SYSTEM AND METHOD FOR DETERMINING HARMONIC CONTRIBUTIONS FROM NONLINEAR LOADS IN POWER SYSTEMS

A Dissertation
Presented to
The Academic Faculty

By

Joy Mazumdar

In Partial Fulfillment
of the Requirements for the Degree
Doctor of Philosophy in
Electrical and Computer Engineering

Georgia Institute of Technology
December 2006

SYSTEM AND METHOD FOR DETERMINING HARMONIC CONTRIBUTIONS FROM NONLINEAR LOADS IN POWER SYSTEMS

Approved by:

Dr. Ronald G. Harley, Advisor
School of Electrical and Computer Engineering
Georgia Institute of Technology

Dr. Thomas E. Michaels
School of Electrical and Computer Engineering
Georgia Institute of Technology

Dr. Deepak M. Divan
School of Electrical and Computer Engineering
Georgia Institute of Technology

Dr. Ganesh K. Venayagamoorthy
Department of Electrical and Computer Engineering
University of Missouri- Rolla

Dr. Thomas G. Habetler
School of Electrical and Computer Engineering
Georgia Institute of Technology

Date Approved: November 13, 2006

ACKNOWLEDGEMENTS

This thesis work was supported by the National Electric Energy Testing Research and Applications Center (NEETRAC) and by the National Science Foundation, USA.

At this very special juncture of my career, I am indebted to many individuals for their support and guidance. I would like to express my sincere gratitude to my PhD advisor Professor Ronald Harley. His guidance, training, constant encouragement and the countless enlightening conversations have not only helped me achieve this goal, but will also help me as an engineer in the years to come. It was an honor for me to work under his exemplary supervision. I would like to acknowledge the efforts of Professor Deepak Divan in completion of this work, and thank him for the innumerable technical discussions and warm encouragement. His immense experience and understanding of the subject helped me tackle some of the difficult challenges in this research. I would also like to acknowledge and thank Professor Thomas Habetler for his contributions in the early stages of this research and most definitely for his time and invaluable inputs. Professor Ganesh Venayagamoorthy had a significant role to play in this research and I would like to acknowledge and thank him for his efforts. This research would never have progressed without the efforts of Mr. Franklin Lambert of NEETRAC. I am very grateful to him for his help, guidance and motivation. Many thanks are due to Professor Thomas Michaels for his technical inputs as well as suggestions and comments in writing a better dissertation.

I wish to thank Dr. Paul Werbos, Professor Herbert Jaeger and Professor Subhashish Bhattacharya for sharing their knowledge and providing me with technical

insights. I wish to thank Georgia Power Company and in particular, Mr. Marty Page, for the field measurements and technical help. During my stay at Georgia Institute of Technology, I have been constantly enriched by many of my IPIC colleagues, whom I also wish to thank. I wish to thank all the IPIC Faculty, in particular Professor Harley, Professor Divan and Professor Habetler, for creating and maintaining an excellent research facility, which has definitely had a positive impact on this work.

Nothing in life is possible without the love and support from one's family. I would like to thank my wife Shilpi for her sacrifices, patience, support and unconditional love. I would also like to thank my sister Jolly for her constant support and encouragement. Last but not the least; I would like to express my undying love and gratitude to my mother and father for a lifetime of support, encouragement and education. Their love and blessings made everything I have accomplished possible.

TABLE OF CONTENTS

LIST OF TABLES

LIST OF FIGURES

NOMENCLATURE

ANN Artificial Neural Network

BP Backpropagation

BPTT Backpropagation Through Time

ESN Echo State Network

FFT Fast Fourier Transform

HG Harmonic Generator

MLPN Multilayer Perceptron Neural Network

MSE Mean Square Error

PCC Point of Common Coupling

PQ Power Quality

PWM Pulse Width Modulation

RMS Root Mean Square

RNN Recurrent Neural Network

SPC Static Power Converter

SRF Synchronous Reference Frame

TDD Total Demand Distortion

THD Total Harmonic Distortion

SUMMARY

The objective of this research is to introduce a neural network based solution for the problem of measuring the actual amount of harmonic current injected into a power network by an individual nonlinear load.

In electrical networks, harmonic currents are injected into the network by non-linear loads such as power electronic equipment, arc furnaces, saturating inductances, and so on. When such loads are supplied from a sinusoidal voltage, their injected harmonic currents are referred to as contributions from the customer. Harmonic currents which flow in any network, cause harmonic volt drops, so that the supply voltage at the customer is no longer sinusoidal. Any other customers, even with linear loads, connected to the terminals (called the Point of Common Coupling, or PCC) of the first customer, will have harmonic currents injected into them by the distorted network voltage at the PCC. Such currents are referred to as contributions from the power system, or supply harmonics. Currently no method exists which can reliably distinguish between load harmonics and supply harmonics. The proposed load modeling method addresses this issue. The theoretical aspect of load modeling is explained. The scheme is verified on a number of different power electronic circuits. It is shown that there is a difference in the current distortion of a load depending on whether the load is served by a clean voltage supply or a distorted voltage supply. To quantify this difference, a new parameter e_m is introduced. The utility is responsible for ensuring there are no resonance conditions created by their use of capacitors on the system. However, if a significant amount of voltage distortion exists on a circuit, customer loads can have an increased level of current harmonics as a result of the voltage distortion. So, it can be difficult to determine

whether a customer is within IEEE519 compliance or not. The proposed load modeling concept is also able to identify the amount of customer injected harmonic current regardless of whether a resonant condition exists on the utility power system.

All loads supplied by the utility are designed and optimized to operate at the supply frequency (60 Hz or 50 Hz, depending on the geographical region of operation). However, the voltage at the PCC is rarely a pure sinusoid and hence loads do not get a clean 60 Hz supply. If several loads are connected to a PCC, another important parameter of interest is to monitor the change in the voltage distortion level at the PCC, if a nonlinear load were to filter out its harmonics. The proposed source modeling scheme addresses this issue. The scheme is verified in simulation as well as on actual field data. The source modeling scheme aids the implementation of IEEE 519 by predicting whether or not the voltage distortion limit at the PCC is restored if corrective action is taken by a nonlinear load in terms of reducing its current harmonics.

The intellectual property of this research is protected. This would help the commercialization of the proposed methods. The main advantages of the proposed schemes are that only waveforms of voltages and currents are required for their operation and they are applicable to both single and three phase systems. Both the schemes are designed as software tools and can be integrated into any existing power quality instrument. This could also be fabricated into a commercial standalone instrument that could be installed in substations of large customer loads, or used as a hand-held clip on instrument.

CHAPTER 1

INTRODUCTION AND OBJECTIVE OF RESEARCH

1.1 Introduction

The development of technology over the years, especially the progress of power electronics applications, has brought about many technical conveniences and economical profits, but it has simultaneously created new challenges for power system operation studies. Driven by challenging environmental constraints, liberalization of the energy market and privatization of the power supply industry, power systems are more and more operating at their maximal performance limits - and frequently beyond them - to maximize asset utilization. To avoid serious functional problems from occurring under these conditions, the system's secure and reliable operation needs to be maintained regarding various aspects of power system operation. One of the main topics of special concern is the aspect of power quality which deals with, among others, voltage characteristics, current characteristics and most importantly control and prediction of harmonics. Dugan et al. published a textbook in 1995 highlighting this aspect [1].

Since the quality of electrical power, e.g. the voltage supplied by the utility or the customer injected current, has become an important feature, the interest in finding, describing and above all, in forecasting system behavior grows continuously. The extensive use of power electronic loads in distribution networks demands alternate methods to forecast power quality problems before they occur in order to maintain reliable system operation. Conventionally, power distribution systems are designed to

operate with pure sinusoidal waveforms and electric utilities strive to meet this requirement. However, the presence of harmonics in the power system represents a threat to sensitive equipments like adjustable speed drives, power electronic loads, computers etc. Simultaneously, during their normal operation, these equipments introduce distortion to the steady-state current and voltages. These circumstances have set the basis for paying considerable attention to the quality of electrical power and addressing the issue of voltage and current harmonic distortion [2], [3]. Attempts to establish steady state harmonic limits in the form of standards for electrical systems containing power electronics or other nonlinear loads emerged as a feasible solution. Standards impose restrictions on harmonic currents which in turn influence the voltage waveform within the system.

Harmonics are an important *measurable* parameter of power quality. The related economic aspects of harmonics [4] and deregulation [5] have all created a need for extensive monitoring of the power system harmonics. Customers with sensitive equipments use harmonic current monitoring to locate the source of harmonic related problems that might occur. On the other side, utilities try to meet the demands of their customers: they monitor the supply voltage to prove that the quality of the offered power is within the pre-specified standards and to obtain the necessary information for solving problems [6], [7]. The utility also reserves the right to measure the amount of the customer's harmonic current injection at any time. These measurements are usually spot checks to locate harmonic sources. Finally, deregulation creates a challenging and competitive new environment, where power quality is a parameter which needs to be measured and monitored continuously.

1.2 What is Power Quality?

The industrial application of power electronics started gaining momentum since the invention of the silicon controlled rectifier (SCR) in 1957. The improved efficiency and productivity provided by the power electronics devices was however offset by the fact that the utility grid was being disturbed due to the injection of harmonic currents by these devices. Hence came the concept of active filtering, first introduced by T. Machida et al in 1971 [8]. In 1977, L. Gyugyi et al [9] and N. Mohan et al [10] did some pioneering work and proposed a family of active filter systems based on pulse width modulated (PWM) current source inverters (CSI) and voltage source inverters (VSI) to reduce the flow of harmonic current from the nonlinear load to the utility system. In the 1980's, with the availability of suitable power semiconductor devices, the application of active filter systems at the industrial level became feasible. As a result, *power quality* as a defined subject was introduced in the early 1980's and by the late 1980's the term *power quality* became a buzzword in the power industry. However, until now there is still disagreement on the usage of this term, how to define it and what it really incorporates. Bollen [11] and Sankaran [12] published textbooks which define power quality and other associated terms.

The term *power quality*, as defined in IEEE 1159 -1995, refers to a wide variety of electromagnetic phenomena that characterize the voltage and current at a given time and at a given location on the power system [13]. IEEE 1159 primarily addresses power quality monitoring issues.

The term *voltage quality* is interpreted as a quality of the product delivered by the utility to the customer. A complementary definition to the voltage quality would be

current quality which is concerned with deviations of the current waveform from a sine wave. Thus, where voltage quality has to do with what the utility delivers to the consumer, current quality is concerned with what the consumer takes from the utility. Both are of course related and if either voltage or current deviates from the ideal it is difficult for the other to be ideal. The next term, *quality of supply,* can be a useful definition as long as the customer's responsibilities are not included, because the word *supply* clearly excludes active involvement of the customer. The supplementary term to quality of supply can be *quality of consumption*, but it is not in common use and therefore of little further interest.

A *power system event* is a recorded (or observed) current or voltage excursion outside the predetermined monitoring equipment thresholds.

A *power disturbance* is a recorded (or observed) current or voltage excursion (event) which results in an undesirable reaction in the electrical environment or electronic equipment or systems.

The term *power problem* refers to a set of disturbances or conditions that produce undesirable results for equipment, systems or a facility [13].

The term *power system event* is typically used to describe significant and sudden deviations of voltage or current from their normal waveform (Figure 1.1) unlike the term *variation* which is used to describe small deviations from the nominal values. The monitoring of events is done using certain triggering thresholds. Voltage or current variations are obtained by continuous monitoring as shown in Figure 1.2.

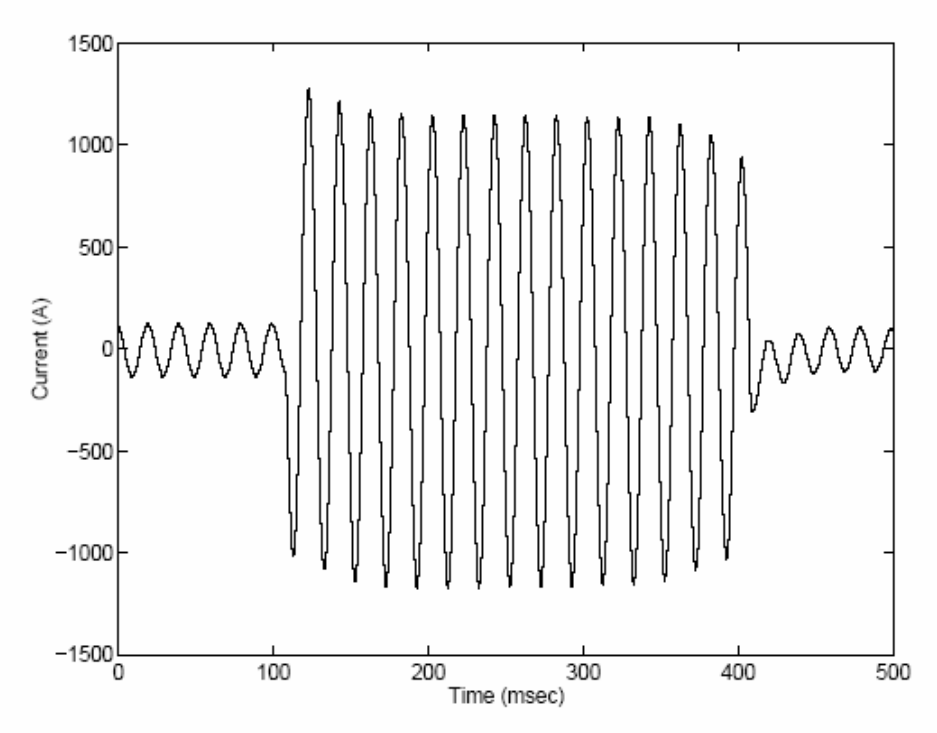

Figure 1.1 Measurement of current during fault

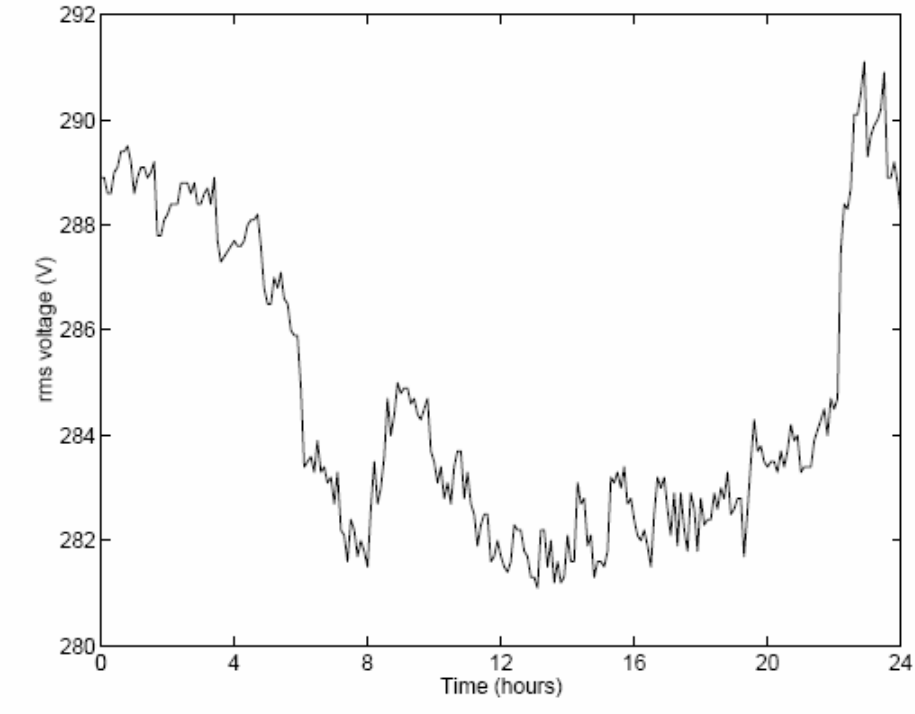

Figure 1.2 Measurement of voltage as an example of monitoring

There are different categories of electromagnetic phenomena that may appear in a power system [13]. This categorization is done in terms of the frequency components (spectral contents) which appear in the voltage signals during the phenomenon, the duration of the phenomenon and the typical voltage magnitude. These phenomena are mainly caused by:

- Factors external to the power system. For example lightning strikes cause impulsive transients of large magnitude;
- Switching actions in the system. A typical example is capacitor switching which causes oscillatory transients;
- Faults which can be caused, for example, by lightning (on overhead lines) or insulation failure (in cables). Voltage dips and interruptions are phenomena related to faults;
- Loads which use power electronics and introduce harmonic currents into the network.

1.2.1 Power Quality Monitoring

The increased requirements on supervision, control, and performance in modern power systems make power quality monitoring a common practice for utilities. Power quality monitoring is necessary to characterize electromagnetic phenomena at a particular location of the network. The objective of monitoring can be [13]:

- The diagnosis of incompatibilities of the power system with the load;

- The evaluation of the electric environment at a part of the system in order to refine modeling techniques or to develop a power quality baseline;
- The prediction of future performance of load equipment or power quality mitigating devices.

For example, an important aspect of power quality monitoring is the collection of information regarding the performance of the system in terms of voltage and current harmonics. For voltage and current harmonics, the obtained information (magnitude and phase) are usually compared with standards like IEEE 519 to evaluate the influence of these events.

In 1981, the IEEE 519 harmonic standard [14] was issued for harmonic related issues; it was revised in 1992. IEEE 519 attempts to establish reasonable harmonic goals for electrical systems that contain nonlinear loads. The objective is to propose steady-state harmonic limits that are considered reasonable by both electric utilities and their customers. The underlying philosophy is that:

- Customers should limit harmonic currents;
- Electric utilities should limit harmonic voltages;
- Both parties share the responsibility for holding harmonic levels in check.

IEEE 519 applies to all voltage levels, including 120 V single-phase residential services. While it does not specifically state the highest-order harmonic to limit, the generally accepted range of application is through the 50^{th} harmonic. Direct current, which is not a harmonic, is also addressed and is prohibited. Since no differentiation is

made between single-phase and three-phase systems, the recommended limits apply to both. A brief outline of the IEEE 519 standard is given in Appendix A.

Harmonic analysis in general can benefit from monitoring [15]. The collected waveforms of voltage and current are also used to test protection and control algorithms [16]. Power quality meters play an important role in the monitoring process.

1.2.2 Power Quality Equipment

Technological advances in digital signal processing, microprocessors and storage devices have made possible the development of metering systems with wide capabilities. These metering systems are designed to accept voltage and current quantities. Typical instrument input limits are 600 V RMS for voltage and 5 A RMS for current. Voltage transducers and current transformers are used to obtain usable signal levels [17]. The Avo-Meggar PA-9 plus meter, which is used in this research is shown in Figure 1.3. Appendix B includes the specifications for this meter.

Figure 1.3 Avo-Meggar PA-9 plus PQ meter

Modern digital monitors utilize analog-to-digital (A/D) converters to convert the analog signals (voltages or currents) into numeric values to be processed by the power quality meter. A/D converters of order up to 20 bits are available for increased resolution. Sampling rates up to 640 samples are typically available, thus increasing the details in the variations in the waveform that can be captured. After the signals have been digitized, the processor of the meter operates on the measurements to derive a number of power quality parameters like harmonic distortion, power factor etc. The measurements and the calculated parameters can be saved in the meter or alternatively be transferred to a host computer. Intranet technologies are employed for the acquisition of the obtained information at the appropriate location [18]. The modems that are used for the transfer can reach a speed of 400 Mb/sec [17].

Typical power quality parameters obtained by most monitors are:

- RMS values of voltage and current;
- Individual harmonics of voltage and current;
- Total harmonic distortion of voltage and current (THD);
- Power factor.

Typically, these parameters are calculated over a short period of time (five cycles) and then their averages are recorded by the meter. Probably the most important task of these meters is to capture power system events without running out of memory while recording. A better solution for saving memory is to analyze the event and then, based on the analysis results, decide whether to store it or not. Automatic processing tools are required in this case.

1.3 Objectives

Nowadays power distribution systems typically operate with nonsinusoidal voltages and currents. Harmonic currents from nonlinear loads propagate through the system and cause harmonic pollution. The need to precisely identify the source of harmonic pollution is growing because the damaging effects of harmonics can no longer be ignored [19]. System designs to prevent the harmful effects of harmonics, like capacitor failures or overheating of conductors, demand analytical methods that require accurate mathematical models to assure reliable system operation both in existing and in planned distribution systems [20], [21]. However such mathematical models are difficult to develop and hence alternate modeling approaches are required. This research proposes one such alternate modeling approach.

As an example, Figure 1.4 shows a simple network structure consisting of a nonlinear load and some other loads, all connected to the point of common coupling (PCC). The PCC is typically a point of metering. There is some flexibility in determining the PCC, but in most instances, it is the point at which the high voltage side of a customer transformer is connected to the distribution network.

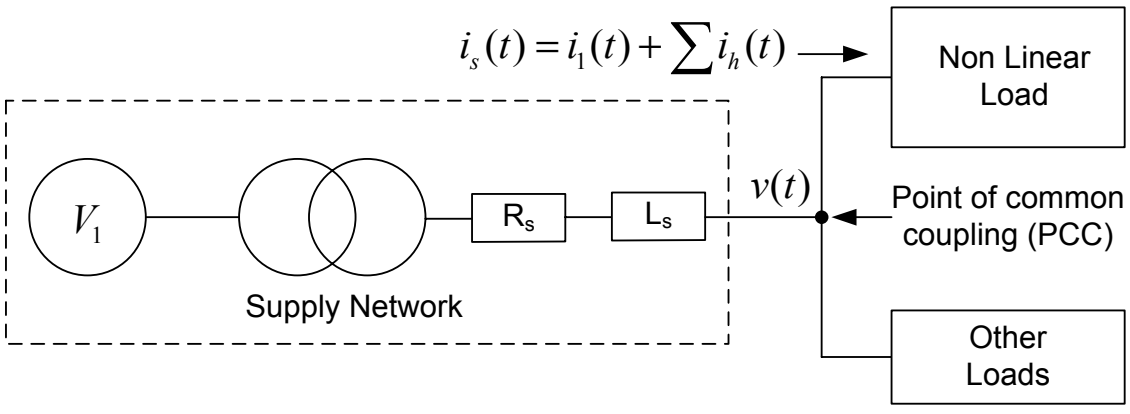

Figure 1.4 Schematic of a simple power distribution network

The nonlinear load current $i_s(t)$ consists of a fundamental component and harmonics. When such loads are supplied from a sinusoidal voltage source, their injected harmonic currents are referred to as *contributions from the load*, or load harmonics.

The nonlinear load produces harmonic current flow in the supply network, which reacts with the network impedance (R_s , L_s) to create voltage drops along this impedance. Hence, the voltage at the PCC is therefore distorted and no longer sinusoidal even if V_1 is sinusoidal. Any other loads, even linear loads, connected to the PCC therefore have harmonic currents injected into them by the distorted PCC voltage. Such currents are referred to as *contributions from the power system*, or supply harmonics.

The premise of IEEE 519 is that there exists a shared responsibility between utilities and customers regarding harmonic control. Maintaining reasonable levels of harmonic voltage distortion depends upon customers limiting their harmonic current emissions and utilities controlling the system impedance characteristics. IEEE 519 includes tables of customer harmonic emissions limits (Appendix A). The tables are created such that the relative size of the customer load, in regards to the utility system at the PCC is taken into consideration. If measurements of current are taken at the PCC, it is expected that those measurements can be used to determine whether the customer is in compliance with IEEE 519. However, results in this research show that the current measurements at the PCC are not always reliable. If there is a significant amount of distortion present in the PCC voltage, then this voltage distortion affects the current distortion measurements. This may create a situation that makes it appear as if a particular customer is not in compliance with the harmonic current limits because of the already distorted utility system voltage. In such a case, it may be necessary to determine

what the customer's true current harmonic distortions would be if the PCC voltage could be a pure sinusoidal voltage.

However, establishing a pure sinusoidal voltage at the PCC may not be feasible since that would mean performing utility switching to reduce the system impedance to almost zero in order to get V_1 to appear at the PCC. An alternative approach is to use a neural network that is able to learn the customer's load admittance. Then, it is possible to predict the customer's true current harmonic distortions based on mathematically applying a pure sinusoidal voltage to the learned load admittance. The proposed method is called *load modeling*. Load modeling predicts the true harmonic current that can be attributed to a customer regardless of whether a resonant condition exists on the utility power system. It is also able to distinguish between load harmonics and source harmonics in a power system network without disconnecting any customer from the network or having to switch parts of the network in or out. If the true harmonic current injections by a customer were known, then a utility could penalize that offending consumer in some appropriate way, including, say, a special tariff or insist on corrective action by the customer.

If a corrective action is taken by the customer, another important parameter of interest is the change in the voltage distortion level at the PCC due to the corrective action of the customer. This research also addresses this issue by predicting the change in the distortion level of the voltage at the PCC if the customer were to draw only fundamental current and filter out its harmonics. This proposed method is called *source modeling*.

The main advantages of the two proposed methods are that only waveforms of voltages and currents are required by them and they are applicable to both single and three phase systems. Most of the other proposed methods aimed at distinguishing between load harmonics and source harmonics, as will be discussed in chapter 2, assume a radial feeder supplying a single load through a known feeder impedance, or multiple loads connected to a PCC which has a sinusoidal voltage and with zero impedance in the supply feeder. Such assumptions are not required here. The largest benefit of the proposed methods is that it is possible to obtain results and draw conclusions about a customer's harmonic profile from the neural network predictions, which otherwise would require switching in the field by the utility and in most instances such switchings are not a desirable action.

Both the proposed methods are designed as software tools and can be integrated into any existing power quality diagnostic instrument. The tools could also be fabricated into a commercial standalone instrument that could be installed in substations of large customer loads, or used as a hand-held clip on instrument.

1.4 Organization

A brief introduction to power quality along with commercially available instrumentation has been provided. A discussion on IEEE 519 standard is also provided. This has been followed by the description of the problem statement and objectives of this research. The remainder of this thesis is organized as follows:

Chapter 2 presents a literature review of various other harmonic identification methods. The theory and control strategies of these methods are summarized. A brief

discussion on harmonic sources, their impact on the power system and tools for analysis of harmonic waveforms are also provided.

Chapter 3 describes the different neural network architectures, fundamentals of the algorithms used for the neural network training, and the suitable adaptation of neural network architectures and the training algorithms to the problem in hand.

Chapter 4 presents the proposed concepts of load modeling and source modeling along with simulation results and laboratory experimental results.

Chapter 5 presents the application of the proposed load modeling and source modeling tool to actual field data from test sites in Georgia.

Chapter 6 presents the theory and application of a special form of recurrent neural network known as an Echo State Network.

Chapter 7 discusses the application of the proposed neural network structure to active filtering.

Chapter 8 presents the conclusions of this thesis and discusses the specific contributions of this research along with recommendations and future work.

CHAPTER 2

LITERATURE REVIEW

2.1 Background Information

Power system harmonics are not a new phenomenon. In fact, a text published by Steinmetz in 1916 devotes considerable attention to the study of harmonics in three-phase power systems. In Steinmetz's day, the main concern was third harmonic currents caused by saturated iron in transformers and machines. He was the first to propose delta connections for blocking third harmonic currents. Steinmetz's contribution and an overall history of harmonics has been published by E.L. Owen [22] .

After Steinmetz's important discovery, and as improvements were made in transformer and machine design, the harmonics problem was largely solved until the 1930s and 40s. Then, with the advent of rural electrification and telephones, power and telephone circuits were placed on common rights-of-way. Transformers and rectifiers in power systems produced harmonic currents that inductively coupled into adjacent open-wire telephone circuits and produced audible telephone interference. These problems were gradually alleviated by filtering and by minimizing transformer core magnetizing currents. Isolated telephone interference problems still occur, but these problems are infrequent because open-wire telephone circuits have been replaced with twisted pair, buried cables, and fiber optics.

The late 80s and early 90s saw the emergence of power electronic loads. Power electronic loads offer advantages in efficiency and controllability. However, they draw nonsinusoidal currents from AC power systems, and these currents react with system impedances to create voltage harmonics and, in some cases, resonance. Studies show that harmonic distortion levels in distribution systems are rising as power electronic loads continue to proliferate [23].

2.2 Harmonic Sources

As previously mentioned, initial considerations identified transformers and rotating machinery as the main source of the waveform distortion since they use magnetic materials that are operated close to - and often in - the nonlinear region for economic purposes. However, the development of technology over decades, especially the growth of the use of switched power semiconductor devices has resulted in rapid proliferation of harmonics within the power systems, such that the harmonics introduced by rotating machinery are nowadays considered negligible compared to those introduced by power electronic devices. Harmonics and inter-harmonics of a waveform can be defined in terms of its spectral components in the quasi-steady state over a range of frequencies. Table 2.1 provides a mathematical definition assuming that f_1 is the fundamental frequency of a power system and h is the harmonic order.

Table 2.1: Definition of Waveform in terms of Spectral Components

Harmonic	$f = h \cdot f_1$, where h is an integer > 0
Interharmonic	$f \neq h \cdot f_1$, where h is an integer > 0
Sub-harmonic	$f > 0$ Hz and $f < f_1$
DC	$f = 0$ Hz ($f = h \cdot f_1$, where $h = 0$)

For general purposes the *harmonic sources* can be divided into three categories [24], [25]:

1. A large number of distributed nonlinear components of small rating (i.e. mass-products), consists mainly of: single phase diode bridge rectifiers, power

supplies of low voltage appliances (SMPS in TV sets, PCs and other IT equipment), and gas discharged lamps.

2. Large static power converters and transmission system level power electronic devices. Static Power Converters (SPC) are used more extensively for controlling loads. There are many forms of SPC: rectifiers, inverters, cycloconverters, single-phase, three-phase, twelve-pulse, six-pulse, but all have the same character. They are all nonlinear and they inject nonsinusoidal current into the power system.

3. Large and continuously randomly varying nonlinear loads. This refers mainly to electric metal-melting arc furnaces with power ratings in the tens of megawatts and connected directly to the transmission network. The furnace arc impedance varies randomly and extremely asymmetrical, since the carbon electrodes in contact with iron have dissimilar impedances between the positive and negative flows of current. Resistance welding has the same characteristics, where the copper electrodes and the steel being welded have dissimilar impedances between the positive and negative flows of current.

2.2.1 Harmonic Producing Loads

In order to understand the injection of harmonic currents in the power distribution network, it is necessary to discuss the general characteristics of nonlinear loads. Nonlinear loads inject harmonic currents or harmonic voltages into the distribution network even when fed by a sinusoidal voltage or current waveform. Nonlinear loads can be broadly divided into two categories;

- Harmonic current source type loads;
- Harmonic voltage source type loads

Thyristor controlled loads such as those used for dc drives, current-source inverters (CSIs), etc. constitute harmonic current source type loads. These loads produce harmonic currents on the ac supply side of the rectifier for their operation, analogous to induction motors which require reactive currents. In contrast, diode rectifiers with dc side capacitors constitute harmonic voltage source type loads. These loads produce voltages on the ac side of the rectifier to operate, and are becoming prevalent due to their use in domestic electronic equipments, variable speed drives (VSDs), etc. Harmonic currents in the supply result due to harmonic voltages and are determined by the ac side impedance. Therefore, harmonic current source type loads can be modeled by a simple current source or Norton equivalent circuit as shown in Figure 2.1.

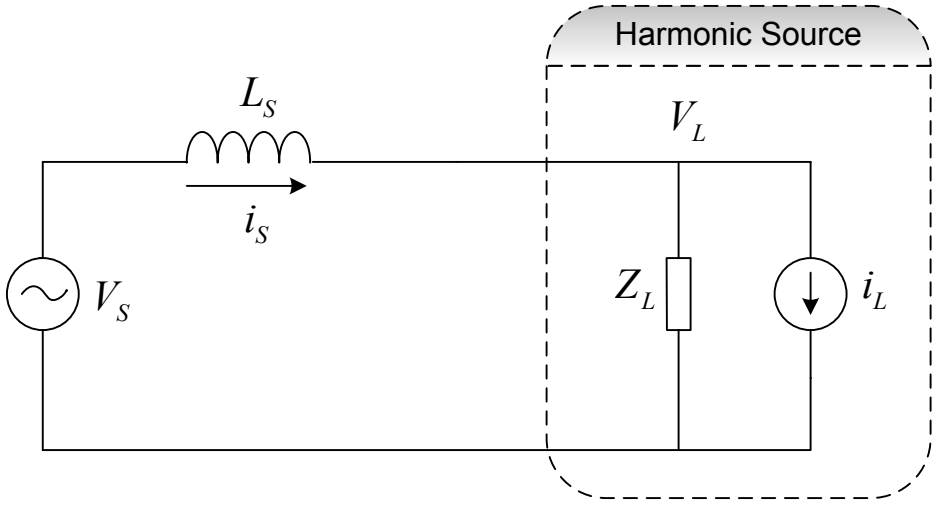

Figure 2.1 Norton equivalent circuit for harmonic current source type load

Similarly, harmonic voltage source type loads can be modeled by simple voltage source or Thevenin equivalent circuit as shown in Figure 2.2.

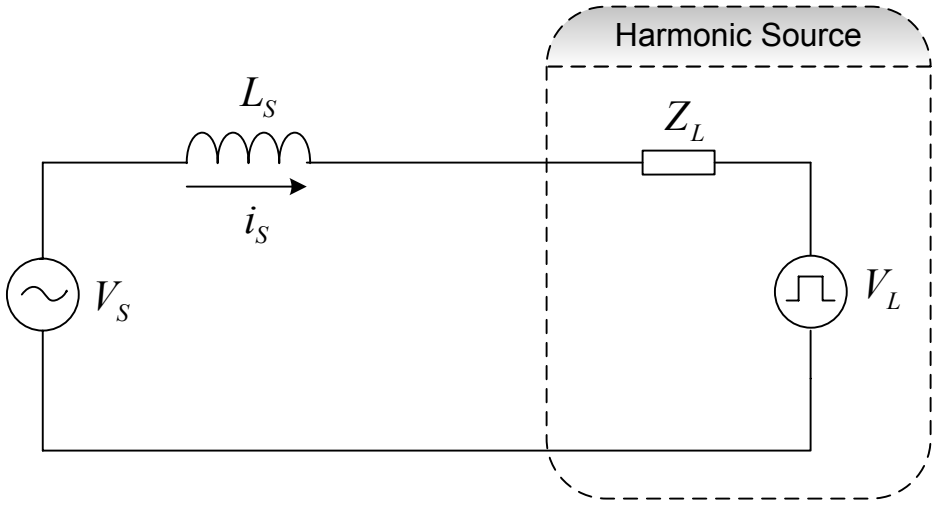

Figure 2.2 Thevenin equivalent circuit for harmonic voltage source type load

These simple Norton and Thevenin equivalent circuit models are however to be used with caution, since under special scenarios such as resonance conditions, they do not accurately model the harmonic sources [26].

2.2.2 Impact of Harmonics

As far as the *impact of harmonics* on power system equipment is concerned, it can be generally stated that harmonics are causing equipment (both in networks and in user's installations) to be subjected to voltages and currents at frequencies for which it was not designed. The effects of such exposure are usually not instantly visible, but can have serious consequences in the medium and long term. Proliferation of three phase diode and thyristor bridge rectifiers for dc power supplies and as front-end rectifiers for inverter

based applications such as VSDs and uninterrupted power supplies (UPS), has resulted in serious harmonic, reactive power, flicker and resonance problems in industrial applications and in transmission / distribution systems. Practically speaking, utilities frequently encounter the following harmonic related problems:

- Voltage distortion in distribution feeders;
- Increased RMS currents, heating and line losses;
- Overheating of power transformers, which requires higher K-factor transformers;
- Derating of distribution equipment;
- Overloading of phase and neutral conductors - neutral currents in a typical commercial office building may carry more than phase RMS currents;
- Amplification of harmonic currents in the utility system due to series and parallel resonances between the utility system and nonlinear loads;
- Overloading and fuse blowing of power factor correction capacitors;
- Tripping of voltage harmonic sensitive equipment;
- Failure of control electronics, micro-processors;
- Reduced accuracy of measuring instruments (such as watt-hour meters);
- Malfunction of solid-state fuses, breakers and relays;
- High failure rate of filter capacitor banks;
- Reactive power and resonance problems;

- Reduced system stability and safe operating margins.

Power quality issues also include unbalanced and sub-synchronous frequency currents (caused by cycloconverters) which contribute to voltage sags and surges, and are the most common cause of VSD nuisance tripping. A rapid increase in the installed capacity of power electronic loads, which is a prerequisite for achieving energy efficiency and productivity benefits, has brought utilities to crossroads. The user achieves energy efficiency at the expense of increased system losses and reduced system stability and safe operating margin for the utilities. The problems and issues, both technical and nontechnical, arising from the proliferation of harmonic producing loads, is a major concern for the utilities as transmission and distribution lines and equipments are operating near their design limits and severe harmonic interactions have caused load and line outages adversely affecting industrial productivity.

The important power quality issues are as follows:

- Displacement power factor;
- Supply / load current harmonics and IEEE 519 harmonic current distortion limits;
- Supply voltage distortion and IEEE 519 harmonic voltage distortion limits;
- Source / sink resonances;
- Line voltage regulation under voltage sags or swells and interruptions;
- Line voltage problems resulting from load switching, network reconfiguration following fault, capacitor switching;

- Transients which include capacitor switching, line voltage notching;
- Nuisance tripping of ASD loads;
- Sensitivity of harmonic filtering solutions to system parameters and operating range;
- Electro-magnetic interference (EMI) issues;

Harmonic currents are injected from harmonic producing loads into the utility network in radial distribution feeders. These harmonic currents affect the operation of other electrical and electronic equipment connected on the same distribution feeder, including the harmonic producing loads. Deeper into the utility distribution and transmission system, it becomes difficult to discern the direction of harmonic power flow, partly due to the highly interconnected and meshed nature of such systems, and partly due to the impact on voltage support capacitors used by the utility and its customers. Resonances between line and transformer reactances, and capacitors in the system can result in amplification of voltage and / or current harmonics. As a result, even small harmonic sources can cause high levels of harmonic current flow between the utility and a customer, and can cause unexpected problems in locations far removed and unconnected with the harmonic source. Further, as utilities and customers change their connected loads, system impedance changes, which can cause resonances and harmonic problems where none existed before. Such problems are not easily identified without a detailed system analysis [27], [28].

In particular the detrimental effect of certain harmonics like even harmonics, triplens etc are listed as follows:

The second harmonic has an impact on peak voltage asymmetry. One half-cycle has a higher peak voltage than the next half cycle and this effect can be accentuated in the presence of other harmonics. There are many loads sensitive to peak voltage asymmetries. For single-phase and three phase rectifiers with large dc filter capacitors, these devices start injecting dc in response to the 2^{nd} harmonic. The dc biases transformers and causes saturation. It causes the voltage zero-crossings to be unequal and disturbs the 6-pulse rectifiers as well [29], [30], [31]. Sources of the 2^{nd} harmonic are e.g.: three-phase half-controlled rectifiers or blasted arc furnaces. However, there are not many field cases reported on annoyances caused by the 2^{nd} harmonic. It is looked upon as a very aggressive harmonic; however its presence in the supply voltage is not high, slightly more than 0.5 %. Other even harmonics are very rare, and are therefore not investigated in this thesis.

The 3^{rd} harmonic (or the other triplens, i.e. 9^{th}, 15^{th}, etc.) is mainly zero-sequence. It raises the potential of the neutral. It has a much stronger effect on communication lines than the 5^{th} and the 7^{th}, because it loads the neutral conductor causing additional losses in the neutral current path, even when the load is balanced but nonlinear.

The fifth was and still is a predominant component in the harmonic mix observed in the voltage [13]. The world wide measurements campaigns have confirmed its significant appearance at every power system voltage level, documenting its steady increasing level even at the high voltage level (about 2 % on many transmission networks). Harmonic surveys show a steady increase of the 5^{th} harmonic level over the last three decades. This increase can be estimated as a constant growth of 1 % point over each 10-year period [13], [23].

The harmonics of order seven, eleven, and thirteen are also present in supply voltages. However their levels are lower than the fifth and vary between 1% to 2%. Their stronger presence compared to the fifth harmonic is mainly caused by resonance phenomena within a power system. The same goes for harmonics of higher orders.

To alleviate harmonic related problems, utilities are beginning to enforce IEEE 519 recommended harmonic standards. IEEE 519 recommends utilities to meet voltage distortion limits, and specifies limits on harmonic currents based on the short circuit ratio at the PCC. As harmonic compensation by itself provides no direct benefit to the user, the widespread use of any form of active filter will only be realized if utilities enforce the IEEE 519 standard for large industrial power electronics loads. This will increase the need for cost-effective and practical approach to the harmonic filter design problem [32].

2.3 Analysis of Harmonic Waveforms

Unlike transient events such as lightning that last for a few microseconds, or voltage sags that last from a few milliseconds to several cycles, harmonics are steady-state, periodic phenomena that produce continuous distortion of voltage and current waveforms [33]. These periodic nonsinusoidal waveforms are described in terms of their harmonics, whose magnitudes and phase angles are computed using Fourier analysis [34].

Fourier analysis permits a periodic distorted waveform to be decomposed into a series containing dc, fundamental frequency, and multiples of the fundamental frequency. The individual harmonics add to reproduce the original waveform. The highest harmonic of interest in power systems is usually the 35^{th} (2100Hz), which is in the low audible

range. Because of their relatively low frequencies, these power system harmonics should not be confused with radio-frequency interference (RFI) or electromagnetic interference (EMI).

2.3.1 General Discussion on Fourier series

Any physically realizable periodic waveform can be decomposed into a Fourier series of DC, fundamental frequency, and harmonic terms. In sine form, the Fourier series is

$$i(t) = I_{dc} + \sum_{k=1}^{\infty} I_k sin(k\omega_0 t + \theta_k) \tag{2.1}$$

where I_{dc} is the DC (i.e., average) value, I_k are peak magnitudes of the individual harmonics, ω_0 is the fundamental frequency (in radians per second), and θ_k are the harmonic phase angles.

The time period of the waveform is

$$T = \frac{2\pi}{\omega_0} = \frac{1}{f_0} \tag{2.2}$$

For a discrete/sampled signal, the frequency spectrum can be obtained as follows:

$$I(k) = \sum_{n=0}^{N-1} i(n) e^{-j2\pi \frac{k}{N} n} \tag{2.3}$$

where N is the number of samples over the period T, $x(n)$ is the amplitude at each sample and $k = 0,1,2,....N-1$. Each frequency is separated by $\frac{1}{T}$, with the highest frequency component at $k = \frac{N}{2}$. The highest frequency becomes $\frac{N}{2T}$.

The sampling frequency to avoid aliasing, also known as the Nyquist frequency, is defined as;

$$f_s > 2f_{(n)} \tag{2.4}$$

where f_s is the sampling frequency and $f_{(n)}$ is the highest frequency component contained in the signal. For power system and harmonic studies, waveforms are normally sampled at 96 – 128 samples/cycle.

Power electronic loads [35], [36] exhibit a special property known as half-wave symmetry. Have-wave symmetry exists when the positive and negative halves of a waveform are identical but opposite, i.e.

$$i(t) = -i(t \pm \frac{T}{2}) \tag{2.5}$$

where T is the period. Waveforms with half-wave symmetry have no even-ordered harmonics.

2.3.2 Total Harmonic Distortion

The most commonly used measure for harmonics is the total harmonic distortion (THD), also known as the distortion factor. It is applied to both voltage and current. If DC is ignored, then the THD for a current waveform is defined as;

$$THD_I = \frac{\sqrt{\sum_{k=2}^{\infty}\left(\frac{I_k}{\sqrt{2}}\right)^2}}{\frac{I_1}{\sqrt{2}}} = \frac{\sqrt{\sum_{k=2}^{\infty}(I_k)^2}}{I_1} \tag{2.6}$$

THD and RMS values are directly linked as shown below;

$$I_{rms} = I_{1,rms}\sqrt{1+THD_I^2} \tag{2.7}$$

Line losses always increase when harmonics are present because these losses are proportional to the square of the RMS current. Sometimes they increase more rapidly due to the resistive skin effect.

While current distortion in loads varies from a few percent to more than 100%, voltage distortion is generally less than 5%. According to IEEE 519, voltage THDs below 5% are considered acceptable, and those greater than 10% are definitely unacceptable and will cause problems for sensitive equipment and loads.

2.3.3 Harmonic Power

Harmonic powers (including the fundamental) add and subtract independently to produce total average power. Average power is defined as;

$$P_{avg} = \frac{1}{T}\int_{t}^{t+T} v(t)i(t)dt \tag{2.8}$$

By substituting the Fourier series for voltage and current in (2.8), the average value of all the sinusoidal terms becomes zero, leaving only the time invariant terms in the summation, or

$$P_{avg} = V_{dc}I_{dc} + \sum_{k=1}^{\infty} V_{k,rms}\cdot I_{k,rms}\cdot dpf_k = P_{dc} + P_{1,avg} + P_{2,avg},...., P_{k,avg} \tag{2.9}$$

where dpf_k is the displacement power factor for harmonic k.

The harmonic power terms are mostly losses and are usually small in relation to the total power. However, harmonic losses may sometimes be a substantial part of total

losses. According to (2.9), if there is no harmonic voltage at the terminals of a generator, then the generator produces no harmonic power. However, due to nonlinear loads, harmonic power does indeed exist in power systems and causes additional losses.

2.3.4 True Power Factor

Voltage and current harmonics produced by nonlinear loads increase power losses and, therefore, have a negative impact on electric utility distribution systems and components. While the exact relationship between harmonics and losses is complex and difficult to generalize, the well established concept of power factor does provide some measure of the relationship, and it is useful when comparing the relative impacts of nonlinear loads, providing that harmonics are incorporated into the power factor definition.

True power factor is defined as [35], [36];

$$pf_{true} = \frac{P_{avg}}{V_{rms} I_{rms}} \tag{2.10}$$

When the voltage and current waveforms are both sinusoidal, (2.10) reduces to the familiar displacement power factor,

$$dpf_1 = \frac{P_{1,avg}}{V_{1,rms} I_{1,rms}} = cos(\theta) \tag{2.11}$$

where θ is the angle between the fundamental voltage and current.

When harmonics are present, (2.11) can be expanded as;

$$pf_{true} = \frac{P_{1,avg} + P_{2,avg} + P_{3,avg} .....}{V_{1,rms}\sqrt{1+THD_V^2} \cdot I_{1,rms}\sqrt{1+THD_I^2}} \tag{2.12}$$

A useful simplification to (2.12) is obtained by making two assumptions;

1. In most cases, the contributions of harmonics above the fundamental to the average power may not be that significant. Hence, $P_{avg} \approx P_{1,avg}$.

2. Since THD_V is normally less than 10%, $V_{rms} \approx V_{1,rms}$

Incorporating these two assumptions into (2.12) yields the following approximate form for true power factor;

$$pf_{true} = \frac{P_{avg}}{V_{1,rms} I_{1,rms}} \cdot \frac{1}{\sqrt{1+THD_I^2}} = dpf_1 * pf_{dist} \tag{2.13}$$

It is obvious in (2.13) that the true power factor of a nonlinear load is limited by its THD_I.Single-phase power electronic loads tend to have high current distortions. Therefore, their true power factors are lower than unity, even though their displacement power factors are near unity.

On the other hand, three-phase power electronic loads inherently have lower current distortions than single-phase loads and, thus, higher distortion power factors. However, if three-phase loads employ phase control, their true power factors may be poor at reduced load levels due to low displacement power factors.

Adding shunt capacitors is not a solution, in general, to compensate for poor distortion power factor. Only the displacement power factor can be improved with capacitors. This fact is especially important in load areas that are dominated by single-phase power electronic loads, which tend to have high displacement power factors but low distortion power factors. In these instances, the addition of shunt capacitors will likely worsen the power factor by inducing resonances and higher harmonic levels [39].

A better solution is to add passive or active filters to remove the harmonics produced by the nonlinear loads, or to utilize low distortion power electronic loads.

2.4 Existing Methods for Determining Sources of Harmonic Distortion

Harmonic distortions have become an important concern for utility companies. Two basic approaches have been proposed in industry for controlling the amount of harmonic pollution present in a distribution system. The first scheme involves the establishment of limits on the amount of harmonic currents and voltages generated by customers and utilities [14], [37], [38]. A second scheme, inspired by the power factor management practice, is an incentive based scheme, proposes to charge harmonic generators an amount commensurate with their harmonic pollution level when the limits are exceeded. A pioneering work in this area was described by Grady et al. [39] and Sasdeli et al. [40].

The biggest challenge towards the implementation of the above schemes is the need to separate the harmonic contribution of a customer from that of the supply system. Srinivasan specifically addressed this issue in [41]. This is not a new issue and researchers have proposed various approaches, mainly analytical, to provide a solution to this problem. Some of the methods adopted by researchers are listed below.

2.4.1 Harmonic Power Flow Direction Method

A common method for harmonic source detection is the power direction method which checks the direction of harmonic power flow. The side that generates harmonic power is considered to contain the dominant harmonic source or to have a larger contribution to the harmonic distortions observed at the measurement point. Detailed work has been reported by Xu et al. in [42] - [45].

The power direction method can be analyzed using a harmonic Norton equivalent circuit of a utility customer interface as shown in Figure 2.3.

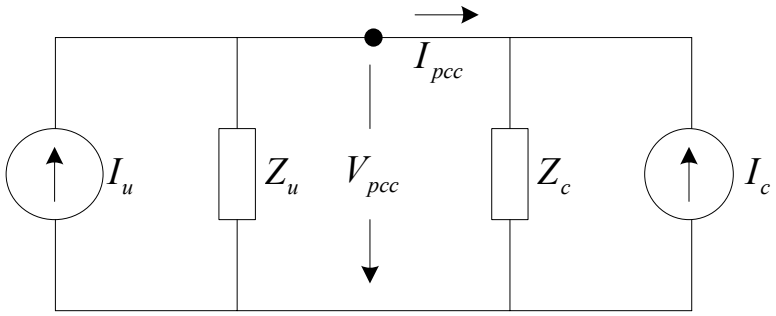

Figure 2.3 Norton equivalent circuit of a utility customer interface

In this figure, the disturbance sources are the customer harmonic source I_c and the utility harmonic source I_u. Z_u and Z_c are the harmonic impedances of the respective parties. The circuit is applicable to different harmonic frequencies (the values will be different). The task of harmonic source detection is to determine which side contributes more to the harmonic distortion at the PCC, subject to the constraint that measurements can only be taken at the PCC. To determine which side causes more harmonic distortion at the harmonic order h, the power direction method first measures voltage and current at the PCC and then calculates the following harmonic power index:

$$P = \Re(V_{pcc}\, I_{pcc}^{*}) \tag{2.14}$$

where V_{pcc} and I_{pcc} are the harmonic voltage and current at the PCC for a particular harmonic number.

The direction of P is defined as positive when it flows from the U side to the C side. Conclusions of the power direction method are the following:

If $P > 0$, the U side causes more h^{th} harmonic distortion

If $P < 0$, the C side causes more h^{th} harmonic distortion

If there is no change in the utility and customer harmonic impedances, then the PCC current flow variation is affected by I_u and I_c only. It is a common practice in industry that utilities provide Z_u information to customers when a plant is built or major changes are made to the utility systems. The data is used for harmonic filter design and for harmonic limit compliance verification. Z_u is normally referred to as the *contract impedance* and should therefore be known [47]. The same applies to Z_c since a harmonic limit compliance check also needs this impedance. An important assumption for this analysis is that both Z_u and Z_c are known to be accurate.

The explanation of harmonic power flow direction is theoretically equivalent to examining the magnitude of $I_u Z_u$ and $I_c Z_c$.

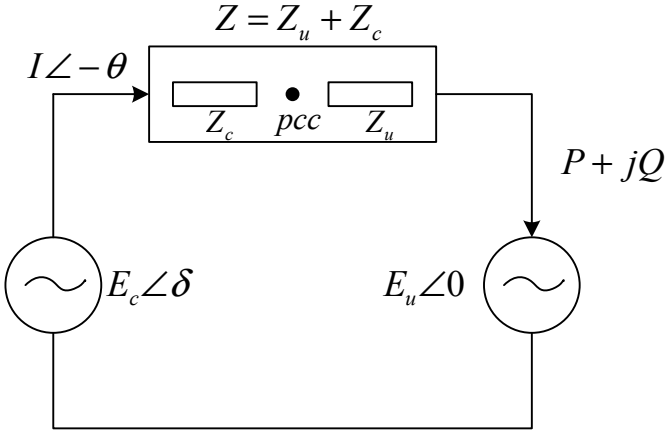

Figure 2.4 Thevenin equivalent circuit of a utility customer interface

If $|I_u Z_u|$ is greater than $|I_c Z_c|$, then it can be shown [47] that the utility side source contributes more to I_{pcc}, and vice versa. Therefore, the circuit of Figure 2.3 is transformed into the Thevenin equivalent circuit as shown in Figure 2.4.

In this figure, $Z = Z_u + Z_c$, $E_u = |I_u Z_u|$, and $E_c = |I_c Z_c|$. The phase angle of E_u is set to zero and that of E_c is denoted as δ . The harmonic source detection problem now becomes to identify which voltage source E_c or E_u has a higher magnitude [47].

However, following the classic power angle equation, if $Z = jX$, then the active power flowing into E_u is:

$$P = E_u I \cos\theta = \frac{E_u E_c}{X} \sin\delta \tag{2.15}$$

The significance of this equation is that the direction of active power is a function of δ instead of the magnitudes of the voltage sources. As a result, the active power direction-based harmonic source detection method may not be accurate, as it cannot reveal the difference between the magnitudes of the two sources [46].

It is common knowledge for power engineers that the phase angles of bus voltages mainly affect the flow of active power while the magnitudes of bus voltages mainly affect the flow of reactive power. On examining the reactive power flowing into E_u ,

$$Q = E_u I \sin\theta = \frac{E_u}{X}(E_c \cos\delta - E_u) \tag{2.16}$$

The above equation shows that the direction of reactive power is indeed related to the voltage magnitudes. Hence the direction of reactive power could indicate the relative magnitudes of two harmonic sources. However, even the reactive power is not a conclusive indicator of the source of harmonic. The reason is, for instance, that reactive power can still flow from the utility side to the customer side if $E_c > E_u$ but $E_c \cos\delta < E_u$.The direction of power flow is always dependent on δ and has to be considered while carrying out any measurements. Li presented this analysis in [47].

2.4.2 Load Impedance variation method

Moustafa et al. proposed this unique method in [48]. This method is based on finding the interrelationship between the distorted voltage waveform, the distorted current waveform, and the link that relates these waveforms, i.e. the load parameters (R and L). Monitoring the load parameter ($R \& L$ values) variations under the influence of harmonics plays an important role for determining the origin of harmonic distortion and evaluating the load nonlinearity. The load with higher $R \& L$ value variations contains more nonlinear elements and produces larger harmonic magnitudes.

A sinusoidal voltage applied to a linear load yields a sinusoidal current. On the other hand, a distorted current waveform will result if a sinusoidal voltage is applied to a nonlinear load. Likewise, if a sinusoidal current is injected through a nonlinear impedance, the voltage across that element will be distorted. Thus, nonlinear loads indicate distorted voltage and/or distorted current waveforms but the opposite is not true. A load with a distorted current or voltage waveform is not necessarily nonlinear. So, considering only the distorted current and voltage waveforms, it is not possible to

pronounce the source of the harmonics. It is mainly dependent on the behavior of the load impedance. Thus, the first step is to find a simple way to monitor the load pattern under the influence of harmonics. Generally for a RL load,

$$v(t) = R(t) \cdot i(t) + \frac{d(L(t) \cdot i(t)}{dt} \tag{2.17}$$

For an incremental time dt, $R \,\&\, L$ can be considered constant, hence the equation becomes

$$v(t) = R \cdot i(t) + L \cdot \frac{di(t)}{dt} \tag{2.18}$$

If $v(t)$ indicates an instantaneous voltage value for a distorted voltage waveform for certain load, and $i(t)$ indicates an instantaneous current value for the corresponding distorted current waveform, then $R \,\&\, L$ indicate the load pattern under the influence of harmonics. For two successive time intervals t_1 and t_2, the equations can be written as

$$\begin{bmatrix} v(t_1) \\ v(t_2) \end{bmatrix} = \begin{bmatrix} i(t_1) & \frac{di(t_1)}{dt_1} \\ i(t_2) & \frac{di(t_2)}{dt_2} \end{bmatrix} * \begin{bmatrix} R \\ L \end{bmatrix} \tag{2.19}$$

Solving the above equation numerically yields the solution as

$$z = [i]^{-1} \cdot v \tag{2.20}$$

The above calculation should be repeated for n successive intervals for the current and voltage waveforms with period T. So for times t_1 to t_n, there are $\frac{n}{2}$ sets of values

for R & L. A sample plot of load parameter variations against time illustrated in Figure 2.5 shows whether it is linear or nonlinear.

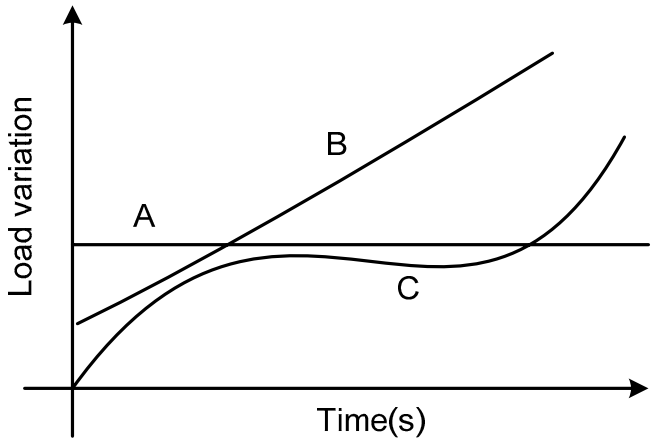

Figure 2.5 Plot of load parameter variation

If the instantaneous R & L parameters represent linear variation or have constant values during the waveform period (pattern A or B), then it indicates that the load under study is linear (nondistorting load). On the other hand, if the instantaneous R & L parameter values have nonlinear variations (pattern C), then it indicates that the load is a source of harmonics.

This mathematical approach can be applied to any set of measured values of v and i, for any load category. From the plots of load parameter variation versus time, it can be predicted whether the load that possesses sharp variations in its R & L parameters would be the higher harmonic producing load.

2.4.3 Online Impedance Measurement

Knowledge of the network impedance values is important for performing power system modeling and simulation. Without this knowledge, it is not possible to simulate or

predict harmonic propagation within a power system. Moreau, Xu, Oliveira, et al. proposed procedures based on current injection for online impedance measurement [49], [50], [51]. Zanotto et al. extended the method for extra high voltage (EHV) transmission networks [52]

Two distinct current injection methods have been used by researchers. The first method proposed by Rhode et al. [53] involves systematically injecting a small sinusoidal current signal at each harmonic frequency of interest. By measuring the phase and amplitude of the voltage and current at the point of injection, the impedance may be calculated at each frequency.

The second method proposed by Thomas et al. [54], [55] involves injecting a narrow current spike to the network. The injected current and voltage transient are recorded and the impedance at the point of injection is calculated. The calculation is carried out in the frequency domain and is given by;

$$Z(f) = \frac{\mathbb{F}(V(t))}{\mathbb{F}(I(t))} \tag{2.21}$$

where $\mathbb{F}$ is the Fourier transform.

The biggest disadvantage of the above methods is the need for need for power electronic converters to inject the current pulse. During online measurements, the converters too becomes a part of the power system and introduces its own nonlinearity.

2.4.4 Probabilistic Methods

Baghzouz and Tan introduced the idea of probabilistic modeling of power system harmonic current injection and propagation [56], [57], [58]. Their research focused on

models which take into account the time varying and probabilistic nature of harmonic loads and their interaction. Correlations exist among currents, voltages and impedances in a power system. Using this information, Testa et al. developed a probabilistic model of impedance [59]. Ribeiro et al. summarized the probabilistic aspects of harmonics and new developments in [60]

Figure 2.6 represents the main links existing among the values assumed by the final quantity of interest (the harmonic voltage V^h) and the values of the quantities of direct influence (the harmonic current I^h, the supply harmonic impedance Z^h and back ground supply voltage V_{BG}^h) and by quantities of indirect influence (the total active and reactive load current I^1 at fundamental frequency, the supply fundamental voltage V^1 and time t).

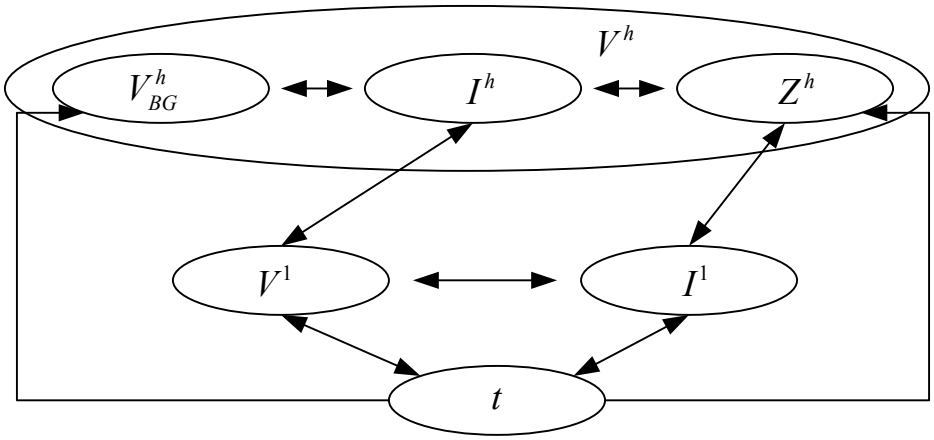

Figure 2.6 Links among different quantities in a power system

Three different modeling approaches are used for evaluating the final quantity of interest, the harmonic voltage V^h;

- The model does not consider impedance variability

- The model neglects the actual correlation effects between currents and impedances
- The model takes into account the actual behavior of currents and impedances

For the analysis, both impedance and current are assumed uniformly distributed between a range of minimum and maximum values.

$$\begin{aligned} Z^h_{min} &= 0 \\ Z^h_{max} &= 1 p.u. \\ I^h_{min} &= 0 \\ I^h_{max} &= 1 p.u. \end{aligned} \tag{2.22}$$

The probability distribution function and cumulative distribution function for V^h is computed under four reference conditions;

a. Constant value for the impedance, which means that,

$$Z^h_{max} = Z^h = 1 \tag{2.23}$$

b. Independence, which means that,

$$P(Z^h \left| I^h \right.) = P(Z^h) \quad and \quad P(I^h \left| Z^h \right.) = P(I^h) \tag{2.24}$$

for different values of Z^h and I^h.

c. Direct dependence, which means that,

$$P(Z^h \left| I^h \right.) = 1 \ \ if \quad \frac{Z^h - Z^h_{min}}{Z^h_{max} - Z^h_{min}} = \frac{I^h - I^h_{min}}{I^h_{max} - I^h_{min}}, \tag{2.25}$$
$$otherwise = 0$$

This means the determination of Z^h has a distance from its minimum value, which is proportional to the distance of the corresponding determination of I^h from its minimum value.

d. Cross dependence, which means that,

$$P(Z^h \mid I^h) = 1 \ \ if \quad \frac{Z^h - Z^h_{min}}{Z^h_{max} - Z^h_{min}} = \frac{I^h_{max} - I^h}{I^h_{max} - I^h_{min}}, \qquad (2.26)$$
$$otherwise = 0$$

and the determination of Z^h has a distance from its minimum value, which is proportional to the distance of the corresponding determination of I^h from its maximum value.

If a physical plot is made for the conditions described above, from the shapes of the probability distribution function and the cumulative distribution function of V^h, it becomes evident that a larger variation of impedance leads to a larger effect on V^h. This approach is useful for the prediction of the corresponding nodal harmonic voltages due to the variation of load impedance, but cannot distinguish between load harmonics and source harmonics.

2.4.5 Neural Network Based Methods

Computational intelligence (AI) techniques, particularly the neural networks, have recently had an impact on power systems and the area of power electronics. Neural networks have created a new and advancing frontier in power systems, which is already a complex and multi-disciplinary technology that has been going through a dynamic evolution in the recent years. Pioneers like Harley [61], Venayagamoorthy [62], Bose

[63], El-Sharkawi [64], Habetler [65] among many others are in the forefront of this effort to promote the application of neural networks in power systems, machines and power electronics.

Specifically in the area of power system applications, Sone et al. [66], Vasquez et al. [67] applied neural networks for harmonic detection in power system waveforms and used it for active power filtering. To detect each harmonic component using the Fourier technique, it needs 2^n sampling points from more than one cycle length of current waveform and the analysis is conducted after all the samples have been input to the system. This method was specifically used to demonstrate the function identification property of neural networks as an alternative approach to FFT based methods.

Bostanci et al.[68], Osowski et al.[69], Chong et al.[70], Richards et al.[70], Chan et al.[72], Arafah et al.[73], Lo et al.[74] have applied neural network techniques for estimation of harmonic components in power systems. Hoffman et al. used neural networks for identification of types of distortion sources in power systems [75]. Neural networks based methods have also been proposed by Suga et al.[76] to predict the voltage at the PCC and also to identify harmonic sources. These methods have been typically useful for predicting the harmonic components of a known waveform and have been shown to be faster since only the harmonics of interest are computed and not the whole spectrum. All these methods assume that the voltage at the PCC is sinusoidal and that the load current contains the true harmonics injected by the load. This thesis extends the work of those earlier neural networks based methods for harmonic identification in order to distinguish between harmonic currents contributed by the load from those harmonic currents contributed by the supply.

2.5 Summary

This chapter has briefly introduced the indices and analysis techniques commonly used in harmonic studies. A description of various methods proposed by researchers to separate customer harmonics from supply harmonics and identification of harmonic sources has been presented. Most of the methods mentioned in section 4 of this chapter assume a radial feeder supplying a single load through known feeder impedance, or multiple loads connected to a PCC which has a sinusoidal voltage and with zero impedance in the supply feeder. A literature review has revealed that many research efforts like the ones mentioned above have been directed at these problems, however, there are still no satisfactory solutions. This has triggered the need for the methods proposed in this research.

Neural networks have been known to be universal function approximators. They are particularly effective in dealing with nonlinear relationships between parameters. Neural networks derive their computing power through their parallel distributed structures and their ability of learn and therefore generalize. Generalization means the neural networks are able to produce reasonable outputs for inputs not encountered during training. Hence, they are capable of blackbox modeling. This feature is exploited in this thesis to provide a solution to the above harmonic measurement problem.

CHAPTER 3

NEURAL NETWORK TOPOLOGIES

3.1 Introduction

Computational Intelligence (CI) techniques, such as expert system (ES), fuzzy logic (FL), artificial neural network (ANN), and genetic algorithm (GA) have been applied widely in power systems, power electronics and motor drives. The goal of CI is to plant human or natural intelligence in a computer so that a computer can reason intelligently like a human being. A system with embedded computational intelligence is often defined as an "intelligent system" that has "learning", "self-organizing" or "self-adapting" capability. Computational intelligence has been debated for a long time, and will possibly be debated for ever. However, there is no denying the fact that computers can be equipped with adequate intelligence to help solve those problems that are difficult to solve by traditional methods. CI techniques are therefore frequently used in industrial process control, image processing, diagnostics, medicine, space technology, and information management system, just to name few. While ES and FL are rule-based, and tend to emulate the behavioral nature of the human brain, the ANN is more generic in nature and tends to emulate the biological neural network directly. The history of the ANN goes back to the 1940's, but its advancement has for sometime been dwarfed by the glamorous evolution of modern-day digital computers.

From the early nineties, the ANN technology started to captivate the attention of a large segment of the scientific community. Since then, this technology has advanced

rapidly and its applications are expanding in different areas. The GA theory (also known as evolutionary computation) was proposed in the 1970's and it is based on principles of genetics (or Darwin's survival of the fittest theory of evolution). Basically, it solves an optimization problem by an evolutionary process resulting in a best (fittest) solution (survivor). Lotfy Zadeh, the inventor of FL, defined ES as hard or precise computing and FL, ANN and GA as soft or approximate computing.

Among all the branches of CI, the ANN seems to have had the maximum impact on the areas of power electronics and power systems as indicated by the number of publications in the literature. However, the literature in this area is hardly more than ten to fifteen years old. In fact, the ANN technology itself has advanced more rapidly in recent years and its applications in different areas are also expanding rapidly. Modern advanced intelligent systems often tend to be a hybrid combination of neuro, fuzzy and GA techniques for improvement of performance. The main body of this chapter describes the principles of different ANN topologies and their learning algorithms.

An artificial neural network (ANN) is a computational device loosely based on the human brain. Simple processing units called neurons (also referred to as nodes) are connected among themselves. It is this interconnected group of artificial neurons that uses a mathematical or computational model for information processing based on a connectionist approach to computation. In most cases an ANN is an adaptive system that changes its structure based on external or internal information that flows through the network. Each neuron receives input signals via a series of connections, coming from either other neurons or the outside world. Each connection has a weight associated with it. In more practical terms neural networks are nonlinear statistical data modeling tools.

They can be used to model complex relationships between inputs and outputs or to find patterns in data [77].

3.1.1 Biological Neuron

An ANN consists of a number of artificial neurons that are interconnected together. The structure of the artificial neuron is inspired by the concept of a biological neuron shown in Figure 3.1. Basically, it is the processing element in the nervous system of the brain that receives and combines signals from other similar neurons through thousands of input paths called dendrites.

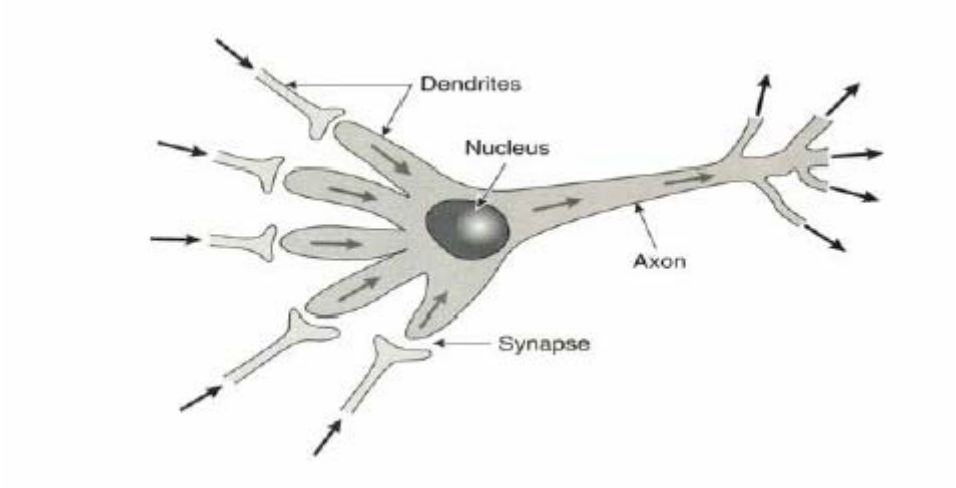

Figure 3.1 Structure of a biological neuron

Each input signal (electrical in nature), flowing through a dendrite, passes through a synapse or synaptic junction. The junction is an infinitesimal small gap in the dendrite which is filled with neurotransmitter fluid that either accelerates or retards the flow of the signal.

These signals are accumulated in the nucleus, nonlinearly modified at the output before flowing to other neurons through the branches of axon as shown. The adjustment of the impedance or conductance of the synaptic gap by the neurotransmitter fluid contributes to the "memory" or "intelligence" of the brain.

The model of an artificial neuron closely matches the biological neuron of Figure 3.1. Basically, it has an op-amp summation type of structure. Each input signal (continuous variable or discrete pulses) flows through a gain or weight (called synaptic weight or connection strength) which can be positive or negative, integer or noninteger. Figure 3.2 illustrates a typical artificial neuron, with connection weights of w_1, w_2, w_3, and w_4 respectively. If signal values of x_1, x_2, x_3, and x_4 are placed on the inputs to this node, as illustrated, the total weighted sum S of the neuron is;

$$S = x_1 \cdot w_1 + x_2 \cdot w_2 + x_3 \cdot w_3 + x_4 \cdot w_4$$

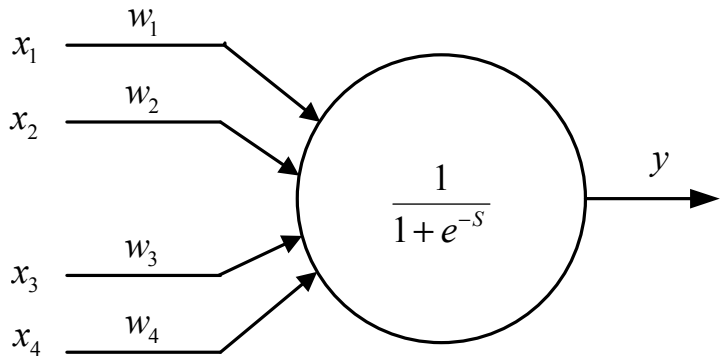

Figure 3.2 Artificial Neuron with connection weights

3.1.2 Activation Functions

Several commonly used types of activation functions used in artificial neuron are shown in Figure 3.3. These are defined, respectively, as linear (bipolar), threshold,

signum, sigmoidal (or log-sigmoid) and hyperbolic tan (or tan-sigmoid). Another type of function that is often used is the Gaussian function, but is not included here. The magnitude of these functions varies between 0 and 1, or -1 to +1 as indicated. The linear function can be unipolar or bipolar.

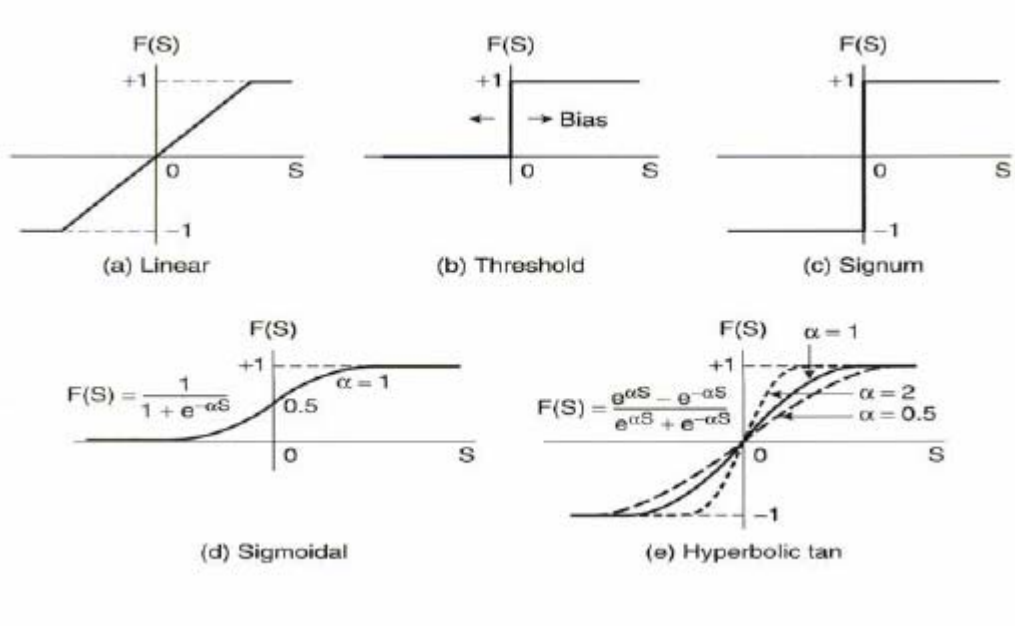

Figure 3.3 Activation functions of artificial neurons

With a slope of infinity, the linear function transforms to the threshold or the signum function, respectively. The sigmoidal and hyperbolic tan functions are commonly used in systems that are nonlinear, such as power electronic systems. Their mathematical expressions are included in Figure 3.3, where α is the gain or coefficient that adjusts the slope or sensitivity. Both these functions are differentiable, and the derivative $\frac{dF}{dS} = 0$ is maximum at $S = 0$. All these functions are squashing in nature, i.e., they limit the neuron response between the asymptotic values. Note that the nonlinear activation function contributes to the nonlinear transfer characteristics of a neuron which permits nonlinear

input-output mapping of ANN as discussed later. However, with linear activation function, this nonlinearity is lost. The activation function used in this research is the sigmoidal function.

The computation performed by any one neuron is simple, but complex behavior emerges when neurons are connected to each other, forming a network. Instead of having to explicitly program them with a particular data processing algorithm, neural networks have the ability to learn from the data presented to them. Learning in a neural network takes place by the modification of the connection weights between nodes.

3.1.3 Learning in Neural Networks

Any neural network requires a learning algorithm to identify or approximate a process. There are three basic classes of learning: supervised, unsupervised and reinforcement learning.

Supervised Learning

In supervised learning, the process starts with teacher data (or training data from the process or plant) which represent examples of the desired model behavior. The teacher data is used to train a ANN such that the ANN approximates (fits) the teacher data. When the trained ANN then receives an input sequence, it should generate an output which resembles the actual output of the original system if it were supplied by the same input. A commonly used cost function is the mean-squared error which tries to minimize the average error between the ANN output and the target value. Minimizing this cost function using gradient descent methods for the class of neural networks called Multi-Layer Perceptrons, results in the well-known backpropagation algorithm for training

neural networks [82]. Tasks that fall within the paradigm of supervised learning are pattern recognition (also known as classification) and regression (also known as function approximation).

Unsupervised Learning

In contrast to supervised learning, the objective of unsupervised learning is to discover patterns or features in the input data with no help from a teacher, basically performing a clustering of input space. In unsupervised learning [83], given some data x, the cost function to be minimized can be any function of the data x and the ANN output $g(x)$.The cost function is dependent on the task and certain a*priori* assumptions (the implicit properties of the model, its parameters and the observed variables).

Reinforcement Learning

In this method, a teacher though available, does not present the expected answer but only indicates if the computed output is correct or incorrect. The information provided helps the network in its learning process. A reward is given for a correct answer computed and a penalty for a wrong answer.

Unsupervised learning and reinforcement learning are not considered in this thesis as it would be inappropriate for the intended application.

3.2 Neural Network Architectures

Neural networks come in many forms and consequently there is no universally accepted definition. They could be characterized as biologically inspired models that typically consist of simple computing units connected in some manner, e.g. Haykin [77]. The structure of the connections between neurons and the computation that a neuron

performs vary between the different neural models. A neural network based modeling is particularly effective when the phenomenon or the process of interest is too complex or unknown in order to be modeled analytically. In such a case, the goal is to build a model in the neural network that will capture the essential properties of the process, by using the observed data and the prior knowledge.

The structure of a biological neural network is not yet well-understood, and therefore, many ANN topologies have been proposed. The ANNs are generally classified as feedforward, and feedback or recurrent types. In the feedforward class, the signals flow only in the forward direction, whereas in recurrent neural network (RNN), the signals can flow in the forward as well as the backward or the lateral direction.

An ANN can be defined as static or dynamic, depending on whether it emulates static or dynamic system. An ANN is characterized by its input-output mapping property. For static mapping, the feed-forward ANNs are preferred, whereas for dynamic or temporal mapping, the RNNs are preferred. A few of the neural network architectures by Haykin [77], as well as some more recent ones are listed as follows.

A. Feed-forward networks:

- Perceptron
- Adaline and Madaline
- Multilayer Perceptron Neural Network (MLPN)
- Radial Basis Function Network (RBFN)
- General Regression Network (GRN)

- Kohonen's Self-Organizing Feature Map (SOFM)
- Learning Vector Quantization (LVQ) Network
- Probabilistic Network (PNN)

B. Recurrent networks:

- Elman Network, Jordan Network
- Echo State Network
- Hopfield Network
- Recirculation Network
- Brain-State-In-A-Box (BSB)
- Adaptive Resonance Theory (ART) Network
- Bi-Directional Associative Memory (BAM) Network

The characteristic of a neural network is that, when trained correctly, the mapping formed by the network can exhibit some capability for generalization beyond the training data. Moreover, typical to neural networks and associated learning algorithms, is that they are somewhat robust against redundant input variables or missing values in the training data. Neural networks are especially useful for classification and regression problems which are tolerant of some imprecision, have lots of training data available, but to which heuristic rules (such as those that might be applied in an expert system) cannot easily be applied.

Many different types of neural networks, such as the Multilayer perceptron neural network (MLPN) as proposed by Rumelhart et al. in 1986 [78] and the Radial basis

function network (RBF) as proposed by Orr et al. in 1996 [79], have been proven to be universal function approximators by Cybenko et al. [80] and White et al. [81]. The universal function approximation property of a neural network means that almost any finite-dimensional vector function on a compact set can be approximated to arbitrary precision if there is sufficient data and sufficient computing resources. A detailed description of all the ANN topologies is beyond the scope of this thesis. Only a few topologies that are most relevant for the proposed application are discussed. Currently, around 90% of ANN applications use feed-forward architecture, particularly the MLPN is most popular. Therefore, a description of this topology is presented in the next section.

3.3 Multilayer Perceptron Neural Network

Multilayer feedforward neural networks, also known as multilayer perceptron neural networks (MLPN), are architectures in which the neurons are assembled into layers, and the connection between the layers flow only in one direction, from the input layer to the output layer, as illustrated in Figure 3.4. There are no connections between the neurons in the same layer. Also, there may be one or several hidden layers between the input and the output layer. Data flows into the network through the input layer, passes through the hidden layer(s) and finally flows out of the network through the output layer.

These architectures are also static, so the mapping between the input and the output is a static function. In practice, this also means that the network does not have memory, where it could store contextual information from the past. Therefore, the input of the network must contain all the necessary contextual information needed to represent the output.

The MLPN is a nonlinear model consisting of number of a neurons organized into multiple layers, forming a mapping $y = g(x, W, V)$ between the input x and the output y, adjusted by the weights W and V. This mapping, with certain architecture and weights, forms a static, nonlinear function. The complexity of the MLPN network can be changed from an almost linear model to a highly nonlinear model by varying the number of layers, the number of neurons in each layer, and the values of the weights.

The network thus has a simple interpretation as a form of input-output model, with network weights as free parameters. A three layer MLPN with input x and output y, interconnected by weight matrices W and V and output error e_0, is shown in Figure 3.4.

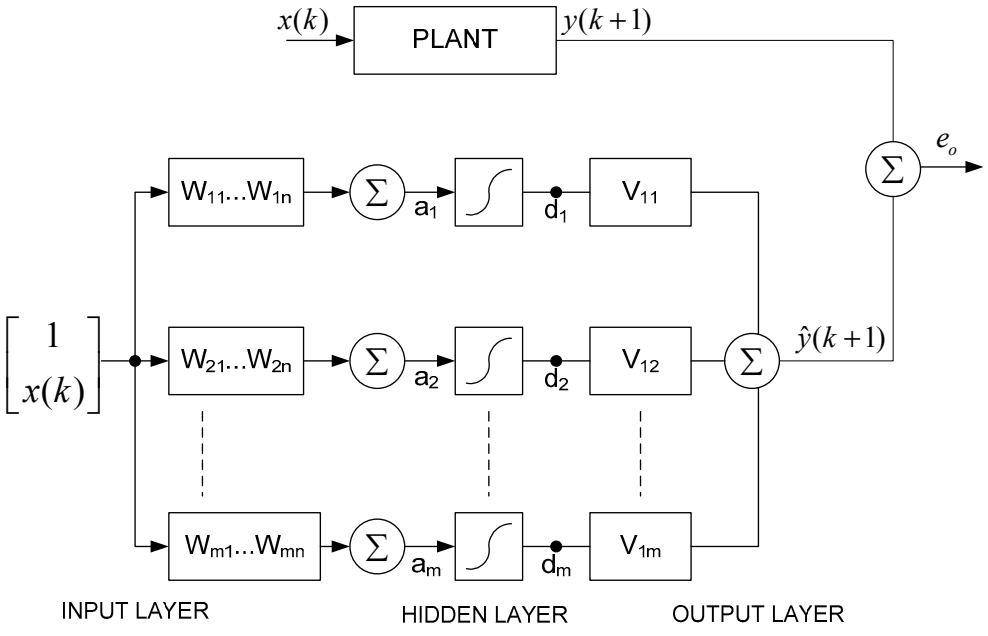

Figure 3.4 Structure of a MLPN network

Parameter estimation of the model is carried out with a training algorithm, which uses the training data to gradually optimize the parameters (or weights) in the MLPN

network. In other words, the training algorithm implements a search method which estimates the values for the parameters of the MLPN.

Gradient descent optimization is one of the methods for estimating the MLPN parameter values. The gradient of the error between the plant and the MLPN output values are computed from the current values. The MLPN parameter values are then corrected in the direction of the gradient, thus gradually driving the MLPN toward the optimal parameter values. A common problem with the gradient descent optimization is difficulty in evaluating whether the MLPN is in a local or in a global minimum. In practice, applied algorithms include different methods which try to prevent from getting trapped to local minima.

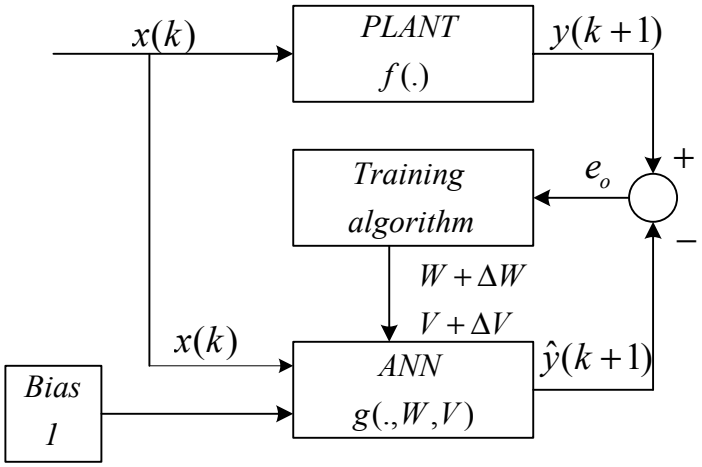

Figure 3.5 Training scheme for a MLPN

The MLPN may be trained to identify or approximate any desired continuous vector mapping function $f(.)$ of a process or a plant as shown in Figure 3.5 over a specified range. Backpropagation learning algorithm based on the gradient descent optimization is the most widely used supervised learning algorithm for MLPNs. This

groundbreaking algorithm was proposed by Werbos in 1974 [82], [84] and has been substantially developed by Harley, Burton, Venayagamoorthy et al. [85], [86] .

The function $g(.,W,V)$ represents the MLPN approximation of the plant function $f(.)$ in terms of it weights W and V. The objective of the training is to modify W and V such that the MLPN function $g(.,W,V)$ approximates the desired function $f(.)$, so that the error e_0 between the desired function output y and the MLPN output $\hat{y}$ is minimal. Two types of supervised learning algorithms exist based on when the weights W and V are updated. The first type is known as Stochastic or online learning, where the weights are adjusted after each pattern presentation. In this case the next input pattern is selected randomly from the training set, to prevent any bias that may occur due to the sequences in which patterns occur in the training set. The second type is known as batch or offline learning, where the weight changes are accumulated and used to adjust weights only after all training patterns have been presented. Continual online training (COT) is required whenever $f(.)$ is a time varying nonlinear function and $g(.,W,V)$ has to track $f(.)$. The generalized equations for backpropagation learning with COT are shown in following section.

3.3.1 Backpropagation Algorithm – Generalized Equations

The online training cycle has two distinct paths;

- Forward propagation and,
- Error backpropagation.

Forward propagation is the passing of inputs through the MLPN structure to its output. Error back-propagation is the passing of the output error e_o to the input in order to estimate the individual contribution of each weight in the network to the final output error. The weights are then modified so as to reduce the output error.

3.3.2 Forward Propagation

Every input in the input column vector $\underline{x}$ in Figure 3.4 is fed via the corresponding weight in the input weight matrix W to every node in the hidden layer. The activation vector $\underline{a}$ is determined as the sum of its weighted inputs. In vector notation;

$$\underline{a} = W\underline{x} \tag{3.1}$$

where the input column vector $\underline{x} \in R^n$, the hidden layer activation column vector $\underline{a} \in R^m$, the input weight matrix $W \in R^{m \times n}$, n is the number of inputs to the MLPN including the bias and m is the number of neurons in the hidden-layer.

Each of the hidden node activations in $\underline{a}$ is then passed through a sigmoid function to determine the hidden-layer decision vector $\underline{d}$.

$$d_i = \frac{1}{1+e^{(-a_i)}}, \qquad i \in \{1,2,....,m\} \tag{3.2}$$

where the decision column vector $\underline{d} \in R^m$.

The decision vector $\underline{d}$ is fed to the corresponding weight in the output weight matrix V. The MLPN output $\hat{y}$ is computed as;

$$\hat{y} = (V\underline{d})^T \tag{3.3}$$

For a single output system output weight matrix $V \in R^{1\times m}$ and $\hat{y}$ is a scalar.

3.3.3 Error Backpropagation

The output error e_o is calculated as

$$e_o = y - \hat{y} \tag{3.4}$$

The output error is back propagated through the MLPN to determine the errors $\underline{e}_d$ and $\underline{e}_a$ in the decision vector $\underline{d}$ and activation vector $\underline{a}$. The decision error vector $\underline{e}_d$ is obtained by back-propagating the output error e_o through the output weight vector V;

$$\underline{e}_d = V^T e \tag{3.5}$$

where the decision error vector $\underline{e}_d \in R^m$.

The activation errors e_{ai} are given as a product of the decision errors e_{di} and the derivative of the decisions d_i with respect to the activations a_i;

$$e_{ai} = \left(\frac{d}{da_i} d_i\right) e_{di}$$

$$= \left(\frac{d}{da_i}\left(\frac{1}{1+e^{(-a_i)}}\right)\right) e_{di}$$

$$= d_i\left(1-d_i\right) e_{di},\ i \in \{1,2,....,m\} \tag{3.6}$$

The derivative of a sigmoidal function can be expressed in terms of its inputs and outputs and computationally it results in multiplication and addition. The subscript i in equation (3.6) indicates element-wise multiplication of the vectors $\underline{d}$, $\underline{1-d}$ and $\underline{e}_d$.

The change in input weights ΔW and output weights ΔV at step k of the training process are calculated as;

$$\Delta W(k) = \gamma_m \Delta W(k-1) + \gamma_g \underline{e}_a \underline{x}^T$$

$$\Delta V(k) = \gamma_m \Delta V + \gamma_g \underline{e}_y \underline{d}^T \tag{3.7}$$

where $\gamma_{m,} \gamma_g \in [0,1]$ are the momentum and learning gain constants respectively. The last step in the training process is the actual updating of the weights at step k ;

$$W(k) = W(k-1) + \Delta W(k)$$

$$V(k) = V(k-1) + \Delta V(k) \tag{3.8}$$

3.3.4 Execution Cycle Computation

All the necessary equations (3.1 – 3.8) required for the computation of forward propagation and error back-propagation are done in vector form. Most of the computations involve either addition or multiplication. Evaluation of the sigmoidal function is the only computationally demanding task. A complete breakdown of the computations required for one MLPN execution cycle is shown in Table 3.1.

Table 3.1 MLPN Execution Cycle Computation

Equation	Multiplication	Addition	Sigmoid
(3.1)	$m \cdot n$	$m \cdot n$	0
(3.2)	0	0	m
(3.3)	m	m	0

Table 3.1 Continued

Forward propagation	$m \cdot (n+1)$	$m \cdot (n+1)$	m
(3.4)	0	1	0
(3.5)	m	m	0
(3.6)	$2m$	0	0
(3.7): ΔV	$2m+1$	m	0
(3.7): ΔW	$m \cdot (2n+1)$	$m \cdot (2n+1)$	0
(3.8)	0	$m \cdot (n+1)$	0
Error backpropagation	$2m \cdot n + 7m + 1$	$3m \cdot n + 4m$	0

Table 3.1 shows that the forward propagation requires m sigmoidal computations. Hence the computation time is directly linked to the size of the hidden layer.

3.4 Neural Networks for Dynamic Systems

The MLPN, discussed in the previous section, can give only static input-output nonlinear (or linear) mapping. In many applications, the ANN is required to be dynamic; that is, it should be able to emulate a dynamic system with temporal behavior, such as identification of a nonlinear time varying function. Such a dynamic network therefore needs storage properties.

3.4.1 Tapped Delay Neural Network

The simplest way to insert memory into the model is to add registers which store consecutive values of the model input as suggested by Mozer et al. in [87]. These registers can be implemented as tapped delay lines, which are fed with a new value at

each time increment, and can store up to k past values of the input. The traditional way of using a tapped delay line neural network is to convert the input sequence into a concatenated vector via a tapped delay line, and to feed the resulting vector as an input to the network. Using the tapped delay line as an input layer in a MLPN was one of the first successful implementations of neural networks in time series prediction by Lapedes and Farber [88]. In the tapped delay line memory the time dimension is converted into spatial representation. In this reconstruction, a neural network approximates the mapping between the input vectors and the desired output. Often the output is a one-step ahead prediction of the time series. In this function approximation procedure, the contextual information between the consecutive input vectors is lost. Also, the time difference between consecutive samples is implicitly assumed to be equal in all input vectors. A typical tapped delay MLPN is shown in Figure 3.6.

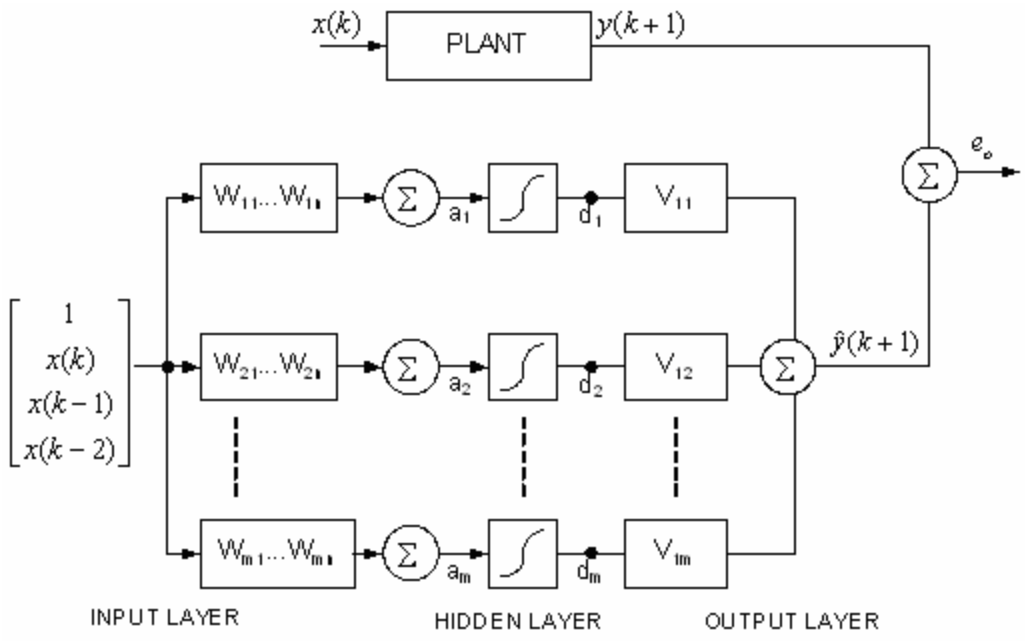

Figure 3.6 Structure of tapped delay line MLPN

In this case, the single input $x(k)$ is fed to a multi-input static neural network through a tapped delay line which generates the sequence of signals with unit time delay $k-1$ and $k-2$ as shown. These signals are then forward propagated through the network structure.

3.5 Recurrent Neural Network (RNN)

One of the most important capacities of the human brain is its ability to remember and base decisions upon present and previous *states* of any process. This ability to store state information makes it possible to perform symbolic manipulation tasks like reasoning.

RNNs are an improvement on MLPN networks, and are characterized by cyclic paths between neurons. Contrary to feedforward networks, RNNs are networks with bi-directional data flow. While a feedforward network propagates data linearly from input to output, RNNs also propagate data from later processing stages to earlier stages. In RNNs, the present activation state is a function of the previous activation state as well as the present inputs. In essence, the recurrent connections allow storing information from the past input and the past state of the network. Adding feedback from the prior activation step introduces a form of memory to the process. This enhances the network's ability to learn temporal sequences without fundamentally changing the training process.

A *simple recurrent network* (SRN) is a variation on the MLPN, sometimes called an "Elman network" due to its invention by Jeff Elman [89] . The structure of a SRN is shown in Figure 3.7. A three-layer network is used, with the addition of a set of "context neurons" in the input layer. There are connections from the hidden layer to these context

neurons with unit delay. At each time step, the input is propagated in a standard feed-forward fashion, and then a learning rule (usually backpropagation) is applied to update the weights. The feedback connections result in the context neurons always maintaining a copy of the previous values of the hidden units (since they propagate over the connections before the learning rule is applied). Thus the network develops memory capability.

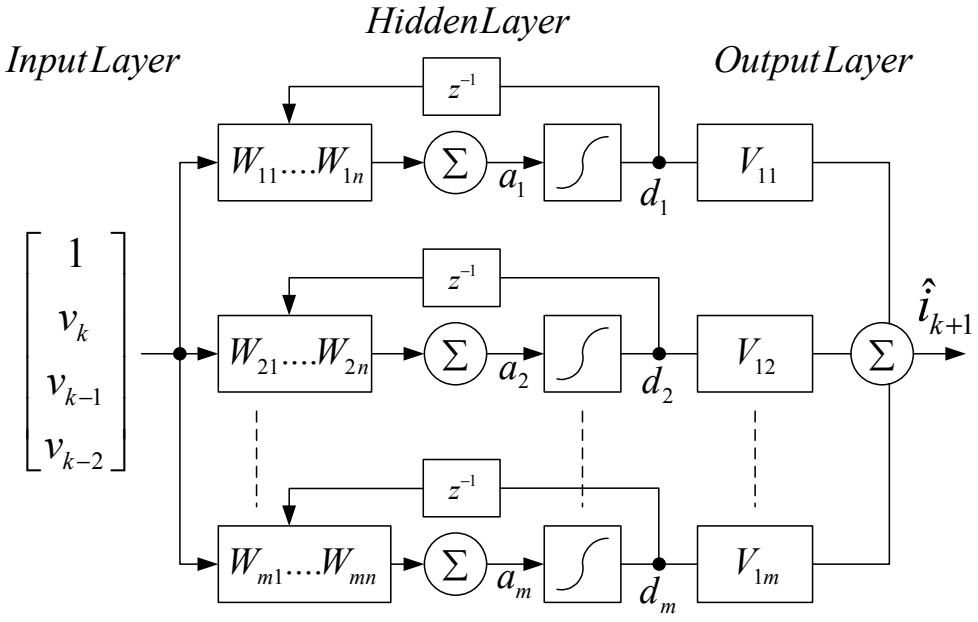

Figure 3.7 Structure of recurrent neural network

Several methods for supervised training of RNNs have been proposed in the literature and the most common one in use today is the *Backpropagation through time* (BPTT) training algorithm. BPTT is an adaptation of the well-known backpropagation training method described in the previous section. BPTT algorithm was also proposed by Paul J. Werbos [90].

3.5.1 Backpropagation through time training algorithm

Backpropagation through time is a general algorithm which is used to train recurrent neural networks. BPTT is based on constructing a static network, which can then be trained with the conventional backpropagation error gradient algorithm. In BPTT, the network is first trained with the training data, and the output error gradient is saved for each time step. Then the network is unfolded in time, as shown in Figure 3.8, originating an equivalent feedforward network called encoding network. This encoding network is a static version of the tapped delay network corresponding to each time step. The static version of the network contains replicated weights corresponding to each time step. Correction terms are then calculated with the standard backpropagation rule for each weight. Finally the correction terms calculated for the static network are accumulated to get correction terms for the weights in the recurrent network.

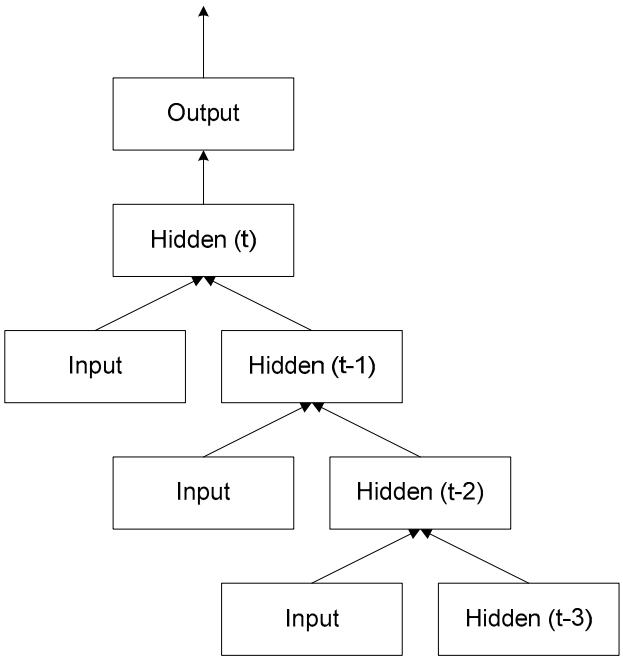

Figure 3.8 Unfolding of a RNN

In a RNN with feedback connection, each time a new input is presented, the hidden neurons compute their activation just as in a feed forward network. However the input of the RNN now contains a term which reflects the state of the network (the hidden unit activation) before the current input was seen by the network. When subsequent inputs are presented, the hidden and output layer states are a function of everything the network has seen prior to the present instant.

The idea of "unfolding in time" can be applied by taking into consideration the history of the network input and state data for a fixed number of time steps. Since the feedback connections in theory have an infinite memory, the BPTT must be truncated to take into account only a predefined number of previous time steps. The number of steps is called the truncation depth and is generally denoted by h. Any information older than h time steps into the past is considered irrelevant and can therefore be ignored. The structure of the BPTT algorithm is presented in Figure 3.9.

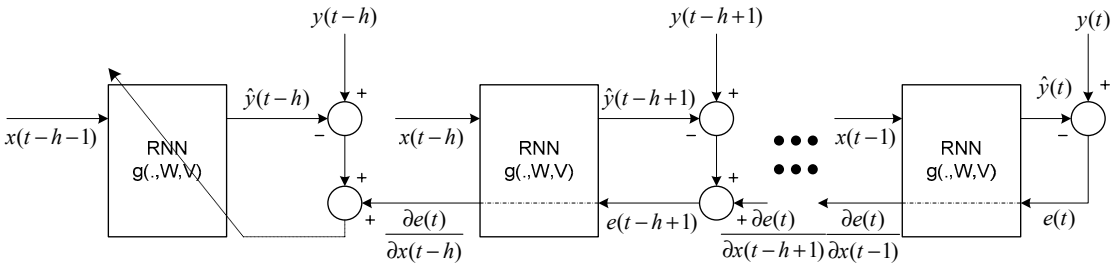

Figure 3.9 Data flow in a RNN with BPTT training

In the BPTT algorithm, the gradient of the sum of squared errors is used to compute the appropriate ΔW and ΔV of the network at the end of each h steps.

The local gradient is defined as

$$\delta(l) = -\frac{\partial(e(l))}{\partial x(l-1)} \tag{3.9}$$

where $t-h<l<t$ and t denotes the time required to learn a temporal task starting from time t_0 all the way up to time t.

For every truncation step l, the local gradient as defined above, is calculated as;

$$\delta(l) = V\begin{bmatrix} d_1(1-d_1) & 0 & 0 \\ 0 & . & 0 \\ 0 & 0 & d_n(1-d_n) \end{bmatrix} W * e(l) \tag{3.10}$$

where $t-h<l<t$.

The local gradient is added to the error e one step before, forming the new error e_{new}.

$$e_{new} = e(l+1) + \delta(l) \tag{3.11}$$

This process is repeated h times until the truncation depth is reached and the final error e is obtained. This output error is backpropagated through the network to adapt the weights W and V. Appendix C shows the execution cycle computation for the RNN.

Drawbacks of using BPTT with recurrent networks include the high computational and memory requirements. More importantly, it has been shown by Bengio et al. [91] that learning long term dependencies is difficult with algorithms based on gradient descent. Since the weight adjustments are calculated as the gradients from the previous values, the adjustments effectively diminish to negligibly small when going further into the past.

Real time recurrent learning (RTRL) proposed by Williams and Zipser in 1989 [92] is another algorithm proposed for training recurrent neural networks. As opposed to BPTT, the training is carried out in "real time", and the correction terms are calculated after each time increment with each new input value to the network. However, even RTRL is computationally demanding. As a result, both these algorithms (BPTT and RTRL) are seldomly applied in practical problems. However, different approximations of these training rules are sometimes employed, allowing faster computations or using less memory [92].

3.5.2 Echo State Networks (ESN)

Complexities with existing algorithms have thus limited supervised training techniques for RNNs from widespread use. When it comes to practical applications, MLPNs still dominate. Echo State Networks are a special form of RNN. The principles of ESN are based on the use of a RNN as a dynamic reservoir. A large (order of 100s of neurons) RNN is used as a "reservoir" of dynamics which can be excited by suitably presented input and output feedback. The connection weights of the reservoir network are not changed by training. In order to compute the desired output dynamics, only the weights of connections from the reservoir to the output units are calculated. This is simply a linear regression problem. The theory and applications ESNs is presented in chapter 6.

3.6 Design of a neural network

Neurons in the hidden layer(s) of a neural network act as memory cells. In most situations, there is no scientific mathematically explicit way to determine the best number

of neurons in the hidden layer without training several networks and estimating the generalization error of each. Too few neurons in the hidden layer, results in a large training error and high generalization error due to under-fitting and high statistical bias. However, having too many neurons in the hidden layer may result in a low training error but will have high generalization error due to overfitting and high variance. Geman et al. discussed how the number of hidden neurons affects the bias/variance trade-off [93]. Moreover, increasing the number of neurons increases the computational effort of the network and severely affects the simulation speed. Essentially there is a tradeoff between the number of the neurons in the hidden layer and the computational and generalization efficiency of the neural network.

Using standard online backpropagation algorithm, however, Lawrence et al. [94] have shown that it can be difficult to reduce the training error to a level near the globally optimal value, even when using more weights than training cases. However, increasing the number of weights makes it easier for standard backpropagation to find a good local optimum, so that an "oversized" network can reduce both the training error and the generalization error.

Some books and articles offer "rules of thumb" for choosing architecture, for example:

- A rule of thumb is for the size of the hidden layer to be somewhere between the input layer size and the output layer size [95].
- Number of neurons in the hidden layer equals: (inputs + outputs) * (2/3).
- One rule of thumb is that the number of neurons in the hidden layer should never be more than twice as large as the neurons in the input layer [96].

Although, the rules of thumb maybe useful for some tasks, they generally do not have much theoretically foundation.

One of the first published works to determine the optimum number of neurons in a neural network, supported by theoretical justifications, was by Hush and Horne in 1993 [97]. They suggest to start the training with a large network size. Such a network will have a large number of redundant information in its synaptic weights. Using *pruning* techniques, the weights and/or nodes which have little or no contribution to the solution are then discarded. Another possibility is *growing* a neural network by starting with a small number of neurons and gradually increasing them until little or no improvement is observed in the network performance.

Baum and Haussler [98] did some groundbreaking work and published their work in 1989 to propose a formula for determining the number of neurons in the hidden layer. For a MLPN with N_W weights and N_N nodes, regardless of the number of layers and the type of activation functions used, Baum and Haussler showed that

$$VCDim \leq 2N_W \times \log_e(N_N) \tag{3.12}$$

A parameter $VCDim$ was defined by Vapnik and Chervonenkis in 1971 [99] and is called the *Vapnik-Chervonenkis Dimension.* This parameter is a measure of the generalization capability of a system, such as a neural network. They showed that the error during the testing stage can be bounded if the number of the training samples exceeds $VCDim$.

To model the harmonic characteristics of a nonlinear load as in this thesis, the neural network architecture needs to address the issues regarding,

(1) The number of layers,

(2) The number of neurons in each layer, and

(3) The hidden layer activation function.

For any nonlinear function identification type problem, at least one hidden layer is required. Additionally, a nonlinear, continuously differentiable hidden layer activation function, such as the sigmoidal function, is required. Depending on the application, the number of ANN inputs and the number of outputs are fixed. The only structural variable then remaining is the number of neurons m in the hidden layer. The ANN execution time and the training convergence is directly dependent on the value of m. Two performance criteria for the measure of ANN training convergence are typically used; they are the absolute value of the tracking error T_e defined as

$$T_e = \left|(y - \hat{y})\right| \tag{3.12}$$

and the Mean Squared Error (MSE) defined as

$$MSE = \frac{1}{r}\sum_{1}^{r}\left|(y - \hat{y})\right|^2 \tag{3.13}$$

where r is the number of training epochs. The tracking error T_e varies at a high rate as training progresses. For this reason it is more convenient to consider the MSE which is a smooth curve due to the averaging process. In neural network training it is not possible to get the MSE to decrease to exactly zero, so the objective is to get it down below some minimum value, typically ($MSE_{min} < 10^{-2}$). This can be achieved by

providing information to the neural network about the history of the system dynamics, typically in the form of delayed inputs and outputs.

The number of neurons in the hidden layer affects the rate and the final value of the MSE convergence, and is typically chosen on a heuristic basis after several iterations. For the specific problem presented in this thesis, based on experimental data and experience, the following formula [98] provides a starting point for choosing the number of neurons in the hidden layer.

$$H_n \approx \frac{K * n}{C \cdot S \cdot MSE_{min}} \tag{3.14}$$

where H_n is the number of neurons in the hidden layer, C is the number of cycles of training data, MSE_{min} is the acceptable MSE in training, S is the number of samples per cycle of the acquired data, n is the number of inputs and K is a constant depending on the number of inputs used and the sampling frequency of data .

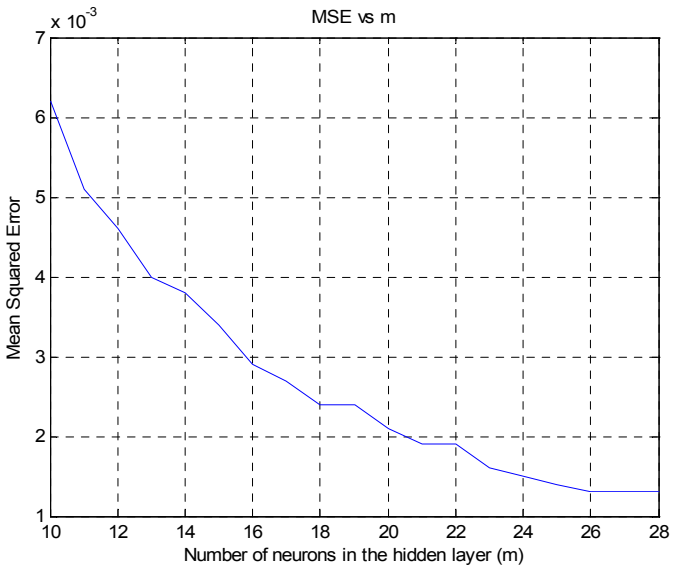

Figure 3.10 Variation of MSE over different values of the number of neurons

Typically power quality recording instruments like the AVO Megger PA-9Plus, the RPM and others, require data to be sampled at 256 samples/ cycle. Starting with random initial values for the ANN weights, and to achieve a MSE_{min} of 0.2% with a 6 cycle snapshot of data, the value of K comes out to be 24. Substituting these values in (3.14), gives a value of H_n as 23.

Figure 3.10 shows the value of MSE obtained experimentally for different values of neurons in the hidden layer for a particular experiment. For most of the experimental results presented in this thesis, the number of neurons used in the hidden layer varies between 20 and 25.

The size of the neural network directly determines the total number of the required mathematical calculations for each training sample as was shown in Table 3.1. This number can serve as an additional measure for selecting the right size and architecture of the neural network. The simulation time required for executing the feedforward and backpropagation paths for each training sample is specifically important for online training applications.

3.7 Summary

Neural networks are good function approximators. They are particularly effective in dealing with nonlinear relationships between parameters. This chapter has introduced the neural network architectures and algorithms available for use in power system applications. Each architecture and algorithm has its own merits and demerits.

This background information on neural networks sets the stage for utilizing the universal approximation property of neural networks to propose a new method to distinguish between load contributed harmonics and source contributed harmonics.

CHAPTER 4

Harmonic Current Identification

4.1 Introduction

Modern day industrial applications extensively use power electronic devices. They have proven to be extremely useful but, unfortunately, due to their switching actions, the power electronic devices can cause power disturbances ranging from line notching to injection of current harmonics [100], [101], [102]. The current waveforms that these devices produce are not sinusoidal. The harmonic content of these nonsinusoidal currents can propagate through the utility's power system and the objective of the electric utility to deliver a sinusoidal voltage at fairly constant magnitude and frequency throughout its network is becoming difficult to meet [103], [104], [105], [106] . The objective of this chapter is to introduce the method used in this research to distinguish between load contributed harmonics and source contributed harmonics.

Figure 4.1 is a one-line diagram of a typical three-phase supply network having a sinusoidal voltage source v_s, network impedance $L_1, L_2, ...L_n, R_1, R_2, ...R_n$ and several loads $i_{h1}, i_{h2}, ...i_{hn}$ (which could be linear or nonlinear) and one specific nonlinear load Z_L, all connected to a PCC. The point at which the high voltage side of a customer transformer is connected to the distribution network is designated as the PCC. The voltage at the PCC is rarely a sinusoid due to many nonlinear loads in the system. As a result, measuring the current waveforms of Z_L yields the combination of nonlinear load

harmonics and nonlinear current due to supply voltage harmonics. For example, if Z_L were a purely resistive load, supplied by a distorted voltage, then the Z_L current would be distorted, appearing as if Z_L was nonlinear.

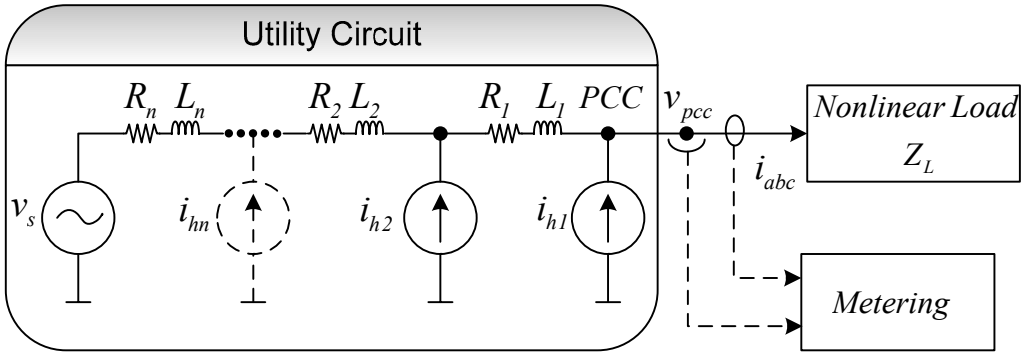

Figure 4.1 Typical power distribution network supplying a nonlinear load

If several loads are connected to a PCC, it is not possible to accurately determine the amount of harmonic current injected by each load, in order to tell which load(s) is injecting any large harmonic currents [107], [108], [109]. If harmonic current injections from individual loads were known, then a utility could penalize the offending consumer in some appropriate way, including say a special tariff or insist on corrective action by the customer. Customers are required to comply with the regulations and when any customer exceeds the limits, the only enforcement power the utility has is to disconnect the customer. Before any action could be taken, an accurate measurement of current is needed. Identification of harmonic sources in a power system has therefore become an important concern for many utility companies. This concern has led to the evolution of various instruments like harmonic analyzers, disturbance monitors, meters etc [110]-[116].

In this research a neural networks based method (called the Load Model Identifier) is proposed to predict the true harmonic current distortion that can be attributed to a customer, without disrupting the operation of any customer. This new method overcomes all the problems discussed in chapter 2. To illustrate this new concept, consider the single line diagram of Figure 4.2 which contains the utility equivalent circuit, the customer and the neural network based Load Model Identifier (LMI).

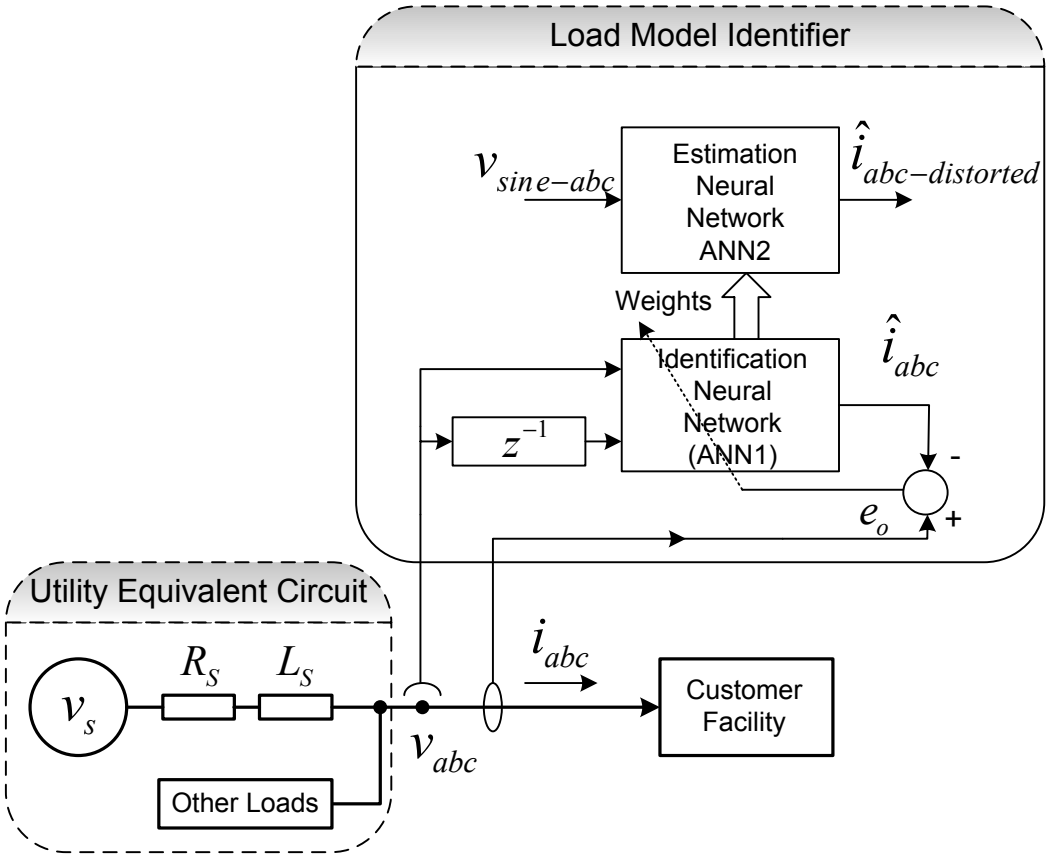

Figure 4.2 Implementation schematic of the LMI method

The utility equivalent circuit comprises of a three-phase supply network having a sinusoidal voltage source v_s, network impedance L_s, R_s and several other loads, which can be linear or nonlinear. The LMI consists of two individual neural network blocks, the **identification** neural network (ANN1) and the **estimation** neural network (ANN2). The

neural network simply consists of software code residing on some processor. The voltage v_{abc} and current i_{abc} at the service entrance of the customer are the parameters of interest and are processed by the LMI.

The nonlinear load injects distorted line current i_{abc} into the network. The identification neural network (ANN1) is trained to **identify** the nonlinear characteristics of the load, or in other words to learn the admittance of the load. At any moment in time after the ANN1 training has been completed, its weights are transferred to the **estimation** neural network (ANN2). ANN2 is then supplied with a mathematically generated sine wave offline to estimate its output $\hat{i}_{abc-distorted}$. Any distortion present in the current waveform $\hat{i}_{abc-distorted}$ can now truly be attributed to the nonlinearity of the load admittance. This procedure is known as load modeling. The function of ANN2 could have been carried out by ANN1, but that would disrupt the continual online training of ANN1 during the brief moments when $\hat{i}_{abc-distorted}$ has to be estimated.

4.1.1 Training the Identification Neural Network

The proposed new LMI method measures the instantaneous values of the three voltages v_{abc} at the PCC, as well as the three line currents i_{abc} at the k^{th} moment in time. The voltages v_{abc} could be line-to-line or line-to-neutral measurements. The neural network is designed to predict one step ahead the line current $\hat{i}_{abc}$ as a function of the present and delayed voltage vector values $v_{abc}(k)$, $v_{abc}(k-1)$ and $v_{abc}(k-2)$. When the *k+1* moment arrives (at the next sampling instant), the actual instantaneous values of i_{abc}

are compared with the previously predicted values of $\hat{i}_{abc}$, and the difference (or error e_0) is used to train the ANN1 weights. This is called continual online training.

Initially the weights have random values, but after several sampling steps, the training soon converges and the value of the error e_0 in Figure 4.2 diminishes to an acceptably small value. Proof of this is illustrated by the fact that the waveforms for i_{abc} and $\hat{i}_{abc}$ should practically lie on top of each other. At this point the ANN1 therefore represents the admittance of the nonlinear load. This process is called *identifying* the load admittance. Since continual online training is used, ANN1 will correctly represent the load admittance from moment to moment. At regular intervals in time after the ANN1 training has converged, its weights are transferred to ANN2. The training cycle of ANN1 continues and in this way ANN2 always has updated weights available when needed.

4.1.2 Prediction by the Estimation Neural Network

ANN2 is supplied with a mathematically generated sine wave to estimate an output while its weights are kept fixed. The output of ANN2, called $\hat{i}_{abc-distorted}$, therefore represents the current which the nonlinear load would have drawn had it been supplied by a sinusoidal voltage source. In other words, this gives the same information that could have been obtained by quickly removing the distorted PCC voltage (if this were possible) and connecting a pure sinusoidal voltage to supply the nonlinear load, except that it is not necessary to actually do this interruption. Any distortion present in the $\hat{i}_{abc-distorted}$ waveform can now be attributed to the nonlinearity of the load admittance. Once a number of $\hat{i}_{abc-distorted}$ cycles have been calculated by ANN2, they

are stored (and subsequently used for harmonic analysis); new weights are then uploaded from ANN1 to ANN2, and a series of new $\hat{i}_{abc-distorted}$ cycles calculated.

4.1.3 Preprocessing the neural network training data

Data preprocessing involves manipulating the data into a suitable form which can be processed further by the neural network. All the necessary computations are carried out in software in vector form. *Normalizing* a vector most often means dividing by a norm of the vector. In the neural network literature [97], "normalizing" also often refers to rescaling by the maximum of the vector. Due to the nature of the sigmoidal transfer function, the outputs of the neurons in the hidden layer are limited to values between 0 and 1. The inputs to the neural networks are therefore limited to values between ± 1. The scaling of the acquired data is done using software and hence that removes any limitations whatsoever on the data acquisition system and the transducers.

4.2 Description of Laboratory Test Circuits and Measurements

For illustrative purposes, consider the network shown in Figure 4.3, where a programmable AC power source is supplying four single phase loads consisting of different power electronic devices, all connected in parallel.

The point of parallel connection is defined as the PCC. The power source used is a California Instruments 5001 iX harmonic generator (HG). The iX Series offers a range of compact, high output AC and DC power units that can be combined to provide up to 30 kVA of power in a small amount of space. The iX Series uses a sophisticated digital signal processor based arbitrary waveform generator and power analyzer. The HG is capable of outputting voltages with programmable distortion levels and zero internal

impedance. The specifications of the HG used in this research are provided in appendix D. Nevertheless, even at its best, the HG still contains 0.2% voltage THD.

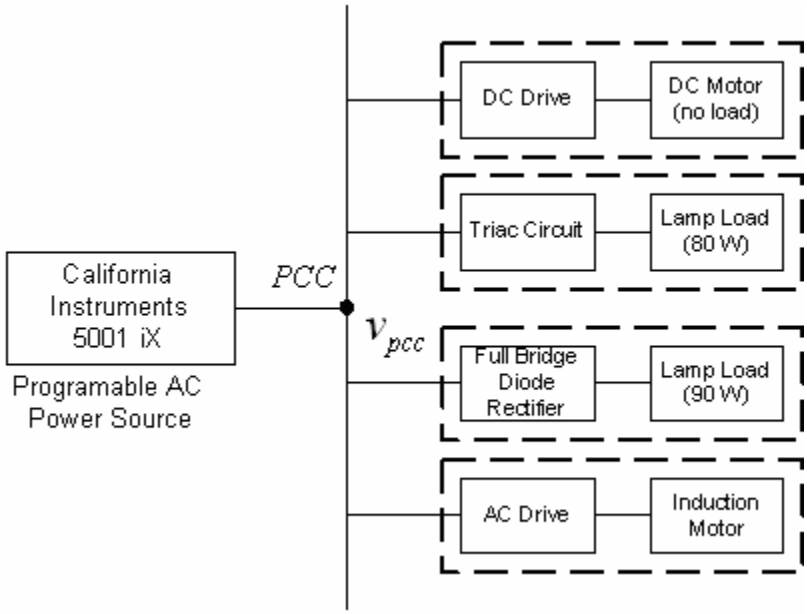

Figure 4.3 Laboratory setup of nonlinear test circuits supplied by the HG

Table 4.1 shows the individual THD of each load in Figure 4.3 when connected one at a time, first to a clean supply from the HG, and then to a distorted voltage from the HG. The voltage distortion of the HG is programmed at 5.91% (which exceeds the IEEE 519 limit of 5 %), made up of 5 % of 3rd harmonic and 3 % of 5th harmonic.

Table 4.1: Sample Measurement Data Using CI 5000 iX to Supply One Load at a Time

	Clean Supply		Distorted Supply	
Load Type	V_{pcc}	I_{load}	V_{pcc}	I_{load}
DC drive with 90% speed ref	0.2%	53.87%	5.91%	62.15%
DC drive with 60% speed ref	0.2%	74.40%	5.91%	77.30%
Diode rectifier with lamp	0.2%	0.34%	5.91%	6.11%
TRIAC with 0° firing angle	0.2%	4.66%	5.91%	7%

Table 4.1 Continued

TRIAC with 30° firing angle	0.2%	29.75%	5.91%	27%
AC drive 60Hz ref	0.2%	85.59%	5.91%	88.18%
AC drive 30Hz ref	0.2%	87.23%	5.91%	89.11%

Some load currents in Table 4.1 have THD values as large as 89%, when no other load is in parallel, but when the supply has 5.91% THD.

An important observation from Table 4.1 is that the current THD of the TRIAC circuit (firing angle 30°) is higher (29.75 %) when it is being supplied by the pure sine-wave (less THD in v_{pcc}) as compared to (27 %) when it is supplied by the distorted v_{pcc}. However for the DC and AC drives, the current THD of the drives are higher when they are supplied by the distorted v_{pcc} as compared to when they are supplied by a pure sine-wave (less THD in v_{pcc}).

When the firing angle for the TRIAC circuit is set to 0°, it behaves as a linear load and its current THD (4.66 %) is lower when supplied by pure sine-wave v_{pcc} as compared to (7 %) when it is supplied by a distorted v_{pcc}. This agrees with the fact that linear loads do not introduce harmonics in the network but do get affected by the distortion in the supply voltage. In a new test with the voltage THD of the HG is programmed to 5.9%, when all the loads in Figure 4.3 are operating together, the THD of the net current from the source is around 52 %. In other words, some harmonic cancellation has taken place.

When several loads are supplied from the PCC, with its own background THD introduced by the HG, the individual load currents are due to the combined effects of the

distorted v_{pcc} and the nonlinearities of the loads. The resulting phase cancellation may reduce the overall harmonic current in the network [117] - [120] and thus benefit some of the nonlinear loads. Hence, it is essential that any harmonic detection or prediction method should be able to analyze the true current injection of each load individually.

4.3 Experimental Results

In most nonlinear circuits, some sort of switching power devices are used as the interface between the supply network and the actual load. The performance of the new LMI method is now further demonstrated with the help of a test comprising the same four loads of Figure 4.3 in a system shown in Figure 4.4 in which the four loads are kept at steady state operation and permanently in parallel. ANN1 is trained to learn the nonlinear characteristics of the triac circuit and ANN2 estimates the true harmonic current distortion of this load. This is then repeated one at a time for the other three loads.

4.3.1 Experiments performed with single phase loads

The switch in Figure 4.4 allows the choice of supplying from either the clean supply or the distorted laboratory supply. The voltage at the PCC is fixed at 120 V RMS, 60 Hz, for both the supply sources.

The nonlinear test circuits are:

- Triac circuit supply a 80 W lamp load (less than 1 Amp).
- Single phase thyristor controlled DC drive supplying a dc motor (2 Amps).
- Diode bridge rectifier supply a 90 W lamp load (less than 1 Amp).
- Single phase IGBT AC drive supplying an induction motor (2 Amps).

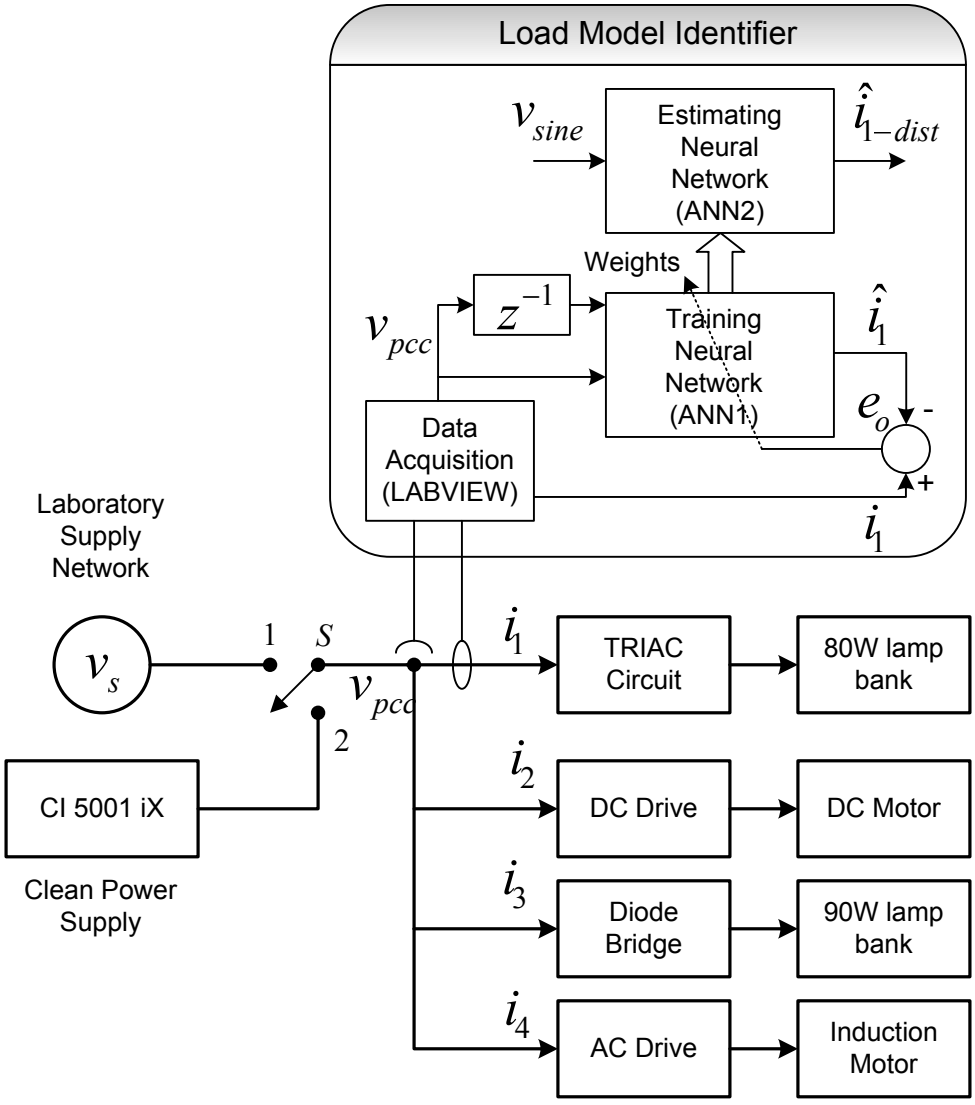

Figure 4.4 Experimental setup for implementation and validation of LMI method

With the TRIAC circuit firing angle set to 30°, the dc drive speed reference set to 90%, and the ac drive reference set to 60 Hz, two different cases are evaluated with switch S either in position 1 or 2.

For case 1, the circuit is supplied from the 120 V laboratory utility wall socket. For case 2, the circuit is supplied from the CI 5001iX. The THD in the voltage and current waveforms are measured with the HP Spectrum analyzer. Data is also acquired

with the NI data acquisition system and stored on a computer. This data is then exported to Simulink and the THD's are calculated in Simulink. It is verified that measurements from both the devices (Spectrum Analyzer and NI Data Acquisition) matched. The recorded measurements for both the cases are shown in Table 4.2.

Table 4.2: Measurement Data for Experiment

	Case 1: S in position 1	*Case 2: S in position 2*
Background THD of voltage at PCC without any loads	4.19%	0.2%
THD of voltage at PCC with all loads connected	4.24%	0.33%
THD of current i_1	27%	30.42%
THD of current i_2	61.53%	53.87%
THD of current i_3	4.38%	0.4%
THD of current i_4	88%	85.59%

The Case 2 measurement data is used to validate the predicted result of the LMI method. The topology for ANN1 and ANN2 is the Elman RNN of Figure 3.7. The LMI method is applied to all the four loads individually. For demonstration purposes, the performance of the LMI method is evaluated for the triac circuit current i_1 and dc drive current i_2 individually. The LMI method is first applied to the triac circuit (i_1). The data obtained from case 1 is used to train ANN1 until the training error converges to near zero, and the output of ANN1 $\hat{i}_1$ correctly tracks the actual current i_1.

Prevention of overfitting is always an important aspect in any neural network training, however if online training is used, overfitting is not an issue. Figure 4.5 indicates how well the training of ANN1 has converged since its output $\hat{i}_1$ lies on top of the actual i_1 waveform. Starting with random weights, the ANN1 requires fifteen cycles of data to achieve initial convergence.

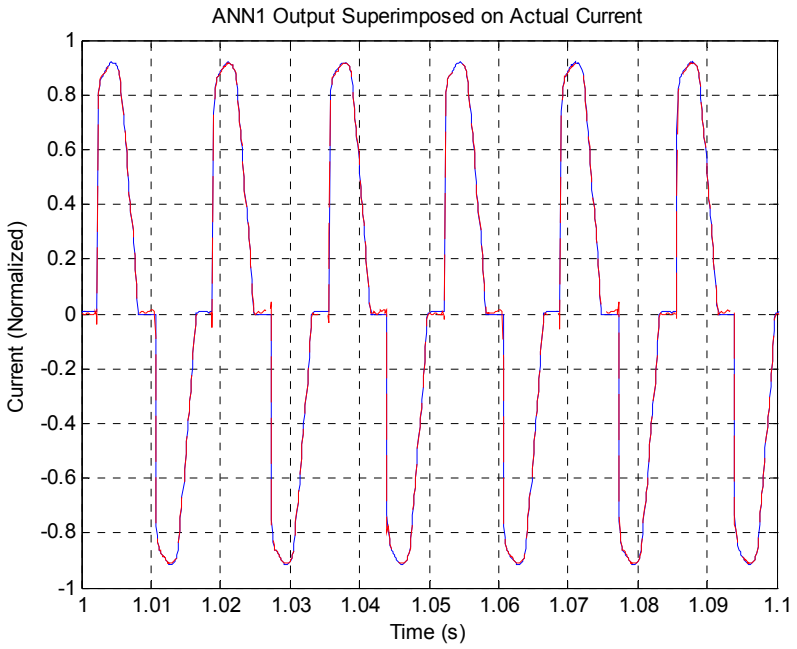

Figure 4.5 ANN1 output $\hat{i}_1$ superimposed on actual current i_1 to indicate convergence

The next step in determining convergence is to compute the MSE using (3.13) of the training. Computation of the MSE while training is in progress is referred to as *training MSE*. Computation of the MSE with weights frozen is referred to as *testing MSE*. Here after, MSE will refer to the *testing MSE*. The MSE in Figure 4.6 is $0.42 \cdot 10^{-3}$. This is sufficiently low to indicate that ANN1 is trained. Once the MSE is below a pre-defined level, it can be concluded that ANN1 has learned the admittance of the TRIAC circuit.

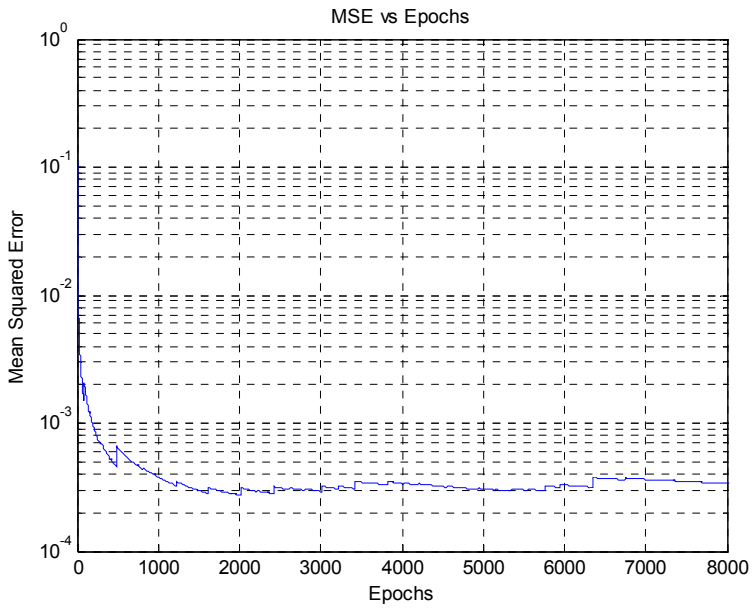

Figure 4.6 Training performance of ANN1 to track i_1 in terms of MSE

The trained weights of ANN1 are now transferred to ANN2 which is supplied with a mathematically generated undistorted sine wave voltage waveform. The ANN2 output ($\hat{i}_{1-dist}$), which is the predicted true current waveform is plotted in Figure 4.7.

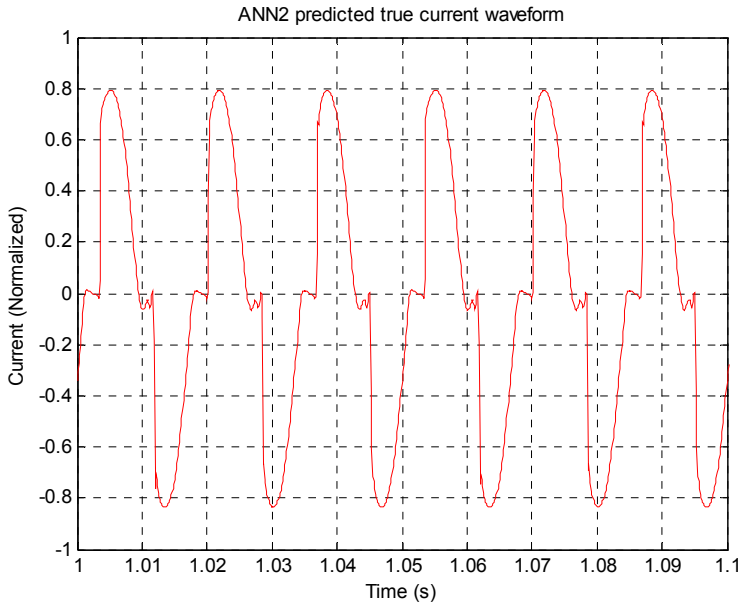

Figure 4.7. True current waveform ($\hat{i}_{1-dist}$) of the triac circuit as predicted by ANN2

Figure 4.7 shows what Figure 4.5 would have looked like if it were possible to isolate the TRIAC circuit and supply it from a pure sine wave. In other words this is the true harmonic current that would be injected by the triac circuit into the network.

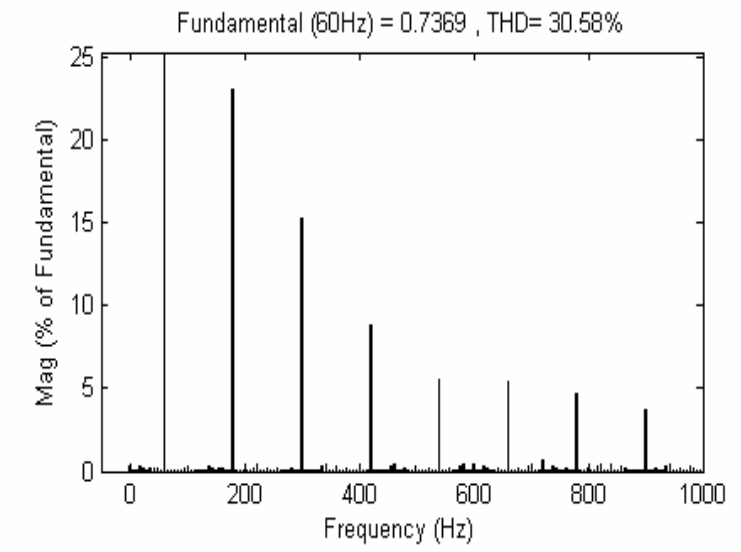

Figure 4.8 FFT spectrum of the true $\hat{i}_{1-dist}$ indicates a THD of 30.58%

Figure 4.8 shows the FFT spectrum of the waveform shown in Figure 4.7. The true current THD of $\hat{i}_{1-dist}$ turns out to be **30.58%** (instead of the **27%** of Figure 4.5). This result agrees well with the measured value of 30.42% obtained in case 2 where the TRIAC circuit was supplied by a 0.2% distorted voltage.

As a second example, the LMI method is applied to identify the current i_2 of the dc drive. The weights are reinitialized with random numbers and the final weights after training are different from those for i_1 and so is the learning time. These parameters are solely dependent upon the admittance being identified. Figure 4.9 verifies the learning capability of ANN1 as its output $\hat{i}_2$ lies on top of the actual i_2 waveform. This is confirmed by Figure 4.10 which shows that the final value of the MSE is about 0.0021.

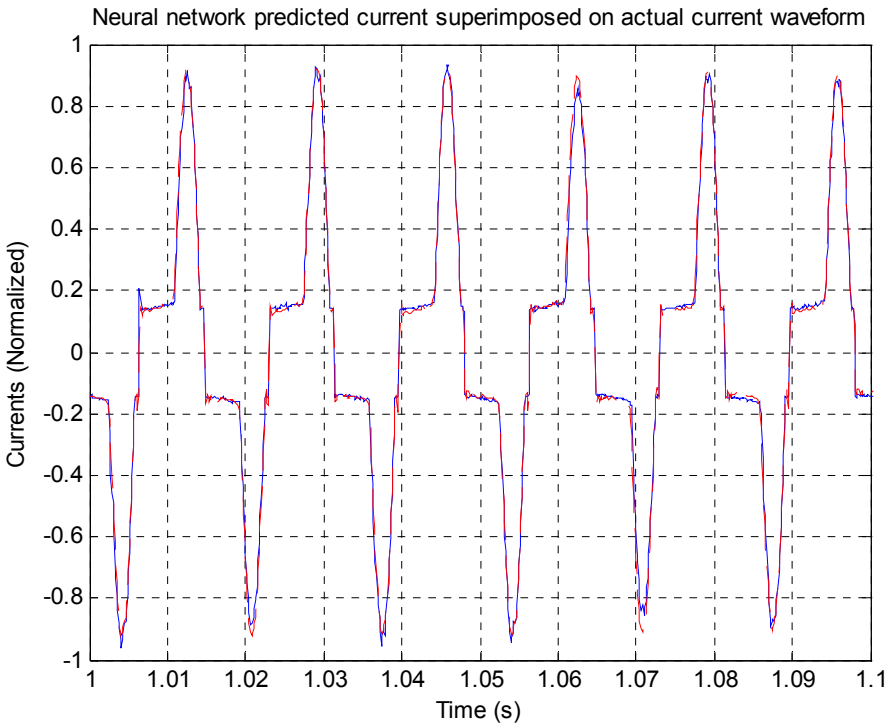

Figure 4.9 ANN1 output $\hat{i}_2$ superimposed on actual current i_2 to indicate convergence

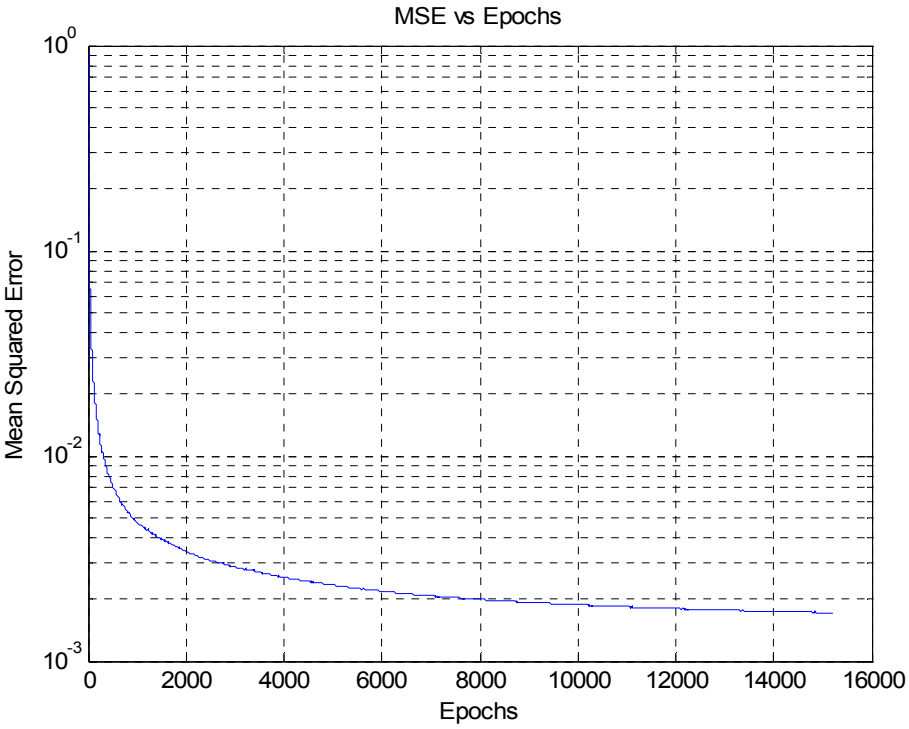

Figure 4.10 Training performance of ANN1 to track i_2 in terms of MSE

The predicted true current $\hat{i}_{2-dist}$ by ANN2 appears in Figure 4.11 along with the FFT spectrum in Figure 4.12. The true current THD of $\hat{i}_{2-dist}$ in Figure 4.12 turns out to be **53.40% (**instead of **61.53%** measured when the dc drive was supplied from the wall socket), which agrees well with the measured value of 53.87% obtained when this was the only load supplied by a 0.2% distorted voltage from CI 5001iX.

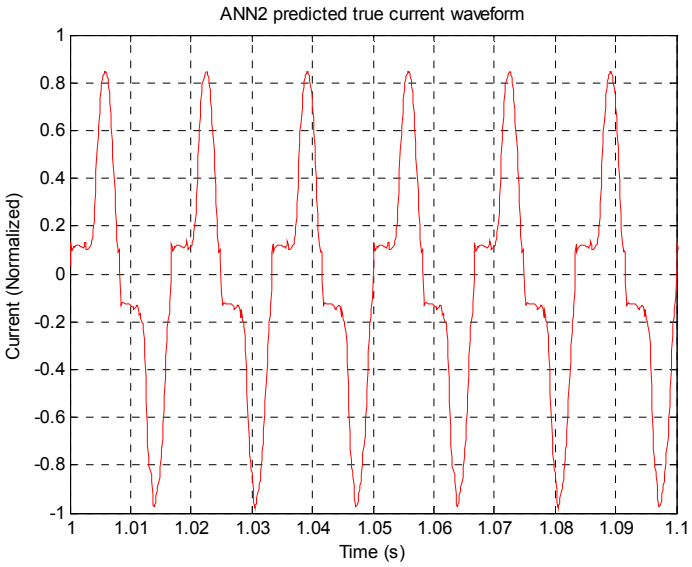

Figure 4.11 True current waveform ($\hat{i}_{2-dist}$) of the dc drive as predicted by ANN2

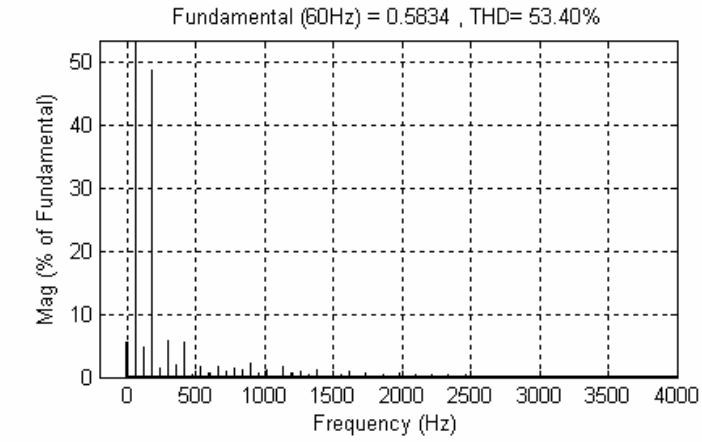

Figure 4.12 FFT spectrum of the true $\hat{i}_{2-dist}$ indicates a THD of 53.40%

4.3.2 Summary of results for single phase loads

As shown in the above experiments, the current distortion levels are different when the loads are served by a clean supply compared to a distorted supply. For the purpose of quantification, a new parameter e_m indicating the change in the THD's, is introduced and is defined as:

$$e_m = (\frac{THD_d - THD_s}{THD_d})\% \tag{4.1}$$

where THD_d is i_{THD} when supplied from a distorted v_{pcc} and THD_s is i_{THD} when supplied from a mathematical sine wave.

The new parameter e_m can be used as an indicator of the error in the measurement if the calculation of THD is done by simply measuring the input current of the nonlinear load. The salient results of all the experiments performed are summarized in Table 4.3.

Table 4.3: Summary of Results for Single Phase Test Circuits

Load	THD_d	THD_s	e_m
TRIAC circuit - 30° firing	27 %	30.58 %	- 13.26 %
DC drive – 90% speed ref	61.53 %	53.40 %	13.21 %
AC Drive	88 %	84.70 %	3.75 %
Diode bridge with lamp load	4.38 %	0.45 %	89.7 %

Table 4.3 shows that e_m can be positive and negative. This important finding shows that it is erroneous to think intuitively that the current THD, when supplied from a distorted v_{pcc} should always be higher than if the v_{pcc} were to have no distortion and vice versa.

4.3.3 Neural Network and Other Experimental Details

For the experiments with the single phase loads, the Elman recurrent neural network architecture (Figure 3.7) is used for ANN1 and for ANN2. Some of the other details are as follows:

- FFT computation : *powergui* block of SIMULINK
- Number of Neurons in the hidden layer: 20
- Time delayed inputs : 2
- Learning gain: 0.05. Momentum gain not used
- National Instruments data acquisition system
- Voltage sensor: LEM LV 25-P
- Current sensor: LEM LAH 25-NP
- Acquired voltage and current waveforms scaled by the peak value of the respective waveforms.
- Sampling frequency for data acquisition: 8000 kHz (~ 128 samples/cycle)

4.3.4 Experiments performed with three phase loads

This proposed LMI method is also applicable to three phase systems. The supply configuration at the PCC for a three phase load is normally:

- Wye connected, neutral grounded or neutral ungrounded
- Delta connected

Harmonics in a three phase system are normally determined on a per phase basis. Hence the proposed scheme has to be applied to each of the three phases individually. A modified method is presented in chapter 5 (Figure 5.7) where a single identification

neural network and a single estimation neural is used for all three phases. For the present experiment, the input to each of the three sets of neural network (one set per phase) is the phase to neural voltage. The neural network tracks the line current or the phase current.

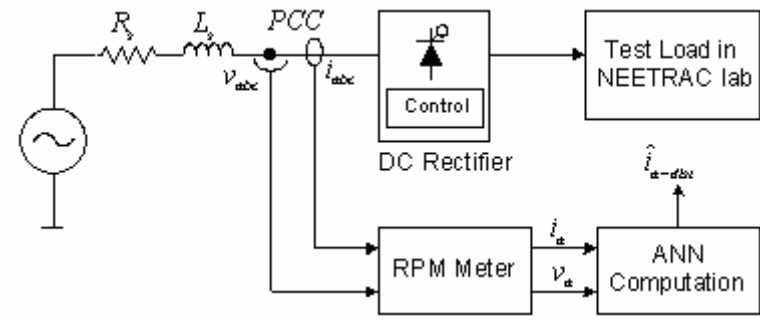

Figure 4.13 Three phase load for implementation and validation of LMI method

The LMI method is applied to the phase A data of a test setup at the National Electric Energy Testing Research and Applications Center (NEETRAC), which is a part of the Georgia Institute of Technology. The system is shown in Figure 4.13 and comprises a utility feeding a RXPO series 30 DC rectifier. The rectifier output load varies between 0 and 3000 A DC. This particular system is chosen since it operates at higher currents, voltages and power than the laboratory circuits tested so far. Nevertheless, it is still a balanced load. Unbalanced loads are tested and reported in chapter 5. The actual phase A to neutral voltage and current THD values are shown in Table 4.4. The waveforms are acquired using a Reliance Power Meter (RPM) and the THD values are recorded from the same meter.

Table 4.4: Load Profile of RXPO Series 30 Rectifier

DC Load (Amps)	Measured v_a THD (%)	Measured i_a THD (%)
3000A	3.71%	31.91%
2500A	3.80%	38.54%

Table 4.4 Continued

2000A	3.39%	46.44%
1500A	2.95%	57.48%
1000A	2.57%	71.36%
500A	1.94%	85.22%

For the case with 2000 A DC loading, the input voltage THD at the PCC is 3.39% and the current THD is 46.44%. This is chosen as the test case and the data acquired is used to train the neural network ANN1. Four cycle snapshots of data is acquired. The training continues until the training error converges to near zero (thirty cycles), and the ANN tracks the actual current i_a. Figure 4.14 indicates how well the training of ANN1 has converged since its output $\hat{i}_a$ coincides with the actual i_a waveform.

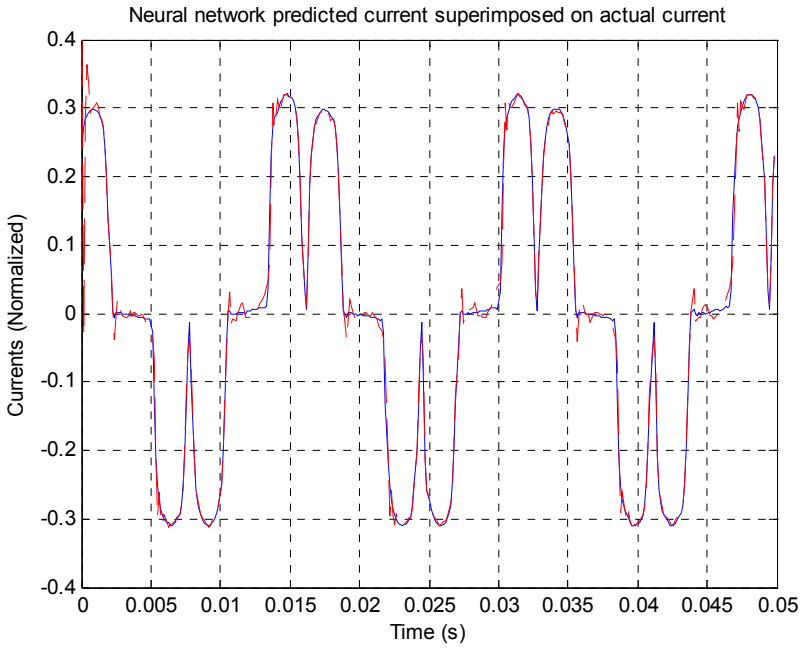

Figure 4.14 ANN1 output $\hat{i}_a$ superimposed on actual current i_a

Figure 4.15 indicates the MSE to be 0.0029. As before, the weights of the trained ANN1 are transferred to ANN2 and ANN2 is supplied with a phase A to neural voltage from a balanced three phase sine wave voltage source. The ANN2 predicted true current $\hat{i}_{a-dist}$ is plotted in Figure 4.16.

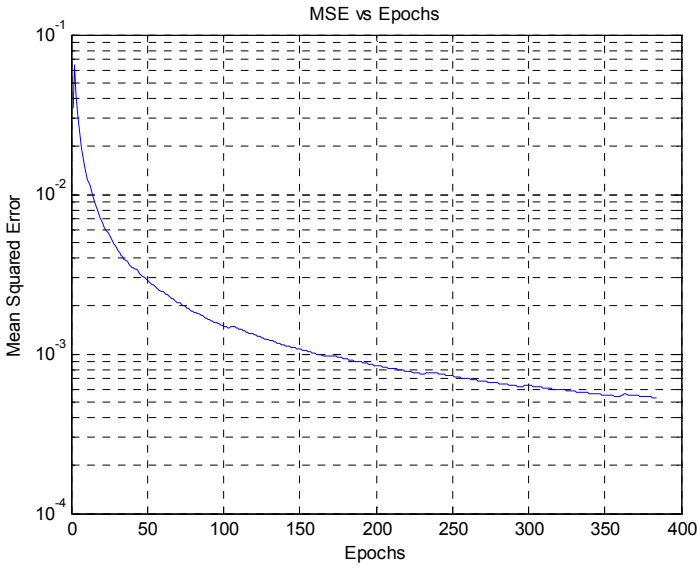

Figure 4.15 Training performance of ANN1 to track i_a in terms of MSE

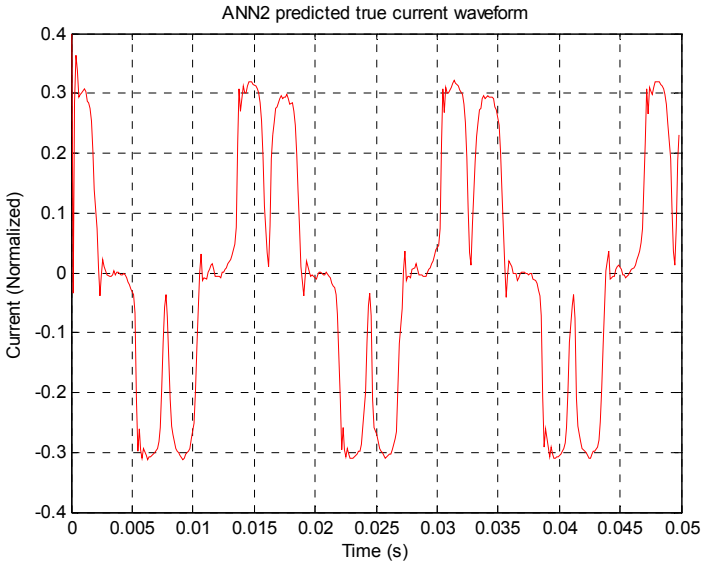

Figure 4.16 True phase A current waveform ($\hat{i}_{a-dist}$) as predicted by ANN2

Figure 4.17 shows the FFT spectrum of the waveform in Figure 4.16. The true current THD of $\hat{i}_{a-dist}$ is **50.63%** (instead of the **46.44%** in Table 4.4).

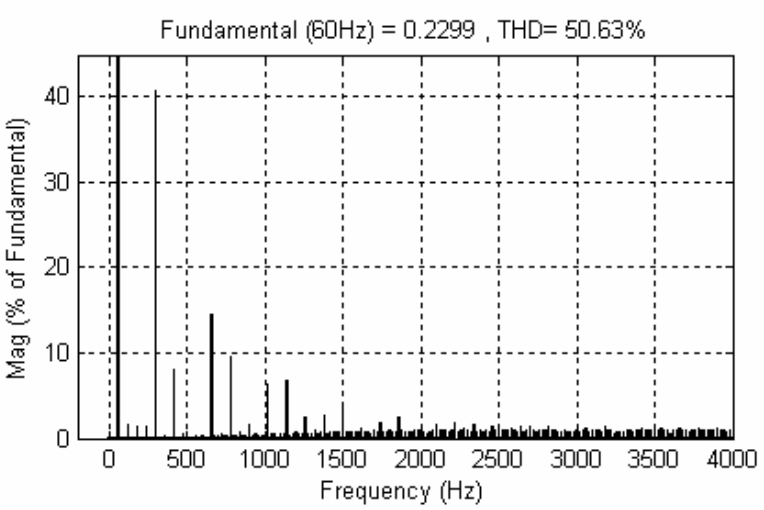

Figure 4.17 FFT spectrum of $\hat{i}_{a-dist}$ indicates a THD of 50.63%

This result indicates that current distortion of six pulse converters may increase when the applied voltage is a pure sinusoid and a low source impedance, i.e. stiff power system. The parameter e_m for this experiment is 8.28%.

4.4 Introduction to PCC Voltage Prediction

Any nonlinear load distorts the voltage at the PCC which in turn affects other loads connected to the same PCC. When several nonlinear loads are connected to the PCC, it is difficult to predict mathematically how each nonlinear load is affecting the voltage distortion level at the PCC. Typically, customers with nonlinear loads apply harmonic filtering techniques to clean up their current and avoid penalties from the utility. When corrective action is taken by the customer, one important parameter of interest is the change in the voltage distortion level at the PCC due to the corrective

action of the customer. A second new method, also based on neural networks, is proposed to predict the change in the distortion level of the voltage at the PCC if the customer were to draw only fundamental current and filter out its harmonics. The proposed method is called source modeling since method looks back to the source side from the load side and predicts the voltage distortion change at the PCC. The proposed source modeling method is a dual of the load modeling method presented earlier in this chapter. The source modeling method would indicate what would happen to the THD of v_{pcc} if the load added front end filters to remove it's harmonics.

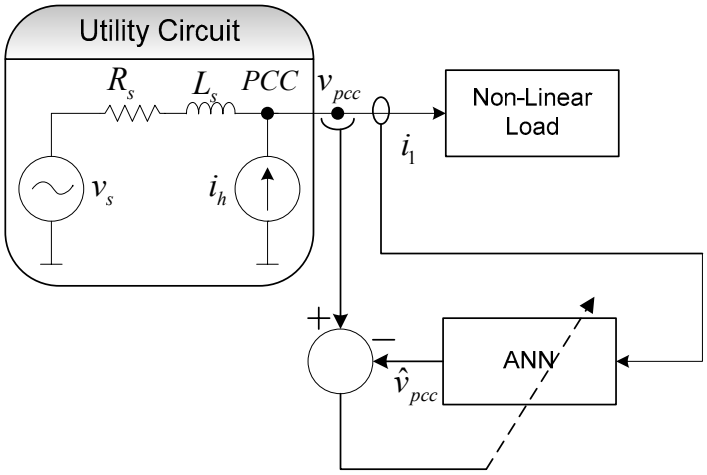

Figure 4.18 Utility equivalent circuit for source model identifier

As an example, Figure 4.18 shows a typical power distribution network consisting of a three-phase supply network having a sinusoidal voltage source v_s, network impedance L_s, R_s, a known nonlinear load and several other loads (which could be linear or nonlinear) represented by i_h. Looking back into the utility side from the nonlinear load, the equivalent circuit now consists of all the other loads (i_h) and the actual source voltage as indicated in Figure 4.18. The schematic proposed for the implementation of

source modeling method is shown as a single line diagram in Figure 4.19, although it could be used on single as well as three phase systems.

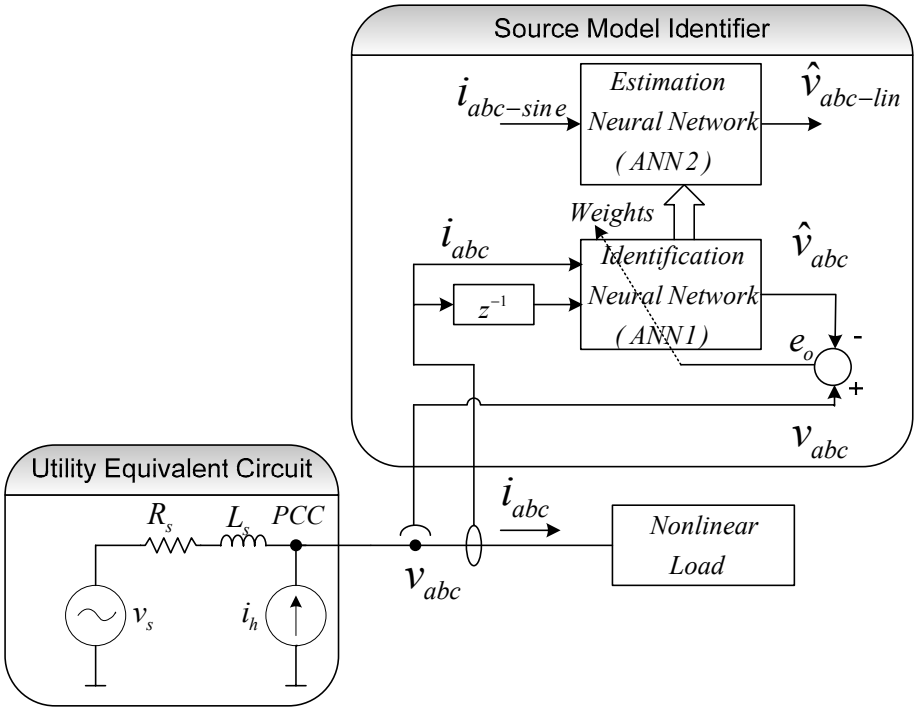

Figure 4.19 Implementation of the source model identifier method

The nonlinear load injects distorted line current i_{abc} into the network. The voltage at the PCC with all loads operating is v_{abc}. The input current i_{abc} is used as the input to the identification neural network (ANN1). ANN1 is trained to **identify** the voltage characteristics at the PCC. At any moment in time after the ANN1 training has been completed, its weights are transferred to the **estimation** neural network (ANN2). If the nonlinear load were to draw a sinusoidal current, then the distortion level of the voltage at the PCC would change due to the absence of harmonics in the nonlinear load's current. This information is obtained when ANN2 is supplied with a mathematically generated sine wave offline to estimate its output $\hat{v}_{abc-lin}$. This output of ANN2 gives the same

information that could have been obtained if in reality the nonlinear load were replaced by a similar sized linear load or it is equipped with front end filters. The difference in the voltage distortion level at the PCC can now be attributed to the nonlinear load harmonics.

4.4.1 Simulation Setup for Source Modeling

To demonstrate the source modeling method, a simulation circuit with two nonlinear loads connected in parallel to a source through inductance L_s is setup in Simulink. The point of parallel connection is designated as the PCC. The loads are a thyristor controlled converter operated by breaker B1 and a diode bridge rectifier operated by breaker B2 as shown in Figure 4.20. The loads are balanced, so currents all three phases are similar. The measurements shown in this section are for the phase A.

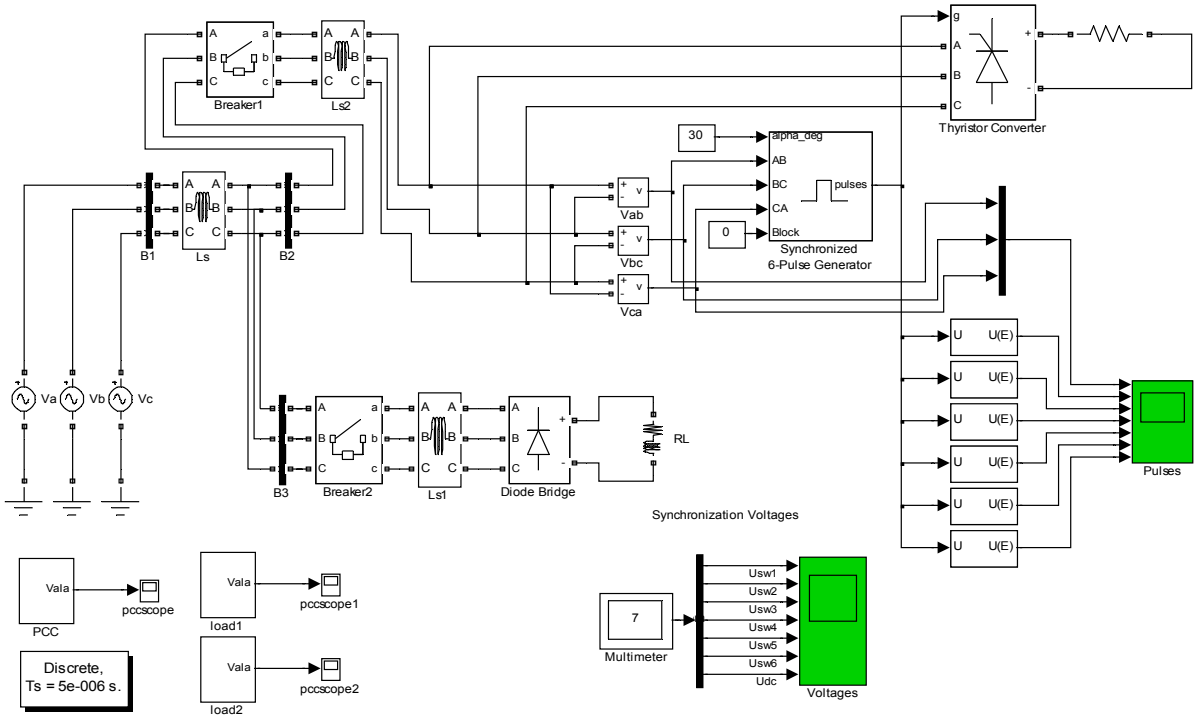

Figure 4.20 Simulation circuit for validation of SMI method

With breakers B1 and B2 ON, the voltage at the PCC is shown in Figure 4.21.The THD of the voltage at the PCC is 7.95%. This exceeds the limit set by IEEE 519 standard. However at this point it cannot be ascertained if this is a violation of the IEEE 519 standard, since the standard states that the voltage distortion should be less than 5% if the load current distortion is within the prescribed limits. With both the breakers on, it is not possible to say, which of the two loads is affecting the voltage more severely.

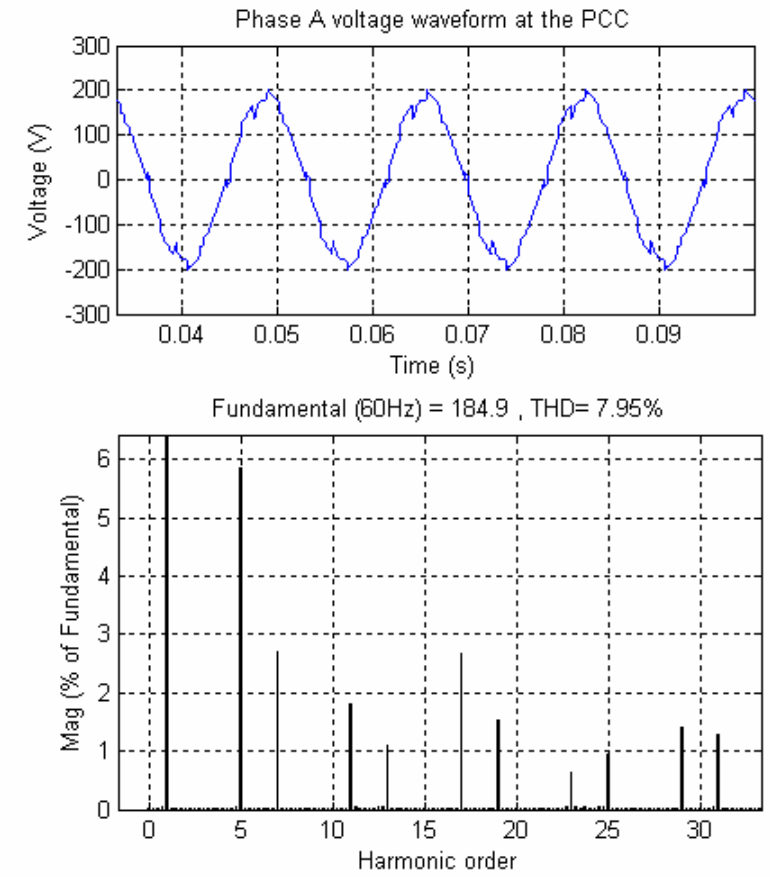

Figure 4.21 Voltage at the PCC with both breakers B1 and B2 ON

As a next step, the total current at the PCC is plotted in Figure 4.22. The current has a THD of 10.08% and the harmonics in this current includes the contributions from both the loads.

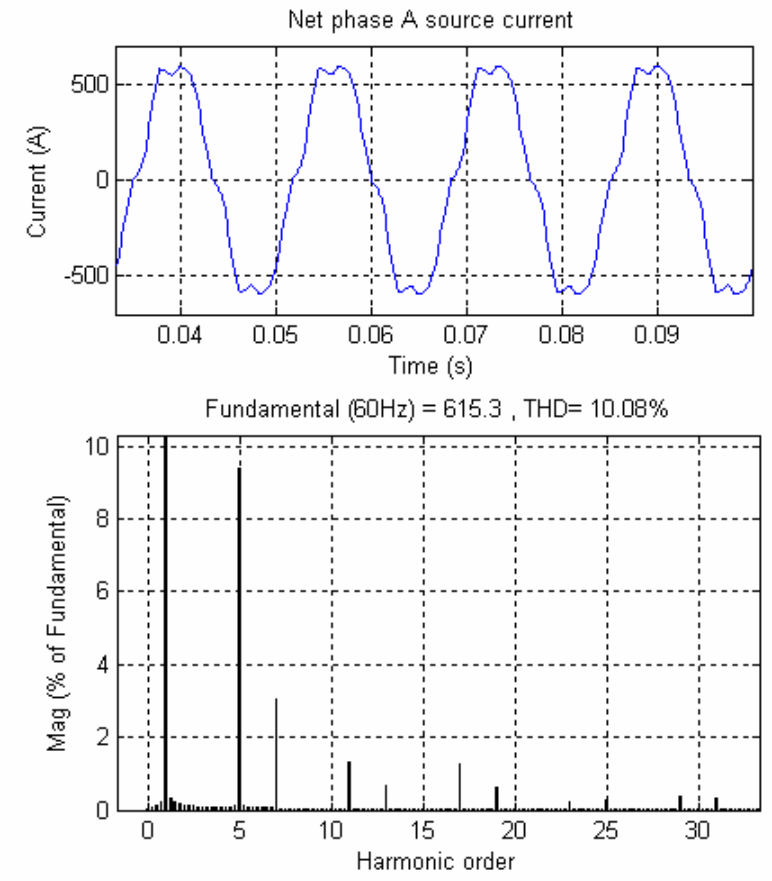

Figure 4.22 Net source current at the PCC with both breakers B1 and B2 ON

The individual current profiles of the thyristor converter and the diode bridge are shown in Figure 4.23 and Figure 4.24 respectively. Even though the current THD of the thyristor converter is 30.29%, the THD of the net current at the PCC is only 10.08%. This indicates the possibility that some amount of harmonic cancellation may have taken place, which results in a current with lower distortion at the PCC.

This is the primary reason why utilities do not see a high distortion in the total current at the PCC, while individual loads connected to the PCC have high current distortions. Hence it is extremely important to be able to predict the actual amount of voltage distortion caused by the harmonics of a particular nonlinear load.

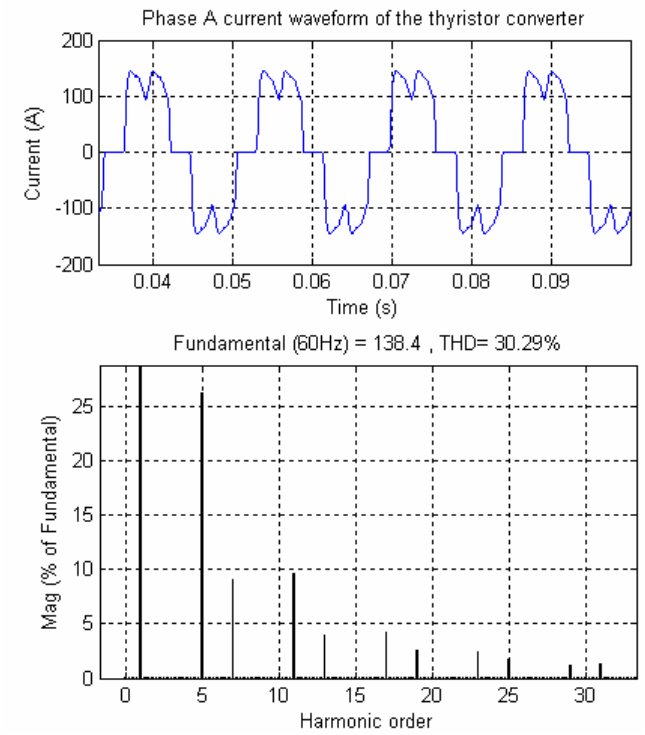

Figure 4.23 Thyristor circuit current with both breakers B1 and B2 ON

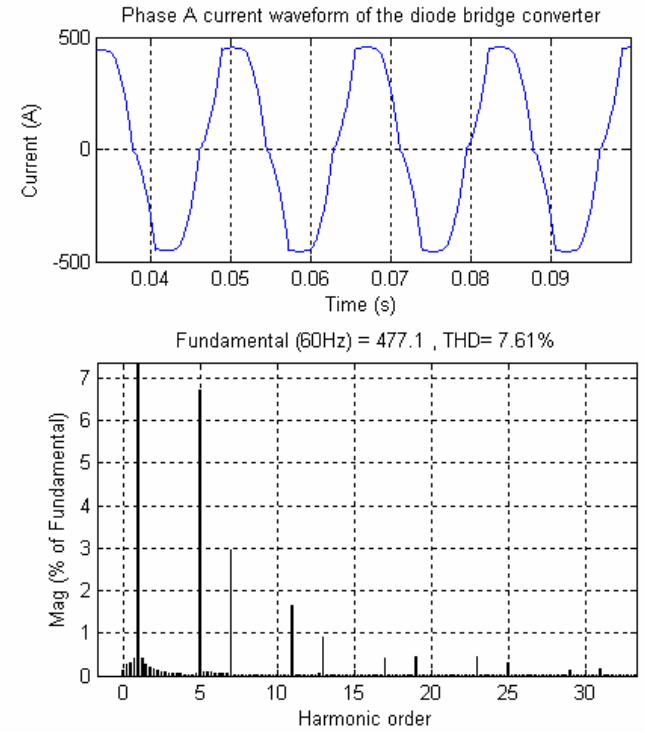

Figure 4.24 Diode circuit current with both breakers B1 and B2 ON

With breaker B1 open, the thyristor converter is isolated from the network. The voltage and current (only that of the diode circuit) at the PCC are recorded again and are shown in Figure 4.25 and Figure 4.26.

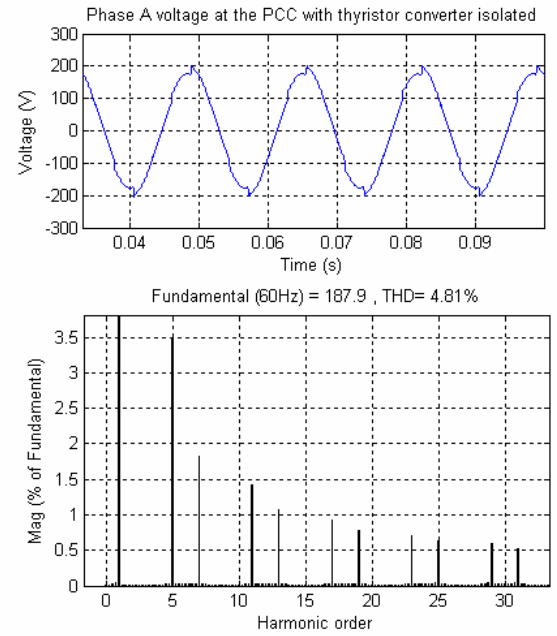

Figure 4.25 Voltage at the PCC with breaker B1 OFF

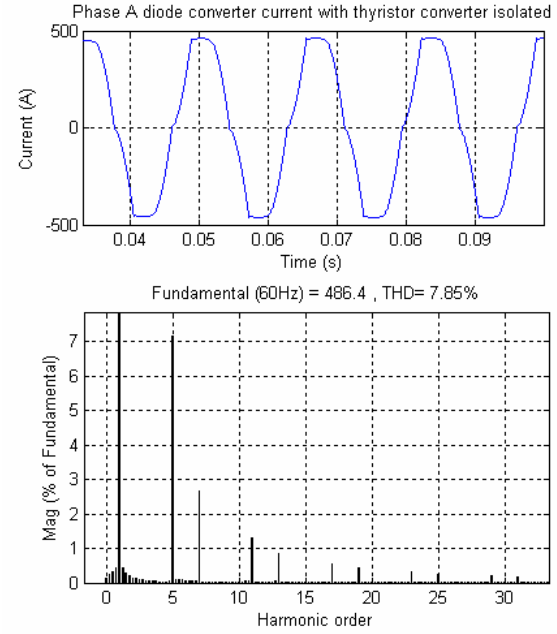

Figure 4.26 Diode load current at the PCC with breaker B1 OFF

The voltage THD at the PCC is now 4.81% which is within the limits of IEEE 519. Hence in this case, the thyristor load is distorting the voltage at the PCC. When the thyristor load is replaced by a similar sized current source with only fundamental current and no harmonics, the voltage THD at the PCC changed to 4.87% (Figure 4.27), which is still within the IEEE 519 limits.

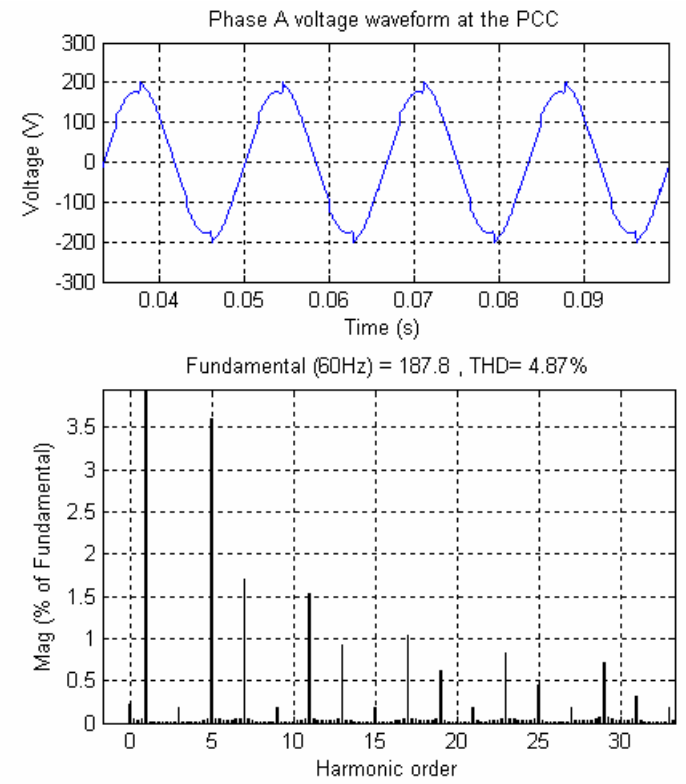

Figure 4.27 PCC voltage with the thyristor circuit replaced by a current source with no distortion

4.4.2 Neural Network Training and Prediction

In a real-life situation, loads with only fundamental current and no harmonics are impractical and probably do not exist. For determining the impact of a specific load on the voltage distortion, the only means the utility has is to disconnect the load and measure

the voltage THD at the PCC. This is not a desirable action. This is where the merit of the proposed method SMI method lies in that the effect of the nonlinear load harmonics can be evaluated on the voltage distortion without interrupting the load.

To validate the SMI method, the thyristor converter from the test circuit described in Figure 4.20 is treated as the nonlinear load of interest. The phase A input current i_a of the thyristor converter is used to train the neural network ANN1 until the the output of ANN1 correctly tracks the voltage at the PCC v_a.

The voltage waveform predicted by ANN1 ($\hat{v}_a$) is plotted along with the actual voltage at the PCC v_a. Figure 4.28 indicates how well the training of ANN1 has converged since its output coincides with the actual voltage waveform at the PCC.

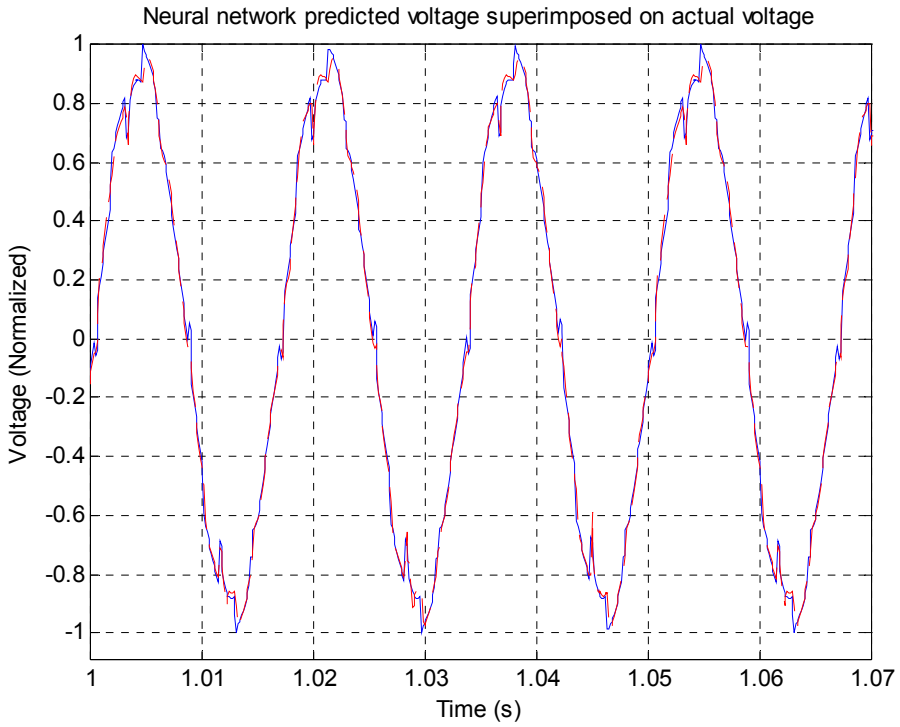

Figure 4.28 ANN1 output $\hat{v}_a$ superimposed on actual current v_a to indicate convergence

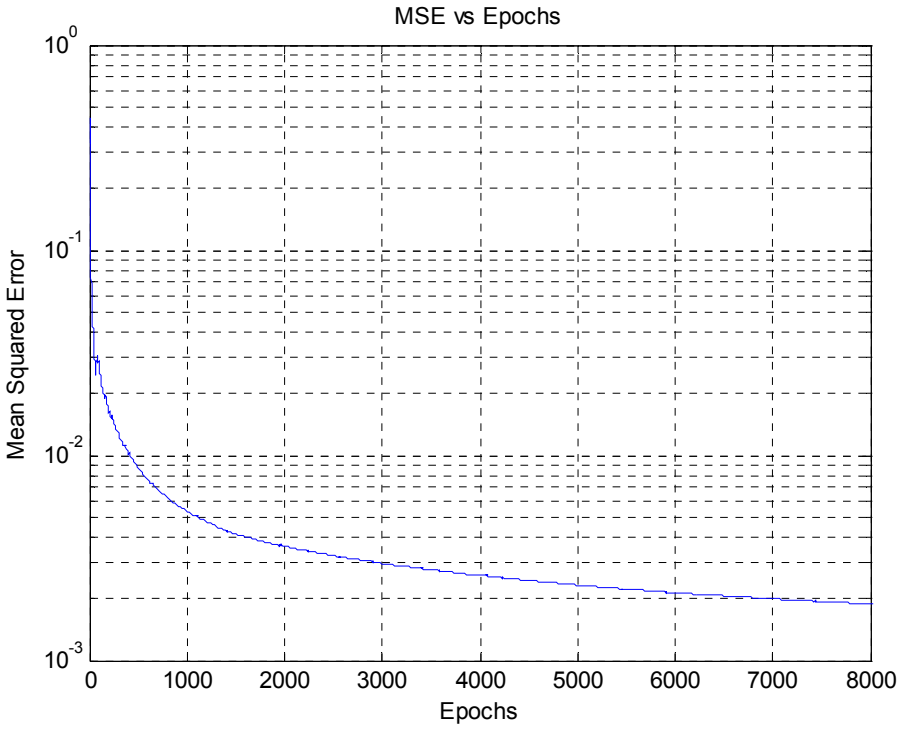

Figure 4.29 Training performance of ANN1 to track v_a in terms of MSE

The MSE in Figure 4.29 is 0.0019. The weights of ANN1 are now transferred to ANN2. The output of ANN2 ($\hat{v}_{a-lin}$) is obtained by using a mathematically generated sine wave current with zero distortion. The output of ANN2 thus predicts the voltage at the PCC if it were possible to disconnect the nonlinear load and replace it by a similar sized linear load which also has front end filters so that its current is purely sinusoidal. Any change in the THD of voltage at the PCC can now be attributed to the thyristor converter.

Figure 4.30 show the output of ANN2 and the frequency spectrum. The voltage THD at the PCC turns out to be **5.41%** instead of the **7.95%** as measured in Figure 4.21. This result agrees well, though not entirely accurate, with the measured value of 4.87%

which was obtained from simulation by replacing the nonlinear load with a similar sized current source. A comparison of the individual harmonics between the normalized waveform of Figure 4.27 and the output of ANN2 in Figure 4.30 is shown in Table 4.5.

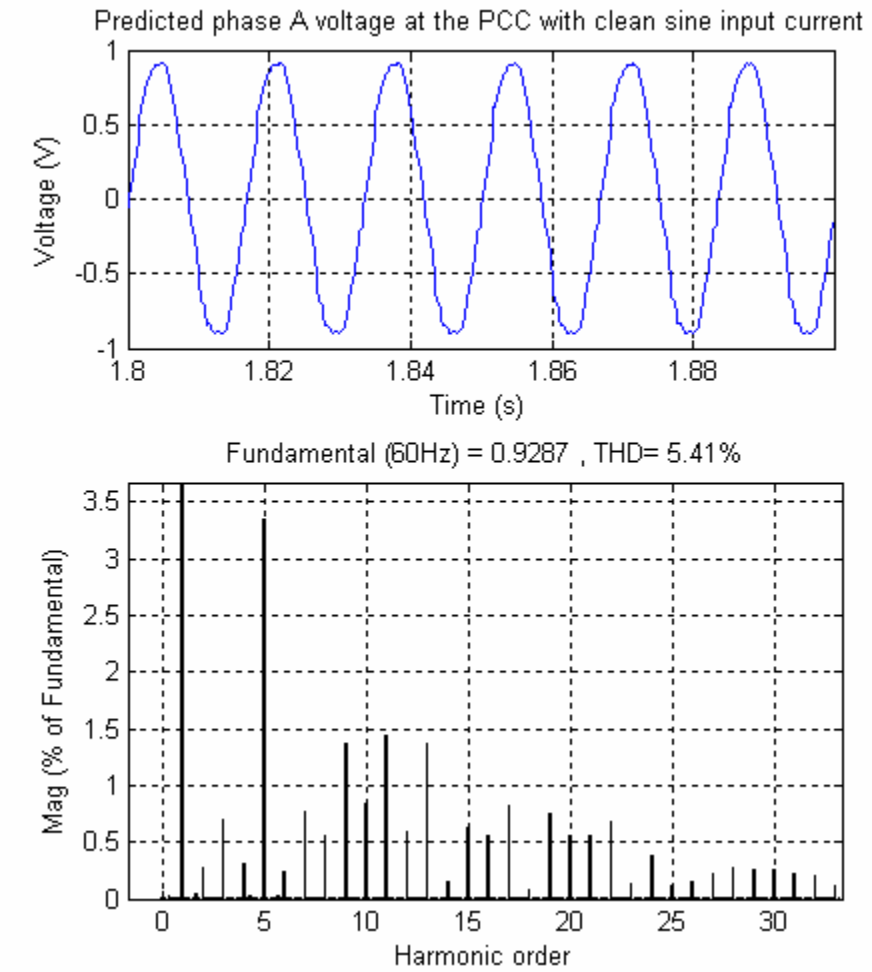

Figure 4.30 True phase A voltage waveform ($\hat{v}_{a-lin}$) as predicted by ANN2

Table 4.5: Comparison of Measured and Predicted Voltage Harmonics

Harmonic	Simulation	ANN2	Error
DC	6.33E-04	5.25E-04	-1.08E-04
1	0.9253	0.9284	3.10E-03

Table 4.5 Continued

5	0.0312	0.0211	-1.01E-02
7	0.0142	0.0162	2.00E-03
11	0.0128	0.0108	-2.00E-03
13	0.0076	0.0064	-1.20E-03
THD	4.87%	5.41%	

In principle, the SMI method is a dual of the LMI method. However both the methods do need independent training and the weights of the SMI network cannot be derived from the weights of the LMI network.

4.5 Computation of FFT Using Simulink

Computation of the FFT of the waveforms is carried out frequently. Using the *powergui* block of SIMULINK, the FFT is calculated as shown in Figure 4.31.

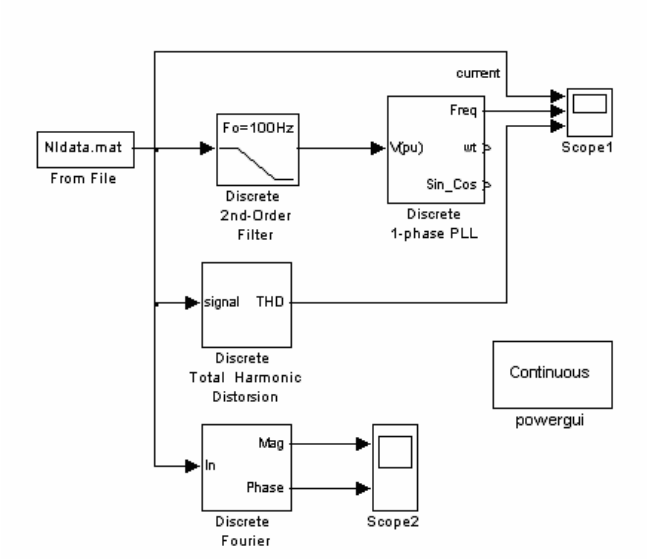

Figure 4.31 FFT computation block using Simulink

This section describes the computation technique using measured data from the circuits. The data acquisition is carried out using LABVIEW. Once the data is acquired, it is imported to the MATLAB workspace.

The THD is measured by a dedicated spectrum analyzer as well as by data acquisition and MATLAB software. Data acquisition is carried out with a system from National Instruments and LABVIEW software which stores the data on a personal computer. This file of data is then imported to the SIMULINK model shown above. In order to find the THD, the correct fundamental frequency has to be determined because THD is an evaluation of harmonic distortion at multiples of the fundamental frequency.

In the SIMULINK model, the data from the file is sent to a phase locked loop (PLL) and filtered by a 2^{nd} order low pass filter which reduces the distortion in the signal. The cut off frequency of the low pass filter is set at 100 Hz. The minimum frequency of the PLL block is set at 45 Hz.

The schematic of Figure 4.31 helps in determining whether the fundamental frequency varies over the measured time period or is fixed. Once the correct fundamental frequency is determined, the *powergui* block of SIMULINK is used to compute the THD of the signal. This THD is then compared with data recorded directly by a spectrum analyzer (when hardware measurements are taken), in order to verify that the LABVIEW and MATLAB computer codes are working correctly. The sampling frequency for data acquisition is 8 kHz which ensures that (theoretically) harmonics up to 4 kHz can be measured. Harmonics above that frequency range are normally in the field removed by harmonic filters.

4.5.1 Training and estimation of ANN1 and ANN2

This section describes the procedure of acquiring data and carrying out the neural network computation for the experiments presented in section 4.3. Data acquisition is carried out by a National Instruments SCXI system and LABVIEW software. The scheme for data acquisition is shown in Figure 4.32.

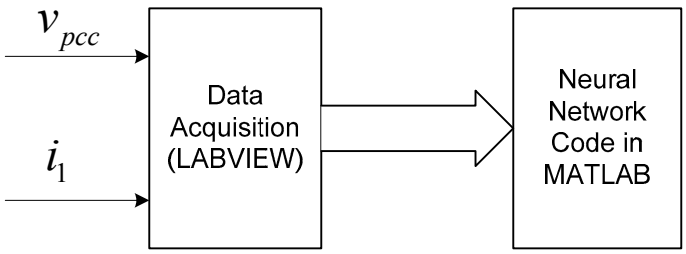

Figure 4.32 Labview Code for Data Acquisition

The data is acquired for two seconds (120 cycles), every one minute with a sampling frequency of 8000 Hz. The code can run as long as the load is running or it can be stopped after a certain time interval. LABVIEW stores data as text files. These text files are then converted to Microsoft excel files and imported to the MATLAB workspace.

The acquired data is used to train the neural network, this contains all the dynamics present in the power system, and hence during training the neural network does not see any particular pattern and is able to incorporate whatever changes are taking place in the load current during the measurement time span. The acquired data for two seconds consists of 16000 sampling points, hence there are 16000 epochs. The computation time for the 16000 epochs on a 3.2 GHz computer is approximately 3.8 seconds.

ANN1 starts with random weights and as the acquired data is presented to the neural network, the weights converge towards the desired weights which represent the load admittance. Once the ANN1 training has converged and the weights transferred to ANN2, five cycles of mathematically generated sine wave are sufficient for the estimation phase of ANN2 to get an accurate THD number.

4.6 Summary

In this chapter, it has been experimentally validated that the proposed load modeling method can indeed learn the dynamics of a nonlinear load and then estimate the true current distortion of the nonlinear load when supplied from a sinusoidal source, without physically disrupting the operation of the load.

The presented experimental results have shown that there is a difference in the current distortion of a load depending on whether the load is served by a clean supply or a distorted supply. To quantify this difference, the index e_m has been introduced. The values of e_m illustrate that this error could be positive as well as negative. Single-phase power electronic loads generate a great amount of triplen harmonics, and triplen harmonics are zero sequence. Three phase power-electronic loads on the other hand, do not generate triplen harmonics. Nontriplen harmonics generated by various single and three-phase loads are likely to have diversity effects due to phase cancellations and attenuation effects that cause the distortion variation in the PCC voltage. This explains why the index e_m is either positive or negative. One important finding from the above results show that it is erroneous to reason intuitively that the current THD, when supplied from a distorted v_{pcc} should always be higher than if the v_{pcc} had no distortion.

In this chapter, the concept of source modeling is also introduced. With the aid of simulation data from three phase circuits, it has been verified in principle that the proposed method can indeed learn the impedance of the nonlinear load and predict the change in the voltage distortion levels at the PCC. This is an extremely important parameter which would clearly indicate whether or not a nonlinear load is responsible for the violation of the IEEE 519 voltage limits at the PCC. The results have shown that requiring a load to add harmonic filters might in fact increase the THD in v_{pcc}.

Both the proposed methods have been applied to single and three phase loads. Chapter 5 presents the results of load modeling and source modeling with actual field data acquired at a site in Georgia.

CHAPTER 5

SITE RESULTS

5.1 Introduction

Harmonics-related problems on electric utility distribution systems are often created by large, primary metered, industrial customers. Typically, these problems are due to large variable speed drives and other switching type of power electronic loads. The significant harmonics are usually 5^{th}, 7^{th}, 11^{th} and 13^{th} with the 5^{th} harmonic being the largest in most instances. Classic utility-side symptoms of harmonic problems are distorted voltage waveforms, blown shunt capacitor fuses, and transformer overheating. Shunt capacitor losses are also sensitive to harmonic voltages, while transformer losses are sensitive to harmonic currents.

Electric loads may be broadly categorized as either linear or nonlinear. A typical power distribution network contains linear as well as nonlinear loads, in most cases, all connected in parallel on the high voltage side of customer's service transformer. Most of the times, the point at which the high voltage side of a customer transformer is connected to the distribution network, is known as the point of common coupling (PCC).

The schemes of load modeling and source modeling introduced in chapter 4 are now applied to site measurements at the substation of large customers. Figure 5.1 show a single line diagram of the test site and the points where the measurements of voltage and current are recorded.

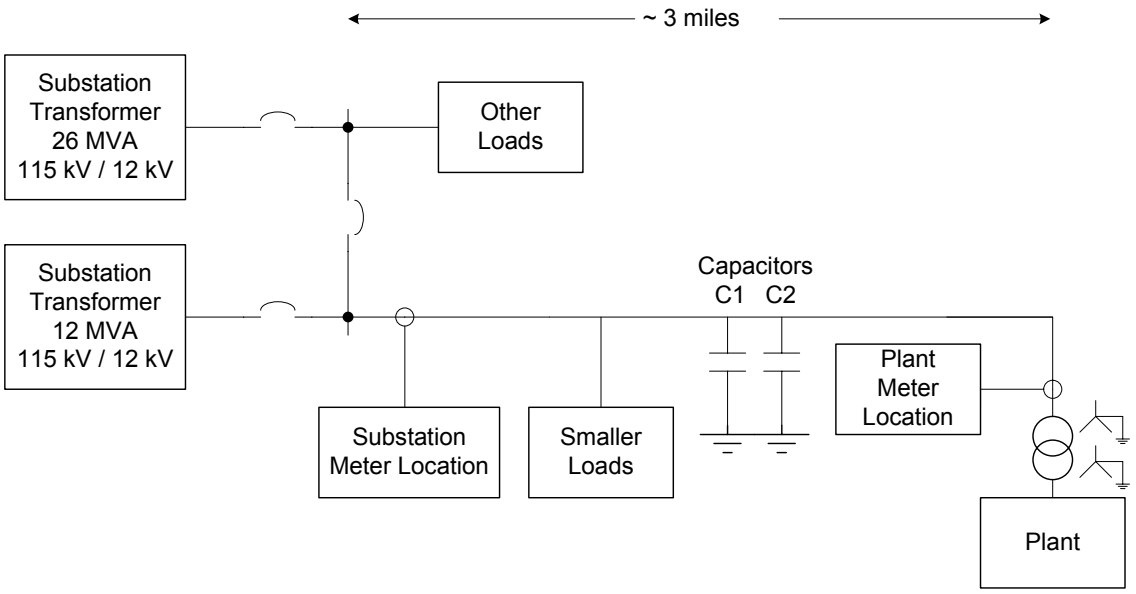

Figure 5.1 Single line diagram of test site

The power system configuration of the feeder circuit is 3 phase 4 wire wye system. Two sets of measurements are taken, one at the secondary side of the substation transformer and the other at the primary side of the customer's transformer. The meters are Metrosonics PA- 9 plus and their specifications appear in appendix C. The customer's load in Figure 5.1 is the largest load on that particular circuit with only a few other customers. The substation has two transformers of ratings 12 MVA and 26 MVA. At the time before any switching action is performed, the customer is supplied from the 12 MVA transformer and other loads in the city as well as load from another nearby substation is supplied from the 26 MVA transformer. The two capacitor banks outside the customer's primary meter are primarily used for voltage control and Var compensation and are initially online [121]. These capacitor banks are automatically controlled by voltage level. Waveforms of the three phase voltages (line-neutral) and the three line currents are acquired as 6 cycle snapshots, repeated at 1 minute intervals, for a period of

6 hours. Each 6 cycle snapshot measurement is designated as an event. There are 375 events recorded. Data is acquired at the rate of 256 samples per cycle [122], [123]. The data is downloaded from the meter to the PC and preprocessed to fall within the limits of ± 1. The scaling is done in software. The data is now suitable for training the neural network. The data acquisition process is illustrated in Figure 5.2.

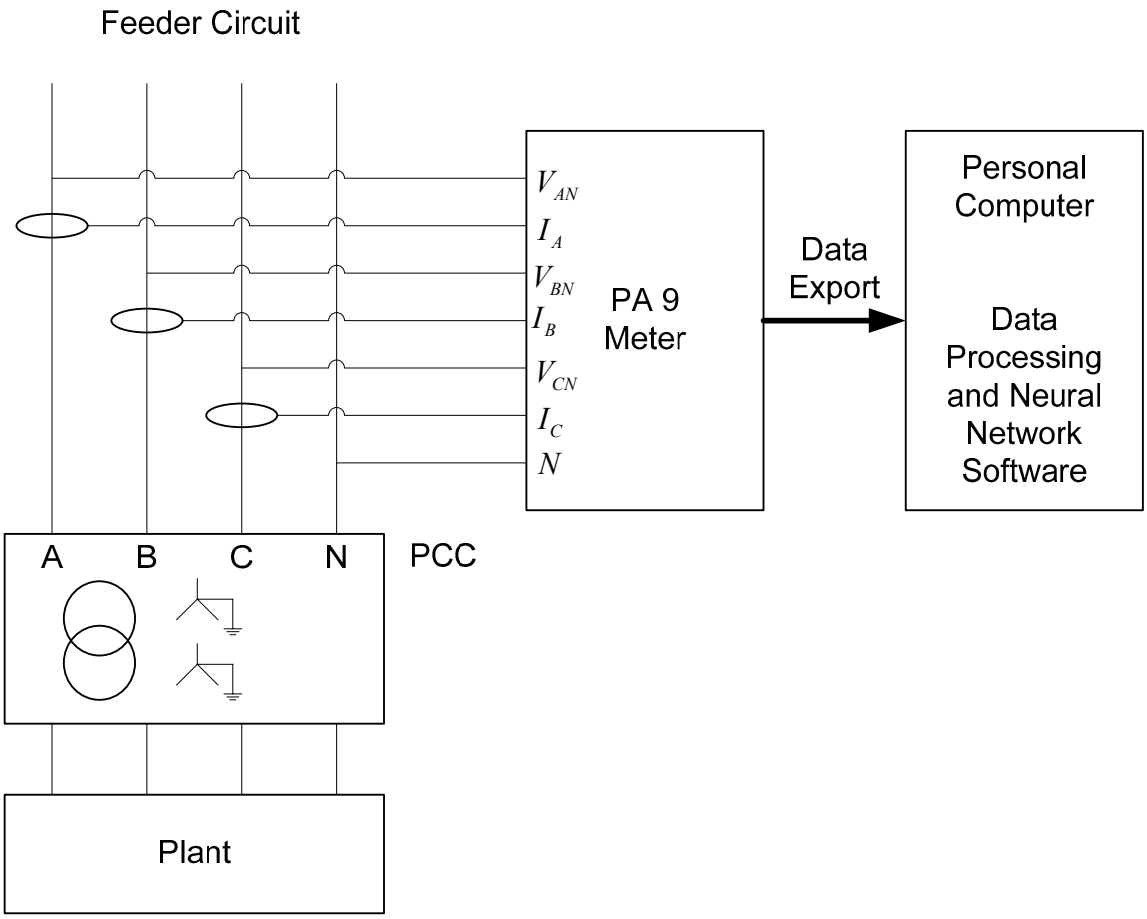

Figure 5.2 Data acquisition and export to a computer

The measurements of voltage and current are recorded for 7 specific conditions of the network, simultaneously at the plant as well as at the substation, as described below.

- The customer is supplied from the 12 MVA transformer and C1, C2 are online: Case 1.
- The 12 and the 26 MVA transformers are tied together and the customer is supplied from there. C1, C2 are online: Case 2.
- The customer is supplied from the 26 MVA transformer and C1, C2 are online: Case 3.
- The customer is supplied from the 26 MVA transformer. At this time, C1 is switched off while C2 is online: Case 4.
- The customer is still supplied from the 26 MVA transformer and both C1, C2 are offline: Case 5.
- The customer is supplied with the 12 and the 26 MVA transformers are tied together and C1, C2 offline: Case 6.
- The customer is supplied from the 12 MVA transformer and both C1, C2 are offline: Case 7.

The neural network load modeling scheme is demonstrated with the data acquired at the plant metering location.

5.2 Site Conditions

The RMS values of 3 voltages and 3 currents along with their frequency spectrums show the operating condition of the network. As an example, the RMS value of Phase A voltage measured at the customer's primary metering location is shown in Figure 5.3 and its total harmonic distortion (THD) over the entire measurement range

appears in Figure 5.4. The voltage remains fairly constant till event 298, after which there is a sudden dip of 200 V. This is the impact of removing the capacitor bank C1 from the network. The second capacitor bank C2 is taken offline during event 323 and the voltage dips by another 100 V. The paralleling of the substation transformers did not have any impact on the voltage magnitude as expected.

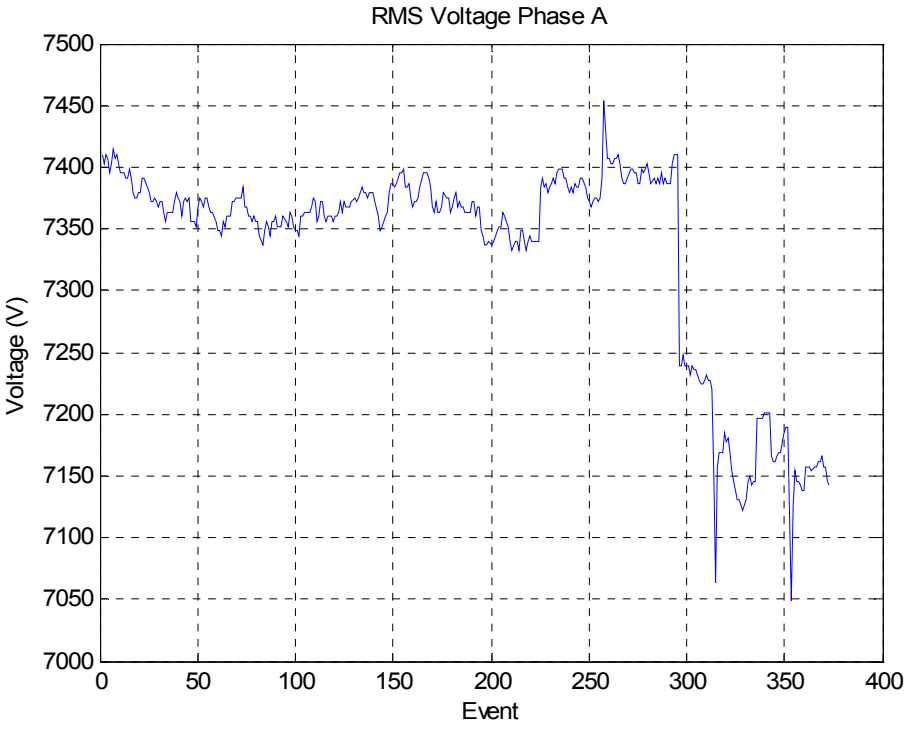

Figure 5.3 RMS value of phase A voltage using the PA 9 meter at the plant location

Inspection of Figure 5.4 reveals that the voltage THD varies from 7.5% to 2% over the entire measurement period. An interesting observation from Figure 5.4 is that during event 255, when the two transformers are tied together and both capacitor banks online, the voltage THD has a sharp decrease from 7.5 % to less than 3 %. When C1 is taken offline, the voltage THD drops below 2%. This indicates a possible resonance condition between the 12 MVA transformer and the capacitor banks.

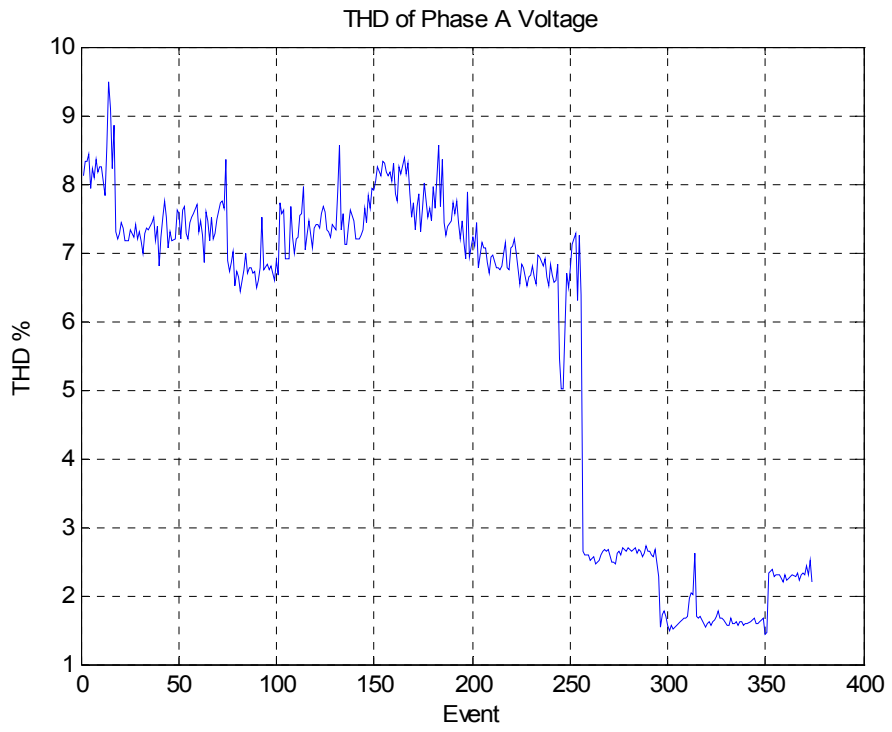

Figure 5.4 THD of phase A voltage using the PA 9 meter at the plant location

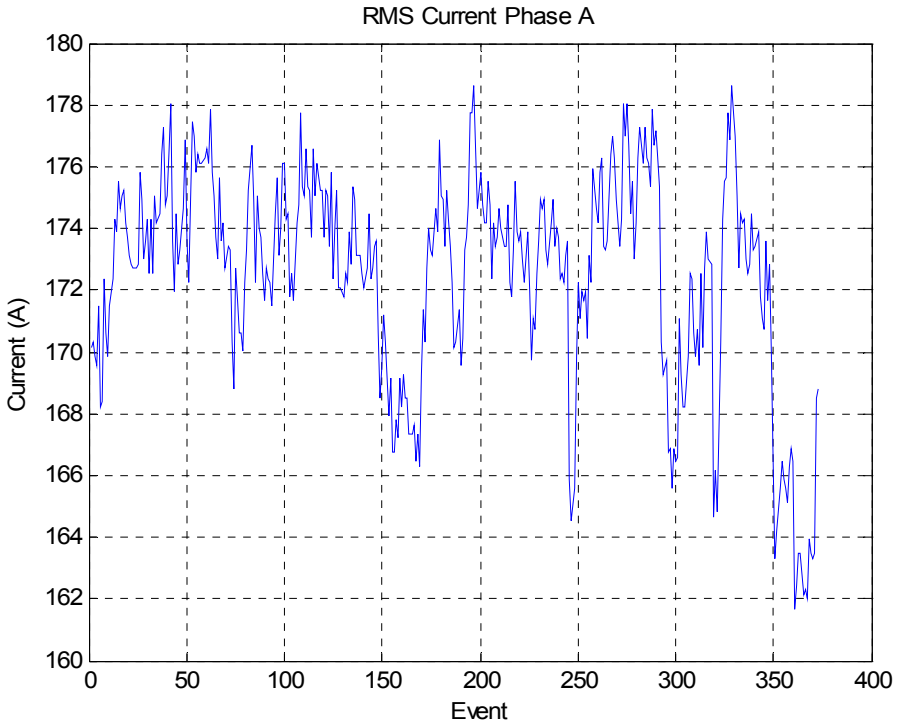

Figure 5.5 RMS value of phase A current using the PA 9 meter at the plant location

Figure 5.5 shows the phase A current over the entire measurement period. The current shows the characteristics of a typical industrial plant with the load going up and down depending on the starting or shutting of machines. The RMS value of current varied between 178 and 162 A. The current THD in Figure 5.7 decreases to a minimum value of 2% over the entire measurement period.

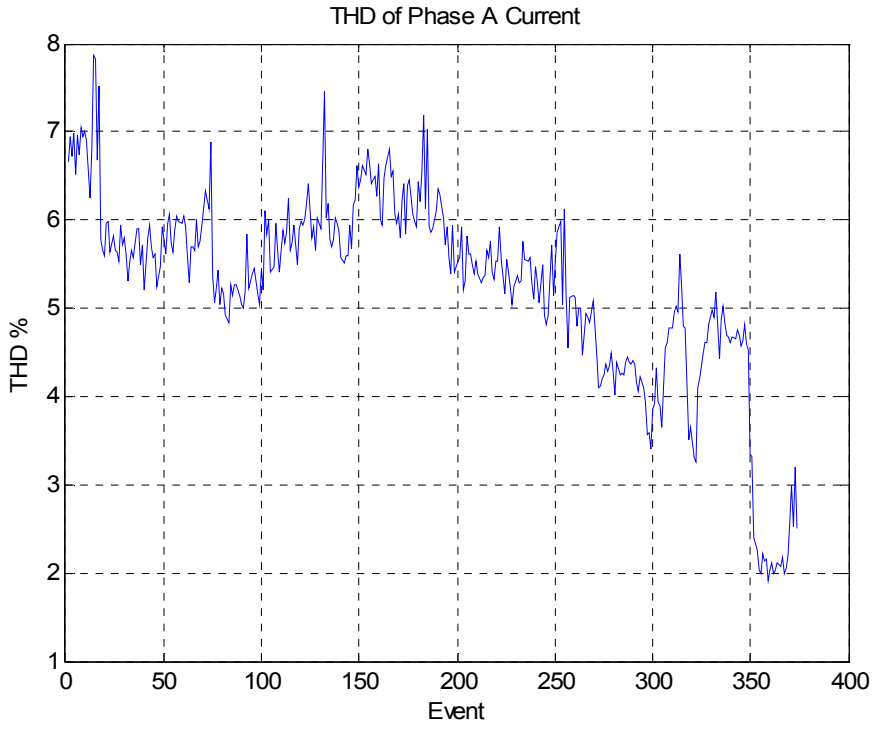

Figure 5.6 THD of phase A current using the PA 9 meter at the plant location

The phase B and phase C voltages and currents exhibit characteristics similar and comparable to those of phase A. However a detailed investigation of the three phase voltages and currents are required and this is presented in the section on experimental results. Hereafter, specific changes in the network operating condition will be referred in terms of the event number rather than time.

Table 5.1 shows the voltage and current measurements at the plant meter as well as the substation meter for a randomly chosen event for case 1, i.e. before any switching action was performed.

Table 5.1: Measurements recorded at the plant and the substation before any switchings

Plant Meter Measurements (Time 10:36:23)								
	Voltage				Current			
Phase	RMS (V)	THD	5^{th}	7^{th}	RMS (A)	THD	5^{th}	7^{th}
A	7343	6.6 %	6.39 % (468.5 V)	1.19 % (87.4 V)	178.12	4.83 %	3.83 % (6.8 A)	2.67 % (4.8 A)
B	7286	6.65 %	6.35 % (461.9 V)	1.27 % (92.6 V)	175.51	4.29 %	2.96 % (5.2 A)	2.76 % (4.8 A)
C	7266	7.58 %	7.34 % (531.5 V)	1.14 % (82.5 V)	166.22	4.72 %	3.74 % (6.2 A)	2.59 % (4.3 A)
Substation Meter Measurements (Time 10:36:11)								
	Voltage				Current			
Phase	RMS	THD	5^{th}	7^{th}	RMS	THD	5^{th}	7^{th}
A	7644	3.3 %	3.23 % (246.6 V)	0.43 % (32.9 V)	190.37	18.1 %	17.6 % (33.1 A)	2.38 % (4.5 A)
B	7644	2.96 %	2.87 % (220.1 V)	0.55 % (41.9 V)	181.86	16.6 %	16.1 % (29 A)	2.61 % (4.7 A)
C	7669	3.03 %	2.94 % (225.4 V)	0.44 % (33.6 V)	182.25	16.2 %	15.9 % (28.6 A)	2.71 % (4.9 A)

All the three phase voltages at the plant meter are exceeding the THD limits specified by IEEE 519. The current THD's are between 4% and 5% with the 5^{th} and the 7^{th} harmonic being the dominant harmonics. Ideally, the measurements of Table 5.1 can

be used to determine whether the customer is in compliance with IEEE519. However, experience as well as results in this research has proven that the current measurements at the customer's primary are not always reliable in that determination. If there is a significant amount of voltage distortion present, then the voltage distortion will affect the current distortion measurements. This may create a situation that makes it appear as if a particular customer is not in compliance with the harmonic current limits because of the already distorted utility system voltage. Under such circumstances, the load modeling tool can be trained to learn the customer's load admittance. Then, it is possible to predict the customers current harmonic current based on mathematically applying a pure sinusoidal voltage to the identified load admittance.

5.3 Implementation of the Load Modeling (LMI) Method

In chapter 4, the implementation of the proposed LMI scheme is presented with one identification neural network and one estimation neural network for each phase. The reason for that was the loads were single phase and even for the three phase loads, the data acquisition was possible on a per phase basis.

A modified implementation of the LMI scheme which requires only one identification network and one estimation network for all the three phases is presented in this chapter, as illustrated in Figure 5.7. Essentially, the modified neural network structure now has three phase voltages as inputs and three currents as outputs. However, each input also requires the present value of the voltage vector and two time delayed values of the voltage vector, as well as a bias. So the actual number of inputs to the neural network is ten.

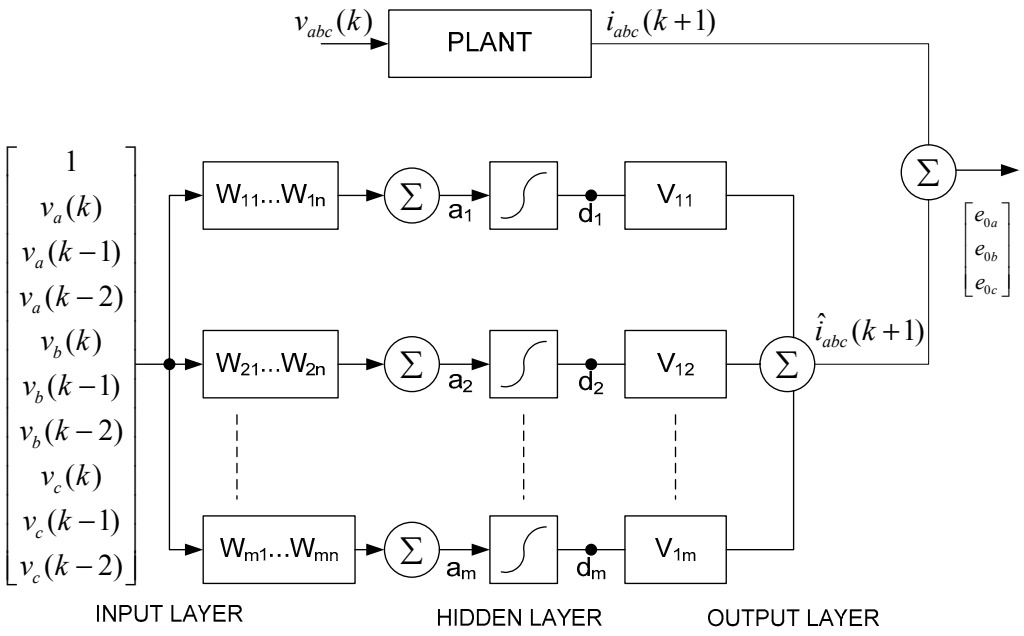

Figure 5.7 Modified LMI method using single ANN1 and ANN2 for all three phases

Figure 5.8 shows the schematic of the implementation of the scheme.ANN1 is trained with snapshots of data acquired before any switchings occurred. The training process begins with the identification neural network ANN1 predicting the line current as a function of present and delayed voltage vector values. Initially the weights have random values. At any moment in time after the ANN1 training has converged, its weights are transferred to the Estimation neural network ANN2, and a true sine wave voltage is computed in software. The undistorted voltage waveform is applied to the input of ANN2 instead of the actual measured distorted voltage at the primary metering location of the customer. The output of ANN2, called $\hat{i}_{abc-distorted}$, gives the same information that would have been obtained if in reality the customer was supplied from an undistorted voltage source.

The error vector $\begin{bmatrix} e_{0a} & e_{0b} & e_{0c} \end{bmatrix}^T$ in Figure 5.7 is a 3 element column vector and is calculated as;

$$\begin{bmatrix} e_{0a} & e_{0b} & e_{0c} \end{bmatrix}^T = i_{abc}(k+1) - \hat{i}_{abc}(k+1) \tag{5.1}$$

The error vector $\begin{bmatrix} e_{0a} & e_{0b} & e_{0c} \end{bmatrix}^T$ is backpropagated through the network to update the network weights W and V, details of which are provided in Appendix E.

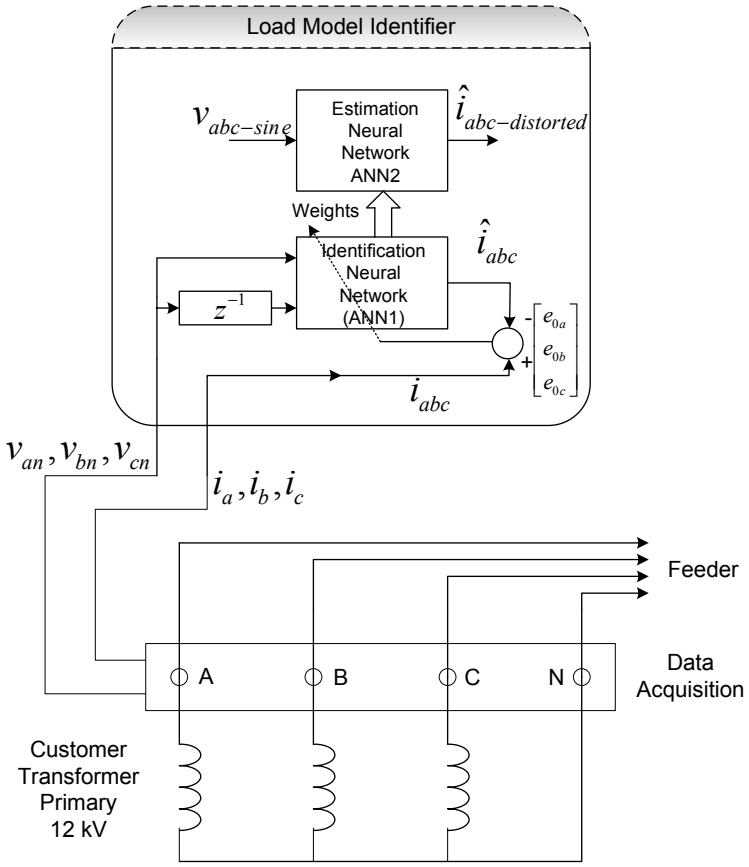

Figure 5.8 Implementation of the LMI method with field data

If the customer was supplied from a pure sinusoidal voltage source, then the distortion level of the customer's current would change due to the absence of harmonics in the PCC voltage. The advantage of this method is that it is not necessary to actually disconnect the customer and reconnect it to a pure sinusoidal voltage source to obtain this information. The increase or decrease in the current distortion level of the customer can

now be classified as either load harmonics or source harmonics. This is valuable information when questions of IEEE 519 compliance arise.

5.4 Prediction of True Load Current

5.4.1 Measurements

The voltages and currents acquired at the plant metering location exhibit harmonics as illustrated in Figure 5.3 to Figure 5.6. It is never known for sure whether the current harmonics are resulting in voltage harmonics or vice versa. In the feeder circuit of Figure 5.1, switching of the capacitor banks can trigger parallel resonance and create voltage harmonics. Saturation of the customer's transformer could lead to increased current distortion. The LMI scheme developed in this research attempts to predict the true current distortion of a customer based on the scheme's ability to learn the admittance of the customers load. Snapshots of phase A voltage and current waveforms for a randomly chosen event before any switching is shown in Figure 5.9 and Figure 5.10.

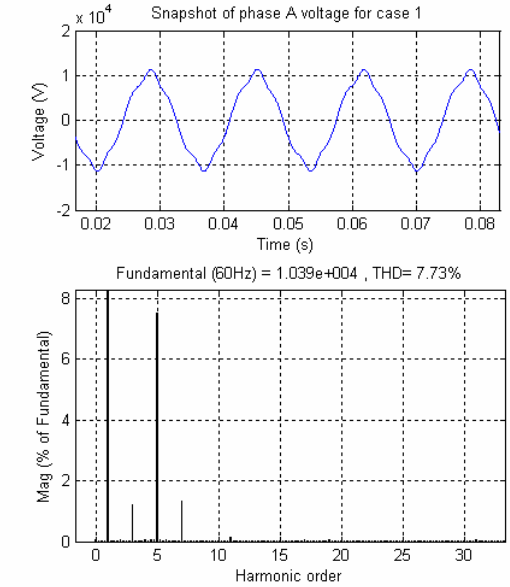

Figure 5.9 Snapshot of phase A voltage at the customers plant meter

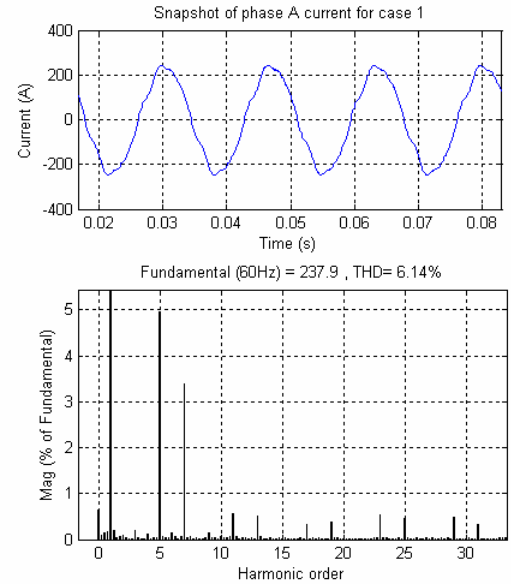

Figure 5.10 Snapshot of phase A current at the customers plant meter

The phase A measured voltage has a THD of 7.73%. This is beyond the IEEE 519 limits and the dominant harmonic in the voltage waveform is 7.51% of 5^{th} harmonic. The measured phase A current has a THD of 6.14% with the 5^{th} and the 7^{th} harmonic being the dominant ones. The other two phases had waveforms with similar characteristics.

5.4.2 Neural Network Training and Prediction

The ANN1 of Figure 5.8 is trained with randomly selected data before any switching took place. The training continues until the MSE of ANN1 in tracking the actual currents for each phase is sufficiently low to indicate that the ANN1 training has been completed. Establishing a pure sinusoidal voltage may not always be feasible since that would mean performing utility switching to change the system impedance characteristics. However, for the validation of the neural network results, the switchings are performed with the customer supplied from the 12 MVA transformer and both the capacitors offline. The possibility of network resonance is eliminated. Variation of phase

A voltage and current THD for the first 13 minutes (events 354 to 366) after the switching, is illustrated in Figure 5.11.

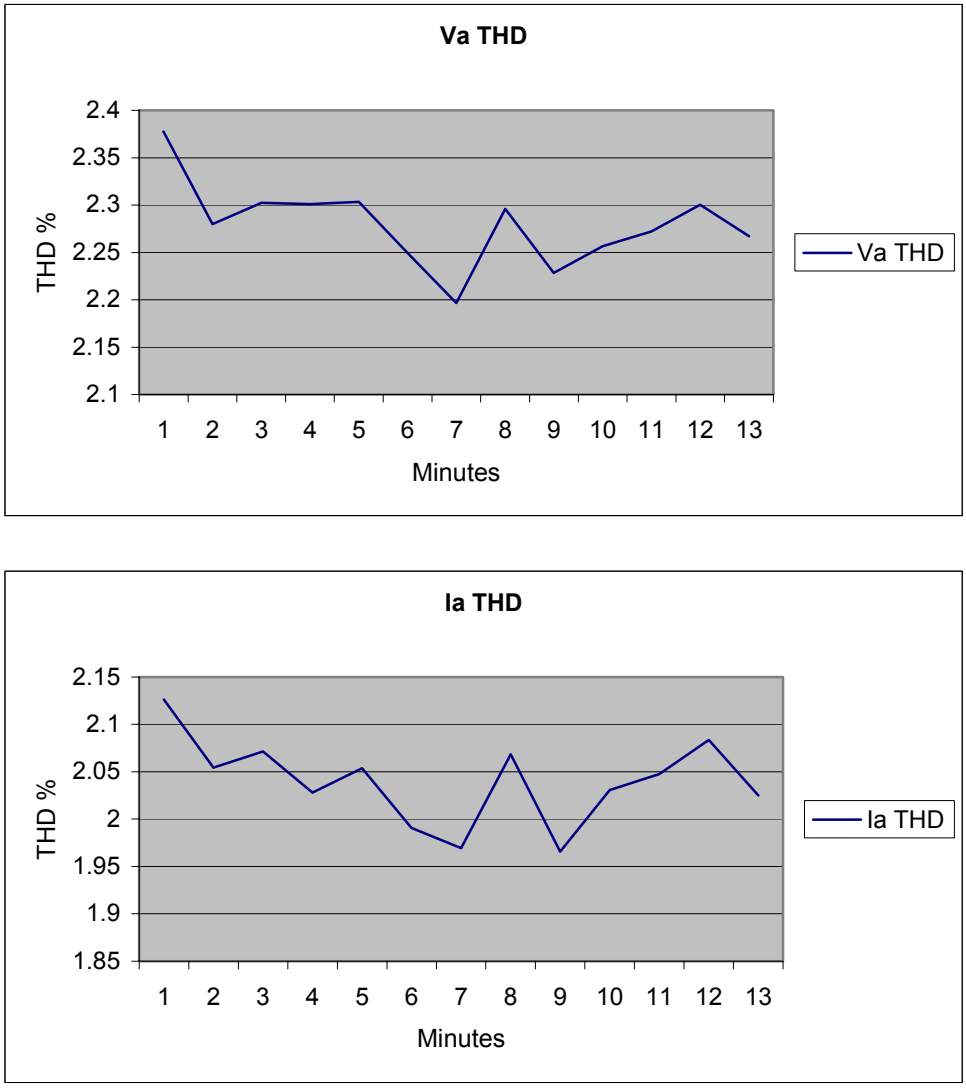

Figure 5.11 THD profile of phase A voltage and current when supplied from 12 MVA transformer and both capacitor banks offline

The same behavior is observed for phases B and C. The THD's are not constant and this is typical in industrial plants due to the constant turning on and off of machines. To validate the training and prediction performance of the LMI scheme, ANN1 is trained with data from the 8th minute to the 11th minute (event 361 to 364) in Figure 5.11 and

then ANN2 predicts the current waveform for the 12th minute (event 365) when supplied with the voltage data from event 365. The predicted current is then compared with the actual measured current to demonstrate the performance of the neural network predictions. The predicted current waveforms appear in Figure 5.12 to Figure 5.14.

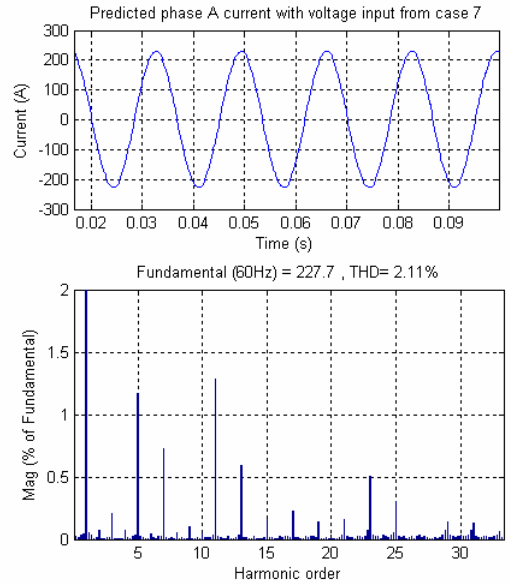

Figure 5.12 Predicted phase A current for event 365

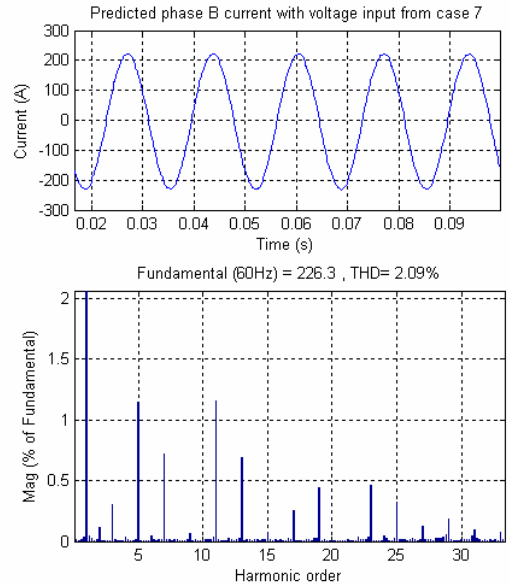

Figure 5.13 Predicted phase B current for event 365

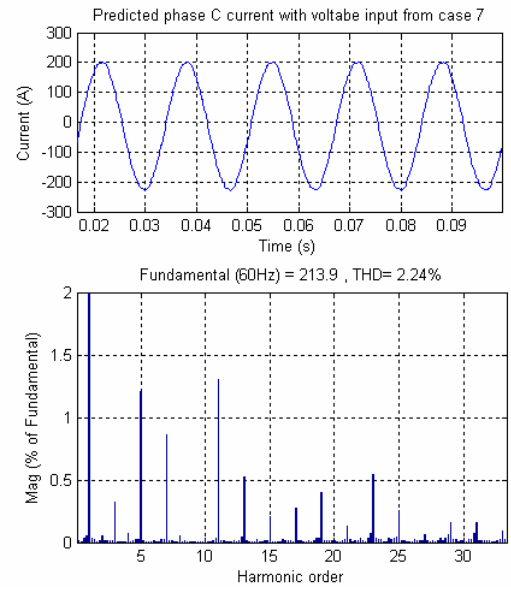

Figure 5.14 Predicted phase C current for event 365

The predicted current waveform for phase A in Fig. 11 has a THD of 2.11 %. The predicted phase B current has a THD of 2.09% (Fig. 12) and the predicted phase C current has a THD of 2.24% (Fig. 13). These THD's are predicted by the neural network based on what it had learned before. The voltage measured at the substation during event 365 has a THD of 1.5%. The voltage measured at the plant has a THD of 2.5%. Since both the capacitor banks are offline, it may be assumed that the increased distortion is due to the harmonic volt drops created by the harmonic current injected by the customer's load.

Table 5.2 provides the measurements recorded at the substation as well as at the customer's primary metering location for event 365. These measurements are compared with the currents predicted by the neural network. Comparison of the predicted current spectrum of Figure 5.12 to Figure 5.14 with actual measured current THD at the plant (Table 5.2) is provided in Table 5.3.

Table 5.2: Measurements recorded at the plant and the substation for event 365

Plant Meter Measurements (Time 15:18:22)								
	Voltage				Current			
Phase	RMS (V)	THD	5^{th} RMS	7^{th} RMS	RMS (A)	THD	5^{th} RMS	7^{th} RMS
A	7159	2.73 %	0.59 % (42.2 V)	0.69 % (46.5 V)	161	2.13 %	1.11 % (1.78 A)	0.84 % (1.35 A)
B	7102	2.58 %	0.47 % (31.9 V)	0.62 % (41.1 V)	160	2.15 %	1.12 % (1.79 A)	0.83 % (1.32 A)
C	7095	2.43 %	0.50 % (35.4 V)	0.49 % (30.4 V)	151.2	2.31 %	1.33 % (2.01 A)	0.72 % (1.23 A)
Substation Meter Measurements (Time 15:24:10)								
	Voltage				Current			
Phase	RMS	THD	5^{th} RMS	7^{th} RMS	RMS	THD	5^{th} RMS	7^{th} RMS
A	7501	1.42 %	0.22 % (16.3 V)	0.36 % (27.3 V)	233.89	2.13 %	1.43 % (3.3 A)	0.42 % (1.0 A)
B	7462	1.52 %	0.41 % (30.5 V)	0.5 % (37.2 V)	222.28	1.95 %	1.19 % (2.6 A)	0.15 % (0.3 A)
C	7537	1.59 %	0.45 % (33.8 V)	0.48 % (36.5 V)	229.80	1.93 %	1.21 % (2.8 A)	0.06 % (0.1 A)

Table 5.3: Comparison of current THD's for validation of neural network predictions

Phases	Measured Current THD	Predicted Current THD	Error in THD	Measured 5^{th} Harmonic	Predicted 5^{th} Harmonic	Measured 7^{th} Harmonic	Predicted 7^{th} Harmonic
A	2.13 %	2.11 %	0.9 %	1.11 % (1.78 A)	1.17 % (1.88 A)	0.84 % (1.35 A)	0.73 % (1.17 A)
B	2.15 %	2.09 %	2.7 %	1.12 % (1.79 A)	1.14 % (1.82 A)	0.83 % (1.32 A)	0.72 % (1.15 A)
C	2.31 %	2.24 %	3.0 %	1.33 % (2.01 A)	1.21 % (1.82 A)	0.72 % (1.23 A)	0.86 % (1.30 A)

The currents predicted by ANN2 with the voltage input data from the measurements of event 365 is within 3% even though the current and voltage THDs are constantly changing and the ANN1 has not seen the data of event 365 during training.

The THD's in Table 5.3 match closely with the THD of the actual measured currents of Table 5.2.

5.4.3 Prediction of Current with Pure Sinusoidal Input Voltage

ANN2 is now supplied with a balanced 3 phase mathematically generated sine wave representing a PCC voltage with no harmonics. The output of ANN2 is the predicted current waveform that would be expected from the customer if it were supplied with a clean sine wave voltage. The prediction performance of ANN2 is demonstrated by comparing the results predicted by ANN2 (clean sine wave input voltage) with the actual plant meter current measurements in Table 5.1. The predicted current waveforms appear in Figure 5.15 to Figure 5.17.

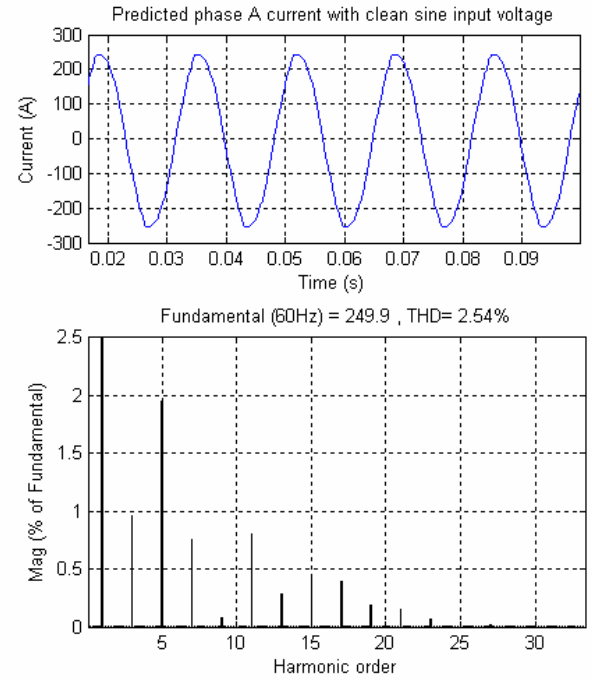

Figure 5.15 Predicted phase A current with clean sine wave input voltage

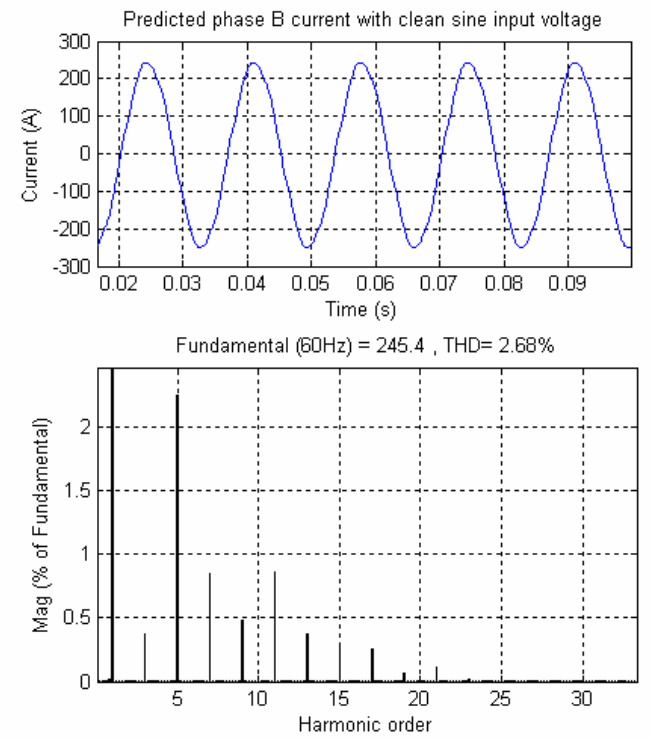

Figure 5.16 Predicted phase B current with clean sine wave input voltage

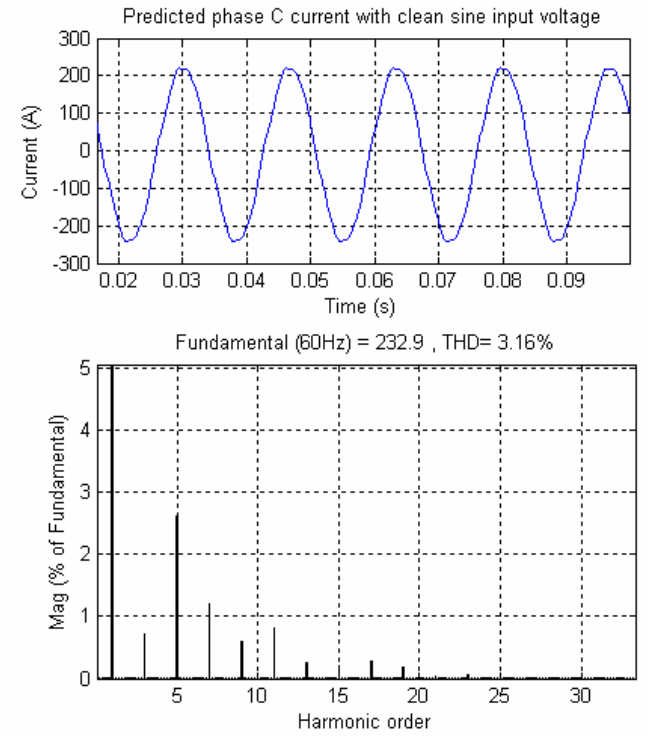

Figure 5.17 Predicted phase C current with clean sine wave input voltage

The predicted current waveform for phase A in Figure 5.15 has its THD reduced from 4.83% in Table 5.1 to 2.54%. The 5^{th} harmonic component reduces from 3.83 % (6.8 A) to 1.95 % (3.45 A). The 7^{th} harmonic component reduces from 2.67 % (4.8 A) to 0.75 % (1.32 A). Similar results are observed for phase B (Figure 5.16) and phase C (Figure 5.17).

For phase B, the overall current THD reduced from 4.29 % to 2.68 %. The 5^{th} harmonic component reduces from 2.96 % (5.2 A) to 2.25 % (3.9 A). The 7^{th} harmonic component reduces from 2.76 % (4.8 A) to 0.84 % (1.45 A).

For phase C, the overall current THD reduced from 4.72 % to 3.16 %. The 5^{th} harmonic component reduces from 3.74 % (6.2 A) to 2.61 % (4.15 A). The 7^{th} harmonic component reduces from 2.59 % (4.3 A) to 1.19 % (1.9 A).

The above results are summarized in Table 5.4.

Table 5.4: Neural network predicted currents with clean sinusoidal voltage input

Phase	Fundamental RMS (A)	THD	5^{th} harmonic	7^{th} harmonic
A	176.7	2.54 %	1.95 % (3.45 A)	0.75 % (1.32 A)
B	173.5	2.68 %	2.25 % (3.90 A)	0.84 % (1.45 A)
C	164.7	3.16 %	2.61 % (4.15 A)	1.19 % (1.90 A)

The customer's load is primarily composed of thyristor controlled drives. The characteristic current harmonic injected by these drives is the 5^{th} harmonic. The above

results show that even when the load is supplied with a clean sinusoidal voltage, the 5th harmonic current still exists. However, the 7th harmonic current reduces to less than 1 % for all three phases. The load modeling scheme predicts that the current harmonic measurements in Table 5.1 at the plant site is not a true reflection of the harmonics that can be attributed to the customer's load alone.

The measurements recorded in Table 5.2 show that the customer's current harmonics can indeed be in the range of 2 ~ 2.5% and this is an indication that the current harmonics predicted by the neural network is converging in the right direction. The measurements used for Table 5.2 contain notches in the voltage waveform at the customer's primary metering location. This results in higher voltage distortion of close to 2.5% for all three phases. At the same time, the voltage distortion measured at the substation is ~ 1.5% for all three phases.

From all the above measurements, it is not difficult to conclude that the presence of the both the capacitor banks result in some form of resonance which results in higher voltage distortion at the customer's site. Removal of both the capacitor banks produces voltage notches as well as reduced voltage (~ 400 V) at the customer's site. The load modeling tool predicts the true current harmonics of the customer's load irrespective of whether a resonance condition exited or not. Even if the utility is able to supply an undistorted voltage waveform at the primary meter of the customer, current harmonics will still exist but, the magnitudes will be lower than what is measured in Table 5.1 Comparison of the measured current THD for case 1 and predicted current THD for all three phases are summarized in Table 5.5.

Table 5.5: Comparison of ANN2 current THD (Table 5.4) with actual current THD (Table 5.1)

Phases	Measured Current THD	Predicted Current THD	Change in THD	Measured 5^{th} Harmonic	Predicted 5^{th} Harmonic	Measured 7^{th} Harmonic	Predicted 7^{th} Harmonic
A	4.83 %	2.54 %	47.4 %	3.83 % (6.8 A)	1.95 % (3.45 A)	2.67 % (4.8 A)	0.75 % (1.32 A)
B	4.29 %	2.68 %	37.5 %	2.96 % (5.2 A)	2.25 % (3.90 A)	2.76 % (4.8 A)	0.84 % (1.45 A)
C	4.72 %	3.16 %	33 %	3.74 % (6.2 A)	2.61 % (4.15 A)	2.59 % (4.3 A)	1.19 % (1.90 A)

The change in THD in Table 5.3 and Table 5.5 is computed as:

$$\frac{(Measured\ Current\ THD - Predicted\ Current\ THD)}{Measured\ Current\ THD} \times 100\% \quad (5.2)$$

5.5 Observations from Load Modeling Experiment

- The voltage distortion at the substation metering location for all three phases is ~3.3% whereas at the plant metering location, it was greater than 6.5% before any switching took place.
- The first steep change (decrease) in the voltage THD waveform at the plant (Figure 5.4) is when both the transformers at the substation are tied together.

The voltage THD drops to around 3% whereas the voltage distortion at the substation is under 1%.

- The lowest voltage distortion measured at the plant metering location is when both the transformers are tied together and both the capacitors are offline. The voltage THD measured is about 1.5%. The current distortion measured during this condition is 2%.
- Removal of both the capacitor banks from the network results in a voltage drop of 200V RMS at the plant metering location.

5.6 Site Results for Source Modeling (SMI) Method

The proposed SMI method of Figure 5.18 (introduced in chapter 4) predicts the change in the voltage THD at the customer's primary metering location if the customer's load were to inject only fundamental current and were to contain no harmonics.

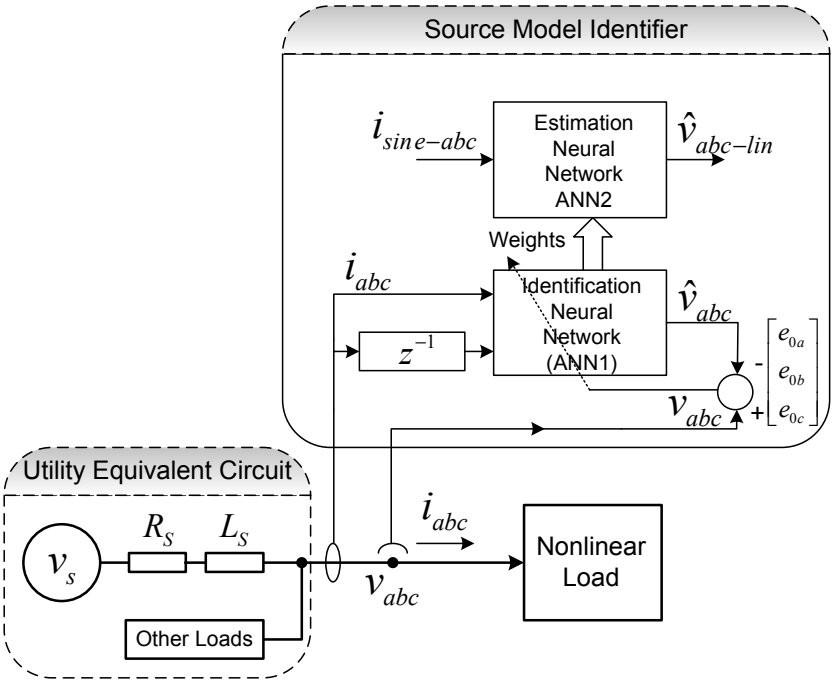

Figure 5.18 Implementation of SMI method with field measurements

In Figure 5.18, v_{abc} is the three phase line-neutral voltage at the PCC and i_{abc} is the line current of the customer. The SMI scheme obtains the instantaneous values of the three voltages v_{abc} as well as the three currents i_{abc} at the k^{th} moment in time from the PA 9 plus data acquisition meter recording data at the plant location. These values are fed to ANN1, which uses this to predict the values of v_{abc} at time instant $k+1$, labeled $\hat{v}_{abc}$. When the $k+1$ moment arrives (at the following sampling instant), and the actual values of v_{abc} are measured, these values are compared with the previously predicted $\hat{v}_{abc}$ values, and the difference (or error $[e_{0a} \quad e_{0b} \quad e_{0c}]^T$) is used to train ANN1 or adjust its weights.

If the customer were to inject only a sinusoidal current, then the distortion level of the voltage at the PCC would change due to the absence of the load injected harmonic current. At any moment in time after the ANN1 training has converged, its weights are transferred to the Estimation neural network ANN2, and a sine wave current waveform $i_{abc-\sin e}$ computed in software, is applied to the ANN2 input instead of the actual measured distorted current of the nonlinear load. The output of ANN2, called $\hat{v}_{abc-lin}$, gives the same information that could have been obtained if in reality the nonlinear load were replaced by a similar sized linear load. In other words, $\hat{v}_{abc-lin}$ represents the true voltage distortion at the PCC due to the removal of all harmonic current injection by the nonlinear load in question, except that it is not necessary to actually disconnect the nonlinear load and connect a pure current source to obtain this information. Any change in the voltage distortion levels between v_{abc} and $\hat{v}_{abc-lin}$ can be attributed to the nonlinearity of the load in question.

Figure 5.19 shows a detailed structure of ANN1 and the training scheme. ANN1 and ANN2 are MLPNs and structurally identical. ANN1 has three line currents as inputs and the three phase voltages as outputs. However, each input also requires the present value of the current vector and two time delayed values of the current vector, as well as a bias.

The error vector $\begin{bmatrix} e_{0a} & e_{0b} & e_{0c} \end{bmatrix}^T$ in Figure 5.19 is a 3 element column vector and is calculated as;

$$\begin{bmatrix} e_{0a} & e_{0b} & e_{0c} \end{bmatrix}^T = v_{abc}(k+1) - \hat{v}_{abc}(k+1) \tag{5.3}$$

Backpropagation of this error vector $\begin{bmatrix} e_{0a} & e_{0b} & e_{0c} \end{bmatrix}^T$ is explained in appendix E.

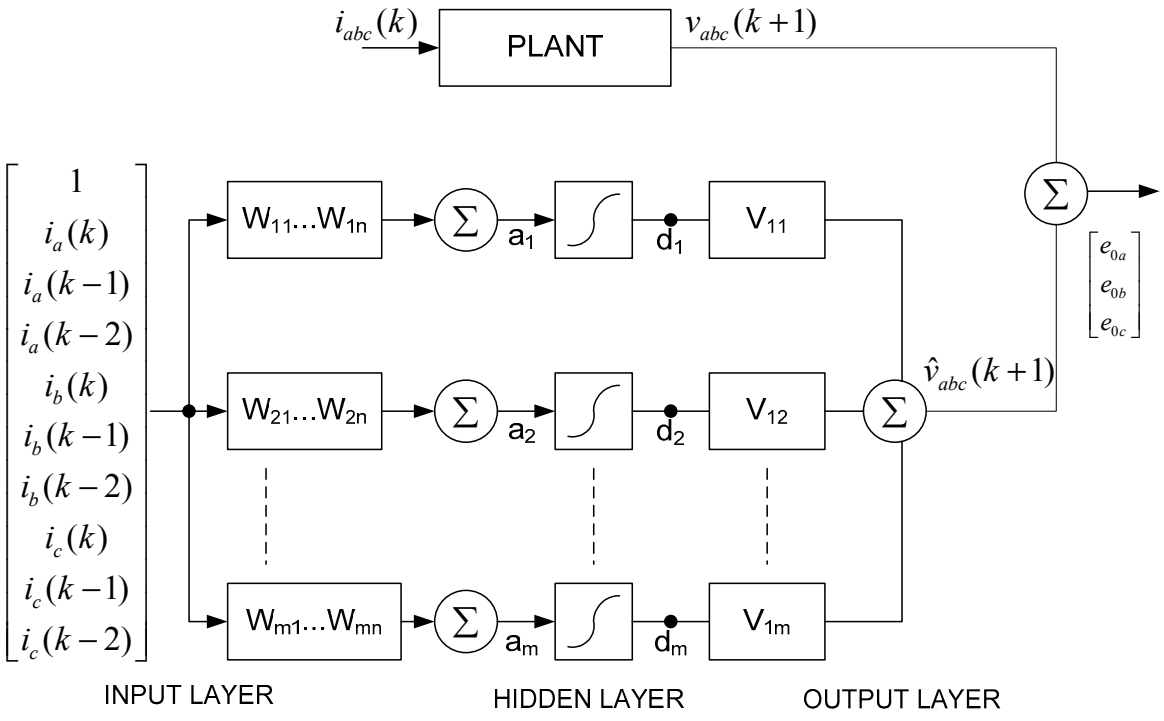

Figure 5.19 Structure of ANN1 for the implementation of SMI method

During the event 366 (case 7), both the capacitor banks are offline and the customer's load is supplied from the 12 MVA transformer. Snapshot of the phase A voltage for event 366 is shown in Figure 5.20.

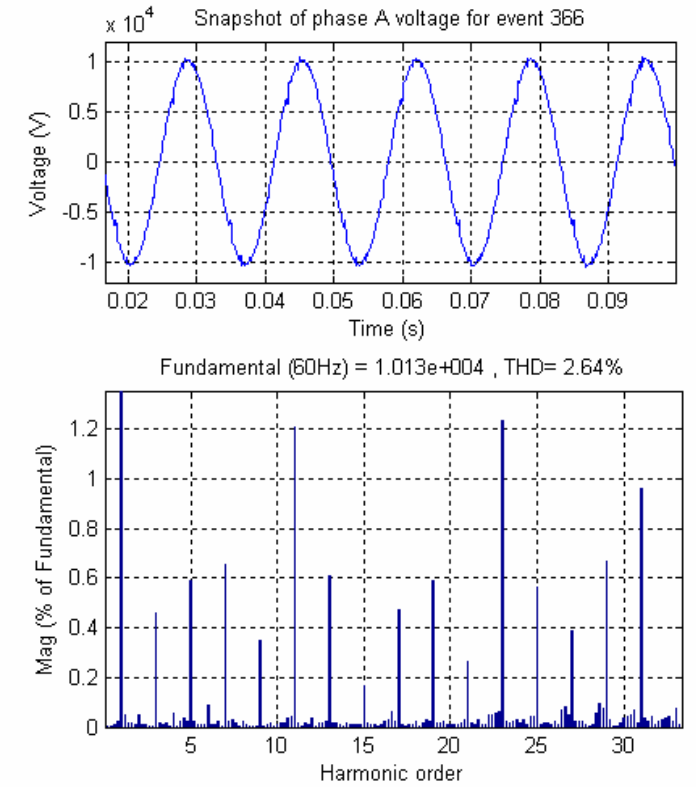

Figure 5.20 Snapshot of phase A voltage using the PA 9 meter at the plant location

Voltage in Figure 5.20 has a THD of 2.64%. Though this is within the IEEE 519 limits, it is important to note the notches in the voltage waveform due to the customer's load. The other two phases exhibit characteristics.

Table 5.6 provides the measurements recorded at the substation as well as at the customer's primary metering location for event 366. Comparison of the plant and substation meter readings for the voltage THD shows the impact of the customer's load current with the downstream impedance of the distribution circuit.

Table 5.6: Recorded measurements for event 366

Plant Meter Measurements (Event 366)				
	Voltage		Current	
	RMS (V)	THD	RMS (A)	THD
A	7160	2.64 %	159	2.12 %
B	7103	2.47 %	158	2.15 %
C	7090	2.31 %	150	2.32 %
Substation Meter Measurements (Event 366)				
	Voltage		Current	
	RMS (V)	THD	RMS (A)	THD
A	7501	1.42 %	234	2.13 %
B	7462	1.52 %	222	1.95 %
C	7537	1.59 %	229	1.93 %

The ANN1 of Figure 5.18 is now trained with randomly selected data from the events of case 7. The training continues until the value of the mean squared error *MSE* of ANN1 in tracking the actual 3 phase voltages, is sufficiently low, thus indicating that the ANN1 training has been completed. At this point the weights of ANN1 are transferred to ANN2. Therefore, ANN2 now represents the customer's average load impedance in time domain.

Convergence in ANN1 training with data from event 366 is demonstrated by the fact that the neural network predicted voltage waveforms coincide with the actual voltage as shown in Fig. 10 and by the decrease in MSE in Fig. 11.

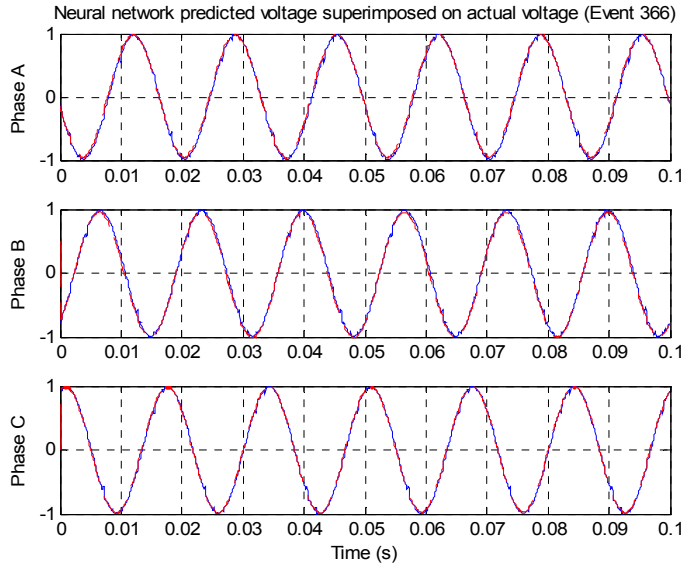

Figure 5.21 ANN1 output superimposed on actual voltage for event 366

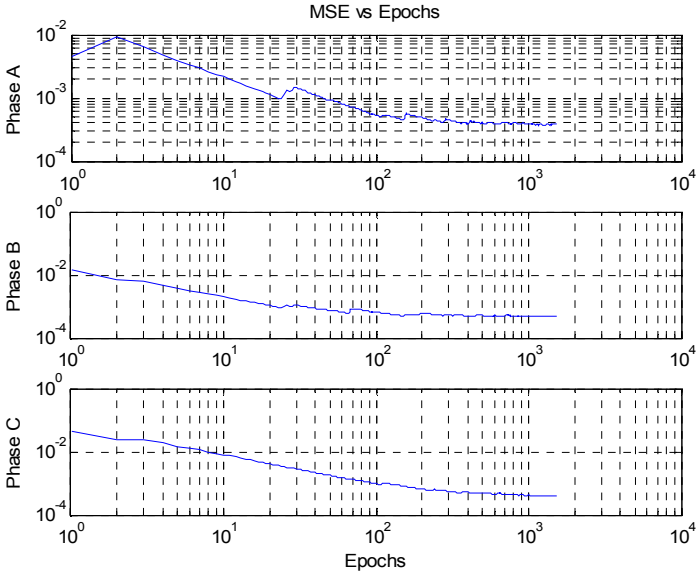

Figure 5.22 MSE in ANN1 voltage tracking for event 366

ANN2 is now supplied with a balanced 3 phase mathematically generated sine wave representing the customer's current with no harmonics. The outputs of ANN2 in Figure 5.23 to Figure 5.25 are the predicted voltage waveforms that would be expected at the PCC if the customer were to has apply filtering techniques to clean up the harmonic currents which it was injecting into the network. The predicted voltage waveforms are then compared with the actual measured voltages of event 366 (Table 5.6) to determine the difference that the customer's filtering action will have on the voltage distortion at the PCC.

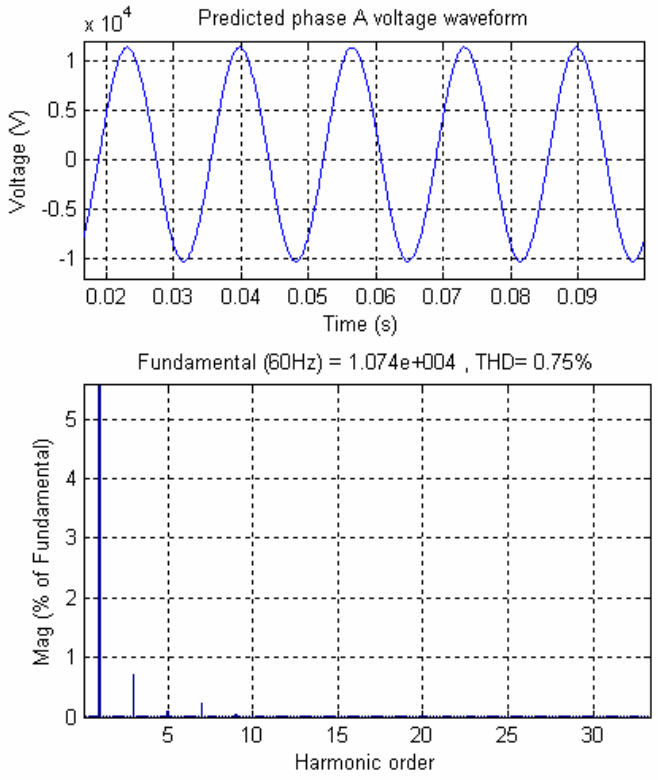

Figure 5.23 Predicted phase A voltage at the primary metering location of the customer by ANN2 with a clean sinusoidal input current

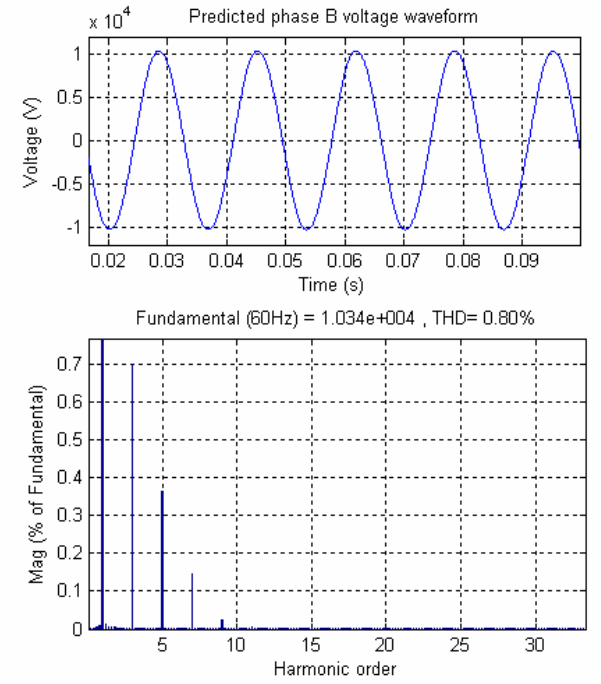

Figure 5.24 Predicted phase B voltage at the primary metering location of the customer by ANN2 with a clean sinusoidal input current

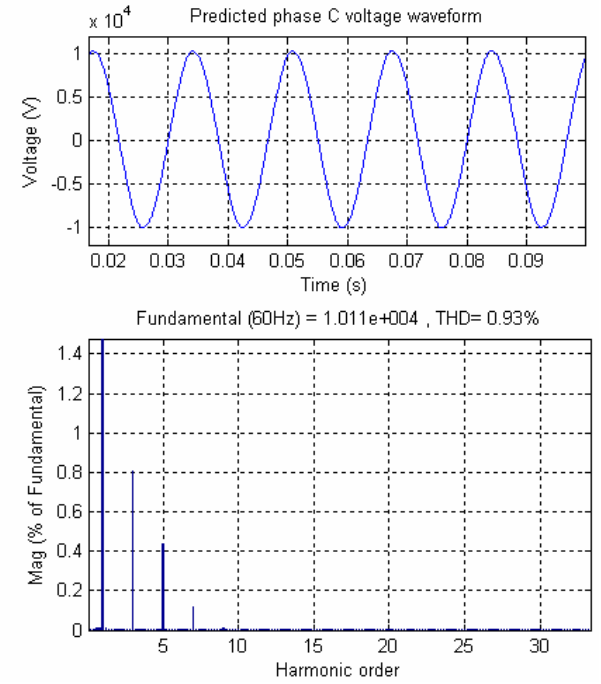

Figure 5.25 Predicted phase C voltage at the primary metering location of the customer by ANN2 with a clean sinusoidal input current

The ANN2 predicted voltage waveforms have THD's less than 1%. This is expected as the customer's load is the dominant load on the feeder circuit and is nonlinear in nature. The other loads on this feeder circuit are residential customers. The customer's load is primarily composed of thyristor controlled drives. The commutation of the thyristors creates notches on the supply voltage and that is seen in Figure 5.20. The characteristic current harmonic injected by these drives is the 5^{th} harmonic. Once the customer's current is assumed to be a clean sine wave, there are no sources of distortion and the voltage THD's reduce from the values measured in event 366.

A comparison of the measured voltage THD and predicted voltage THD for all three phases at the PCC is presented in Table 5.7.

Table 5.7: Comparison of the voltage THD's at the PCC for event 366

Phase	Measured Voltage THD (Event 366)	ANN2 Predicted Voltage THD
A	2.64 %	0.75 %
B	2.47 %	0.80 %
C	2.31 %	0.93 %

To give a quantitative meaning to the THD values predicted by ANN2, a percentage change is computed using (5.1). For this particular site, the phase A voltage THD reduces by 71.5%, phase B voltage THD reduces by 67.6% and phase C voltage THD reduces by 59.7%.

5.7 Summary

This chapter demonstrates the ability of a single neural network to learn the nonlinear characteristics of a three phase load and utilize the trained neural network to predict the true nonlinear load characteristics caused by that load. The proposed load modeling scheme is shown to be able to identify the amount of customer injected harmonic current regardless of whether a resonant condition exists on the utility power system. The proposed source modeling is also applied to actual plant data. This chapter also shows the feasibility of applying the proposed scheme to actual field data and the possibility of training the neural network with snapshot data. The scaling of the acquired data is done using software and hence that removes any limitations whatsoever on the data acquisition system and the transducers. Both the schemes, load modeling and source modeling, are designed in software and hence can be integrated into any commercially available power quality diagnostic instrument.

CHAPTER 6

ECHO STATE NETWORKS

6.1 Introduction

This chapter investigates the application of Echo State Networks (ESN) as an extension of the recurrent neural networks used in chapters 3 and 4. Complexities with existing algorithms have thus far limited supervised training techniques for RNNs from widespread use. When it comes to practical applications, MLPNs still dominate. ESNs are a special form of RNNs. RNNs are fundamentally different from feedforward architectures in the sense that they not only operate on an input space but also on an internal state space, a trace of what already has been processed by the network. Connectivity is an important part in a RNN. A fully connected RNN means that a neuron in one layer is connected to all the neurons in the previous layer. Generally, tasks requiring some form of memory are candidates for RNN modeling.

During the last decade, several methods for supervised training of RNNs have been explored. Currently, the most important ones in use are: backpropagation through time (BPTT), real-time recurrent learning (RTRL), and extended Kalman filtering based techniques (EKF). Although, all of the above algorithms are mathematically complex and there are no clear winners, BPTT is probably the most widely used due to its similarity with the standard backpropagation algorithm.

ESNs present a newer approach to training RNNs. Invention of ESN is credited to Herbert Jaeger [124]. ESNs have been proposed for modeling complex dynamic systems

[125]-[129]. The principles of ESN are based on the use of a Recurrent Neural Network (RNN) as a dynamic reservoir. A large (order of 100s of neurons) RNN is used as a "reservoir" of dynamics which can be excited by suitably presented input and output feedback.. The connection weights of the reservoir network are not changed by training. In order to compute the desired output dynamics, only the weights of connections from the reservoir to the output units are calculated. This is simply a linear regression problem.

6.2 ESN Architecture

ESNs have three basic layers: input later, the Dynamic Reservoir and the output layer. The input layer is linked to the dynamic reservoir through the input weights W^{in}. The dynamic reservoir has internal weights W which define the recurrent connections inside the reservoir. The dynamic reservoir to the output layer is linked through the output weights W^{out}. The output is fed back to the dynamic reservoir through feedback weights W^{fb}. Structurally, the main difference between an ESN and a RNN is the connectivity of neurons within the dynamic reservoir. The ESN is a sparsely connected RNN with W^{in}, W and W^{fb} fixed apriori to randomly chosen values. In contrast to RNNs where the input and output weights are adjusted based on the minimization of the mean squared error (MSE), ESNs only calculate the output weights W^{out} leading from the dynamic reservoir to the output layer. Figure 6.1 shows the structure of an ESN.

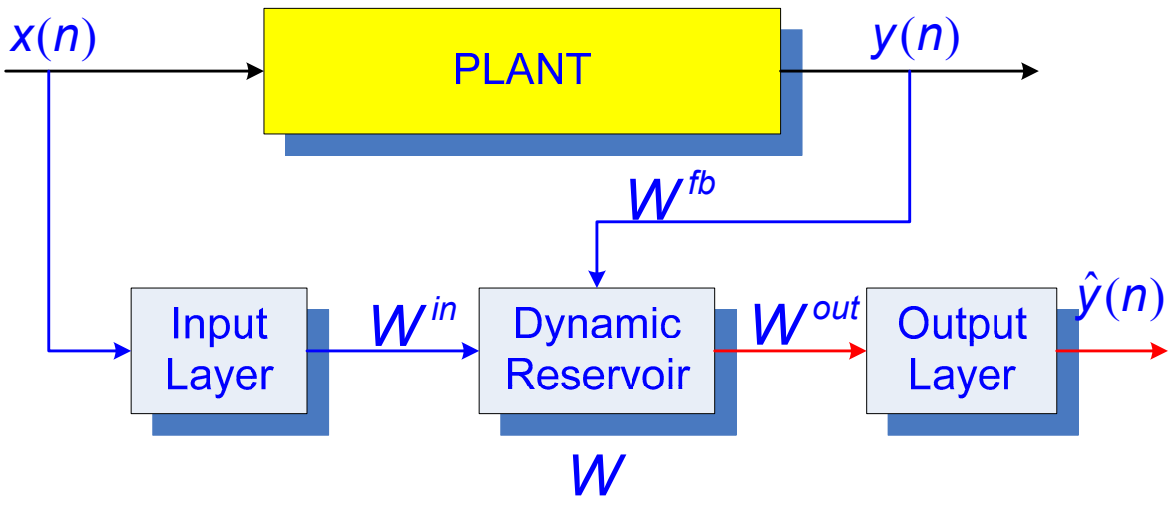

Figure 6.1 Block diagram of Echo State Network

6.2.1 ESN Parameters

The main parameters of the ESN based on Figure 6.1 are defined below:

- A discrete-time input sequence $\underline{x}$ and a corresponding output sequence $\underline{y}$.
- K input neurons, i.e., $\underline{x} = [x(1), ...x(K)]^T$.
- N neurons in the dynamic reservoir, i.e. the output of the dynamic reservoir is the state vector $\underline{d} = [d(1), ..., d(N)]^T$.
- M output neurons i.e., $\underline{\hat{y}} = [\hat{y}(1), ...\hat{y}(M)]^T$
- Input weight matrix W^{in} of size $N \times K$
- Hidden layer weight matrix W of size $N \times N$
- Output weight matrix W^{out} of size $M \times (K + N)$
- Feedback weight matrix W^{fb} of size $N \times M$

- Sigmoidal activation function for the dynamic reservoir

6.2.2 ESN Theory

The key to understanding ESN training is the concept of echo states [130], [131]. Having echo states (or not having them) is a property of the network prior to training, that is, a property of the weight matrices W^{in}, W, and W^{fb}. Intuitively, the echo state property says, "if the network has been run for a very long time [from minus infinity time in the definition], the current network state is uniquely determined by the history of the input and the teacher forced output". A formal definition of ESN is provided in Definition 1.

Definition 1: Assume an untrained network with weights W^{in}, W and W^{fb} is driven by teacher input $x(n)$ and teacher-forced by teacher output $y(n)$ from compact intervals X and Y. The network (W^{in}, W, and W^{fb}) has echo states with respect to X and Y, if for every left-infinite input/output sequence ($x(n)$, $y(n-1)$), where n = ..., -2,-1,0, and for all state $d(n)$ and any arbitrary state $d'(n)$ compatible with the teacher sequence, i.e. with state update equation;

$$d(n+1) = sig(W^{in}x(n+1) + Wd(n) + W^{fb}y(n)) \tag{6.1}$$

$$d'(n+1) = sig(W^{in}x(n+1) + Wd'(n) + W^{fb}y(n)) \tag{6.2}$$

it holds that $d(n) = d'(n)$ all $n \leq 0$.

An equivalent way of stating this is to say that for every internal state signal $d_i(n)$ there exists an echo function e_i which maps input/output histories to the current state:

$$e_i : (X \times Y)^{-\mathbb{N}} \to \mathbb{R}$$
$$(....., (x(-1), y(-2)), (x(0), y(-1)) \mapsto d_i(0) \tag{6.3}$$

It is often stated, somewhat loosely, that a (trained) network (W^{in}, W, W^{out} and W^{fb}) is an echo state network if its untrained "core" (W^{in}, W, and W^{fb}) has the echo state property with respect to input/output from any compact interval $X \times Y$.

One of the conditions referred to as the state contracting property is shown to be equivalent to echo states.

Definition 2: With the same assumptions as in Definition 1, the network (W^{in}, W, and W^{fb}) is state contracting with respect to $X \times Y$, if for all right-infinite input/output sequences $(x(n), y(n-1)) \in (X \times Y)$, where n = 0,1,2,... there exists a null sequence $(\delta_n)_{n \geq 1}$, such that for all starting states $d(n)$, $d'(n)$ and for all $n > 0$ it holds that $|d(n) - d'(n)| < \delta(n)$, where $d(n)$ and $d'(n)$ is the network state at time n obtained when the network is driven by $(x(n), y(n-1))$ up to time n after having been started in $d(0)$ and $d'(0)$.

Unfortunately, there is no known necessary and sufficient algebraic condition which allows to decide, given (W^{in}, W, and W^{fb}), whether the network has the echo state property. However a condition sufficient for the nonexistence of echo states is connected to the algebraic properties of the weight matrix W.

Definition 3: Assume an untrained network (W^{in}, W and W^{fb}) with state update equation (1) and with sigmoidal activation function. Let W have a spectral radius $|\lambda_{\max}| > 1$, where $|\lambda_{\max}|$ is the largest absolute value of an eigenvector of W. Then the

network has no echo states with respect to any input/output interval $X \times Y$ containing the zero input/output $(0,0)$.

In Definition 3, the input and feedback weights (W^{in} and W^{fb}) are not used. It seems that these weights are irrelevant for the echo state property. In practice, it is found that they can be freely chosen without affecting the echo state property.

For practical purposes, the following procedure for determining W seems to guarantee echo state networks:

Generate a sparse random matrix W_0 in the range [-1,1]

Scale the matrix by it's highest eigen value $|\lambda_{\max}|$

Multiply the matrix by α known as the spectral radius. $[\alpha \in 0,1]$

$$W = \frac{\alpha \cdot W_0}{|\lambda_{\max}|} \tag{6.4}$$

6.3 ESN Training

Given the ESN and the I/O sequences of the plant, the network is trained to learn the plant characteristics. The available I/O sequences are divided into three parts:

- An initial part, which is not used for training but serves the purpose of getting rid of initial transients in the network's internal states.
- A training part, which is used in the actual learning procedure of adjusting the output weights.

- A testing part, which is used to test the newly trained network on additional data. W^{fb} is not used during the testing.

6.3.1 Training Procedure

- Randomly generate an internal weight matrix W_0. The matrix should be sparse. The MATLAB command for the same is *sprand*. Apply (4) to obtain W. The size is W is depended on the length of the training sequence T_L. As a thumb rule, N should not exceed an order of magnitude of $\frac{T_L}{10}$ to $\frac{T_L}{2}$. Ideally ESNs are suitable for periodic data and for such data N should be closer to $\frac{T_L}{2}$.

- Randomly generate input weights W^{in} and feedback weights W^{fb}. Then, the untrained network (W^{in}, W, W^{fb}) is an echo state network, regardless of how W^{in} and W^{fb} are chosen.

- The spectral radius α depends on the application and needs to be hand tuned. A starting value of α is 0.8.

- The next step is to sample the network dynamics. This is a mechanical step and involves no heuristics. First, the network's internal state vector $\underline{d}$ is initialized to zero state, i.e. $\underline{d}(0) = 0$.

- Drive the network by the training data for times $n = 0,...T$ by presenting the input $x(n)$ and forcing the output $y(n-1)$ to the dynamic reservoir. The new state of the network for the next time step is calculated as;

$$d(n+1) = sig(W^{in}x(n+1) + Wd(n) + W^{fb}y(n)) \tag{6.5}$$

- The information from initial time steps, $n = 1,....T_0$ is not used for training because the network's dynamics are partly determined by the initial arbitrary starting state of $\underline{d}(0) = 0$. By time T_0, the effects of the arbitrary starting state die out. As an example, for a 500 point data sequence, T_0 could be set to 100. This is known as the initial washout time.

- For each time larger or equal than an initial washout time T_0, collect the input $x(n)$ and the network state $d(n)$ as a new row into a state collecting matrix M. In the end, size of M works out to be $(T - T_0 + 1) \times (N + K)$.

- Similarly, for each time larger or equal than an initial washout time T_0, the sigmoid inverted teacher output $\tanh^{-1} y(n)$ is collected in the teacher collecting matrix T of size $(T - T_0 + 1) \times (L)$ (this should not be confused with the final time step also designated as T).

- Once the training is over, multiply the pseudoinverse of M with T, to obtain a $(K + N) \times L$ sized matrix W^{out}.

$$W^{out} = M^{-1}T \tag{6.6}$$

6.3.2 Testing Procedure

- The network (W^{in}, W, W^{fb} and W^{out}) is now ready for use. It can be driven by novel input sequences $x(n)$ and using the output equation, the predicted output is obtained. The output at time $n+1$ is computed as;

$$\hat{y}(n+1) = lin(W^{out}(x(n+1), d(n)) \tag{6.7}$$

Here the commas mean vector concatenation. It is important to remember that the output update equation is not used during training, since the output weights are not yet set to their final values. Instead, the output nodes are just overwritten by the output part of the I/O sequence.

- Now the output of the system approximates the actual system output by the equation,

$$\hat{y}(n) \approx y(n) = \sum_{i=1}^{L} W_i^{out} \cdot d(n) \tag{6.8}$$

- More specifically, the output weights are computed such that the mean squared training error is minimized.

$$MSE = \frac{1}{r}\sum_{n=1}^{r}(y(n) - \hat{y}(n))^2 = \frac{1}{r}\sum_{n=1}^{r}(y(n) - \sum_{i=1}^{L} W_i^{out} \cdot d(n))^2 \tag{6.9}$$

where r is the length of the I/O sequence used for testing.

6.4 ESN Applied to Load Modeling

The method proposed in chapter 4 predicts the true harmonic current distortion that can be attributed to a load. Instead of using traditional neural network topologies, the load modeling method now uses ESNs. Figure 6.2 is a one-line diagram of a three-phase supply network having a sinusoidal voltage source v_s, network impedance L_s, R_s and several loads (one of which is nonlinear) connected to a PCC.

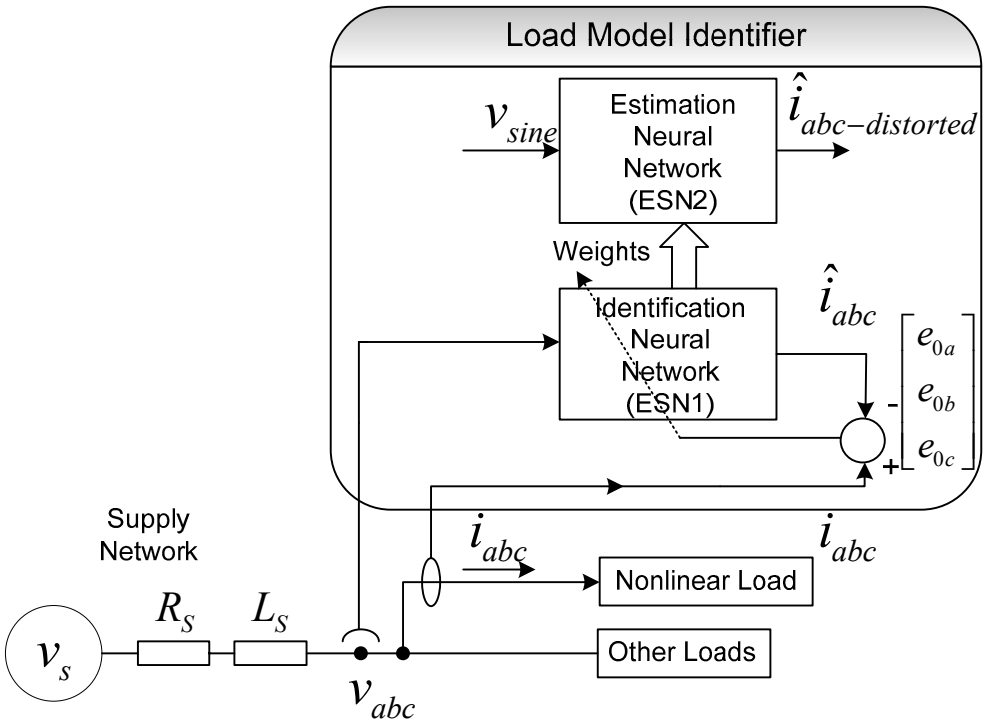

Figure 6.2 Implementation of LMI method (v_{abc} is the voltage at the PCC)

The nonlinear load injects distorted line three-phase line current i_{abc} into the network. The Identification Neural Network (ESN1) is trained to identify the nonlinear characteristics of the load. The Estimation Neural Network (ESN2) predicts the true harmonic current that would be injected by the load into the network, if it were possible to isolate the load and supply it from a pure sinusoidal source. ESN2 is an exact replica of the trained ESN1 structurally.

The proposed method measures the instantaneous values of the three voltages v_{abc} at the PCC, as well as the three line currents i_{abc} at the k^{th} moment in time. The voltages v_{abc} could be line-to-line or line-to-neutral measurements. ESN1 predicts the line current $\hat{i}_{abc}$ as a function of the present voltage vector value. The length of the training samples is predetermined. The training is done offline. Once all the samples are

processed by ESN1, the output weights are computed. Now the actual instantaneous values of $\hat{i}_{abc}$ are compared with the previously predicted values of $\hat{i}_{abc}$, and the difference (or error e_{0-abc}) is used to recomputed the ESN1 output weights, where

$$e_{0-abc} = i_{abc} - \hat{i}_{abc} \tag{6.10}$$

e_{0-abc} is used to compute the MSE. If MSE is not within acceptable limits, the DR is reinitialized and whole process of training is repeated. After several runs, the training converges and the value of the error e_{0-abc} diminishes to an acceptably small value. Proof of this is illustrated by the fact that the waveforms for i_{abc} and $\hat{i}_{abc}$ should practically lie on top of each other. At this point the ESN1 therefore represents the admittance of the nonlinear load. This process is called identifying the load admittance.

ESN2 is supplied with a mathematically generated sine wave voltage to estimate its output using (6.8). The output of ESN2 called $\hat{i}_{abc-distorted}$ therefore represents the current which the nonlinear load would have drawn had it been supplied by a sinusoidal voltage source. In other words, this gives the same information that could have been obtained by quickly removing the distorted PCC voltage (if this were possible) and connecting a pure sinusoidal voltage to supply the nonlinear load, except that it is not necessary to actually do this interruption. Any distortion present in the $\hat{i}_{abc-distorted}$ waveform can now be attributed to the nonlinearity of the load admittance.

6.5 Experimental Results with ESN

For illustrative purposes, the scheme is applied on a three phase variable speed drive on a per phase basis. The drive is supplied from the utility source as well as from a

clean power source. The clean power source used is the same HG used in chapter 4. The HG is capable of outputting voltages with programmable distortion levels and near zero internal impedance. Figure 6.3 shows the experimental setup.

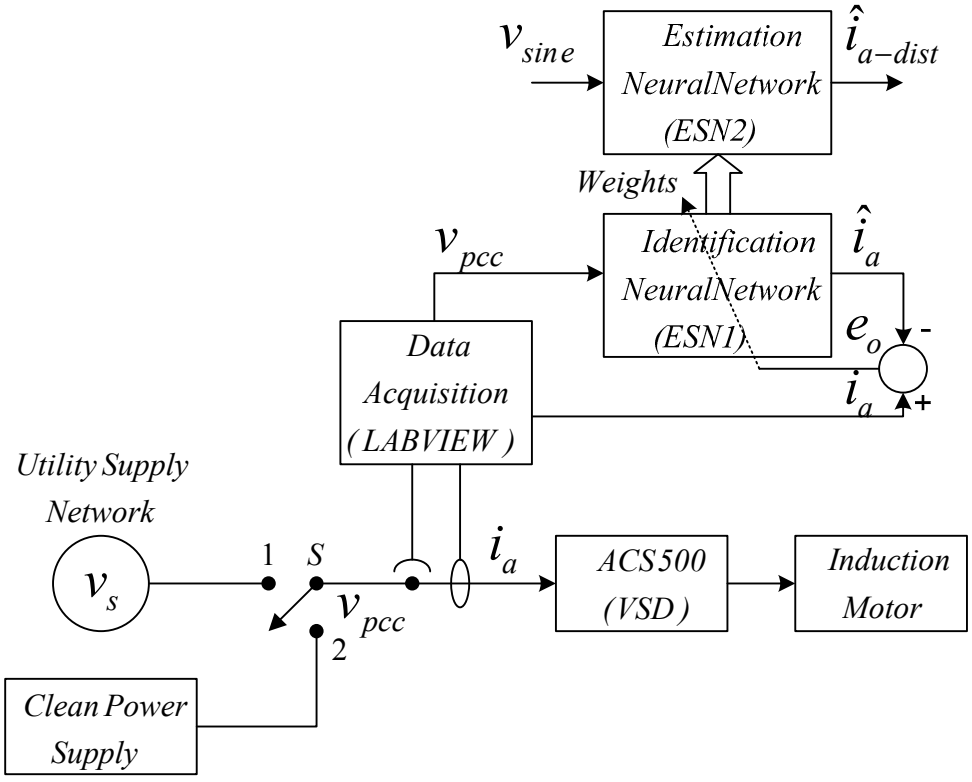

Figure 6.3 Experimental setup for validation of LMI method with ESN

The scheme has to be applied to each phase individually. The method of using online trained ESNs to identify the load admittance and utilizing the trained neural network to estimate the harmonic current of the VSD, is now demonstrated for phase A. With switch S in position 1, the VSD is supplied from the utility source. The three phase line to neural voltages and the phase currents are recorded. Now with switch S in position 2, the drive is supplied from the clean power source. The measured phase A voltage and current waveforms with switch in position 1 are shown in Figure 6.4.

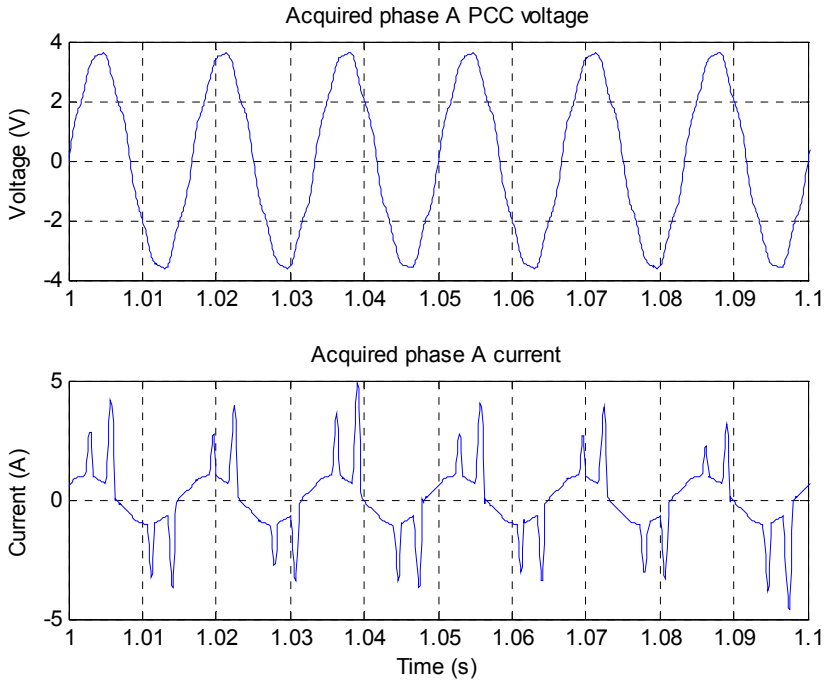

Figure 6.4 Measured voltage and current with S in position 1

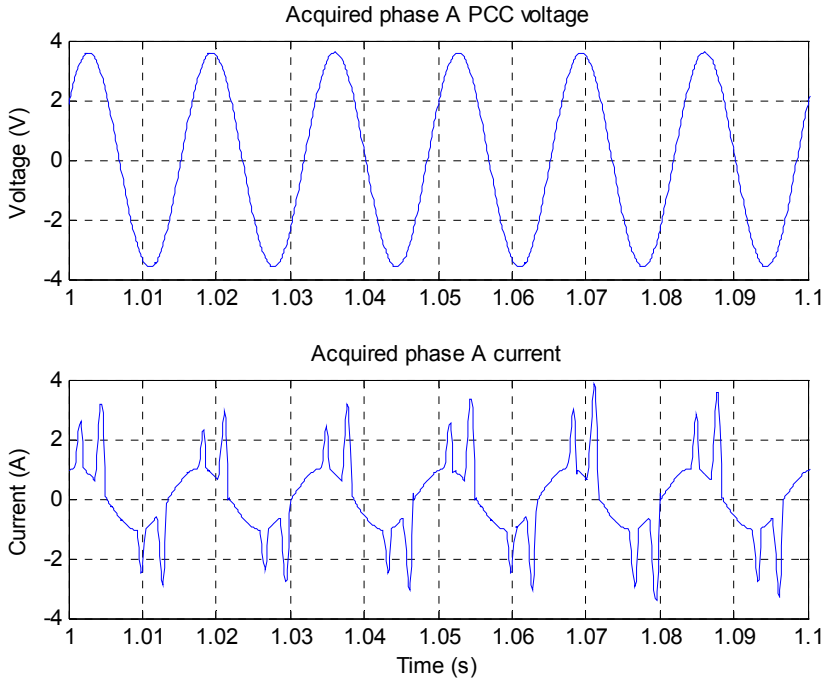

Figure 6.5 Measured voltage and current with S in position 2

Figure 6.5 shows the measured phase A voltage and current waveforms with the switch in position 2. The total harmonic distortion (THD) of the utility voltage at the PCC is 4.5% and the THD of the CI 5001 iX voltage at the PCC is 0.2% (near sinusoidal).In a real life application, the use of the clean power source is not required for the implementation of this scheme, nor will such a power source be available.

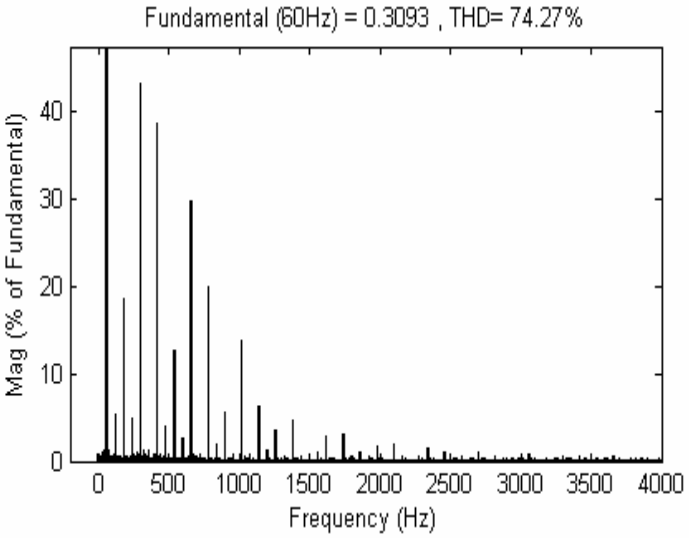

Figure 6.6 FFT spectrum of current with S in position 1

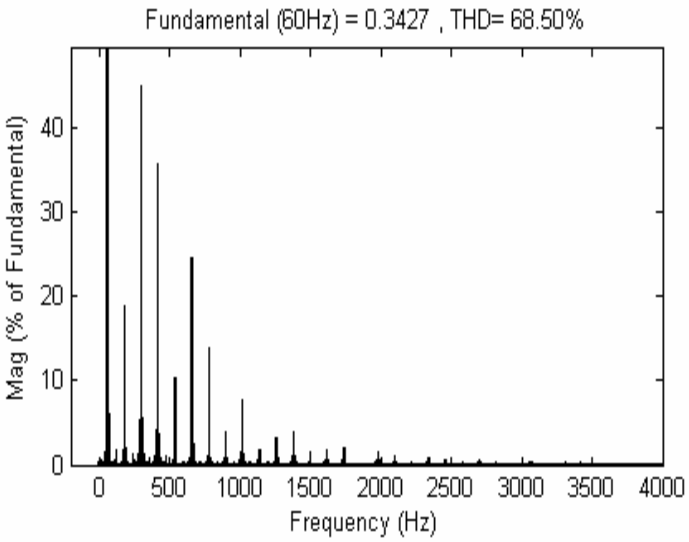

Figure 6.7 FFT spectrum of current with S in position 2

The THD of the load current with switch S in position 1 is 74.27% and the THD of the load current with switch S in position 2 is 68.5%. The FFT spectrums are shown in Figure 6.6 and Figure 6.7.

The sampling rate for data acquisition is set at 128 samples per cycle. The dynamic reservoir is constructed with 20 neurons. Data acquisition is carried out by a National Instruments data acquisition system. The voltage transducers used are LEM LV 25-P and the current transducers used are LEM LAH 25-NP. The FFT of the acquired waveforms are computed using the *powergui* block of SIMULINK. The dynamic reservoir of the ESN is constructed with 20 neurons.

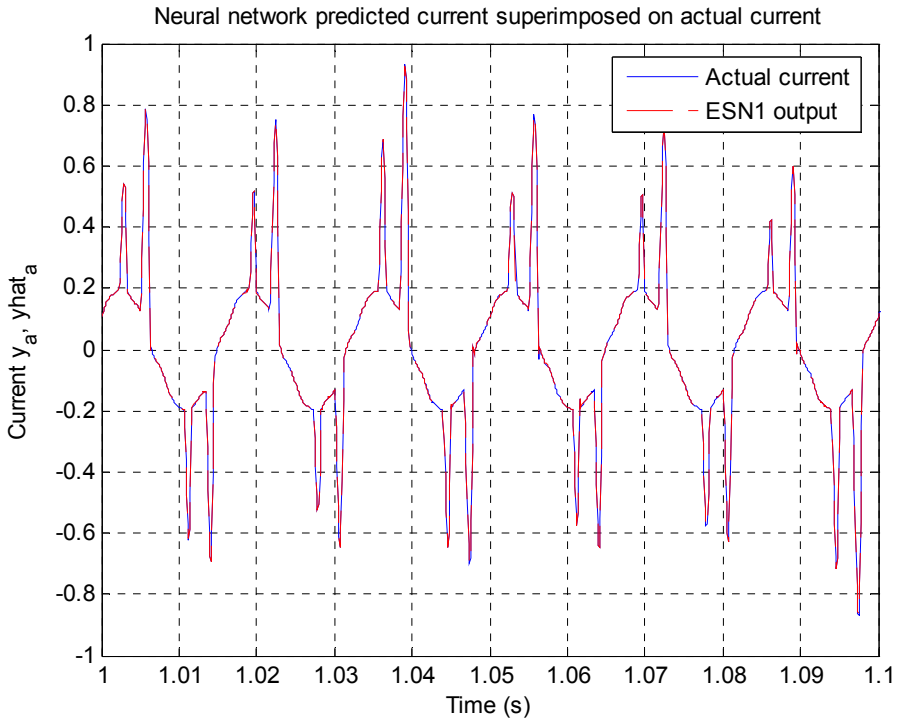

Figure 6.8 ESN1output superimposed on actual phase A drive current

The data obtained with switch S in position 1 is used to train the neural network ESN1 until the training error converges to near zero, and the output of ESN1 correctly

tracks the actual current i_a. Figure 6.8 indicates the training result of ESN1 by creating a plot of $\hat{i}_a$ coinciding with the actual i_a waveform. The convergence of the training is also verified by considering the MSE of ESN1 in Figure 6.9.

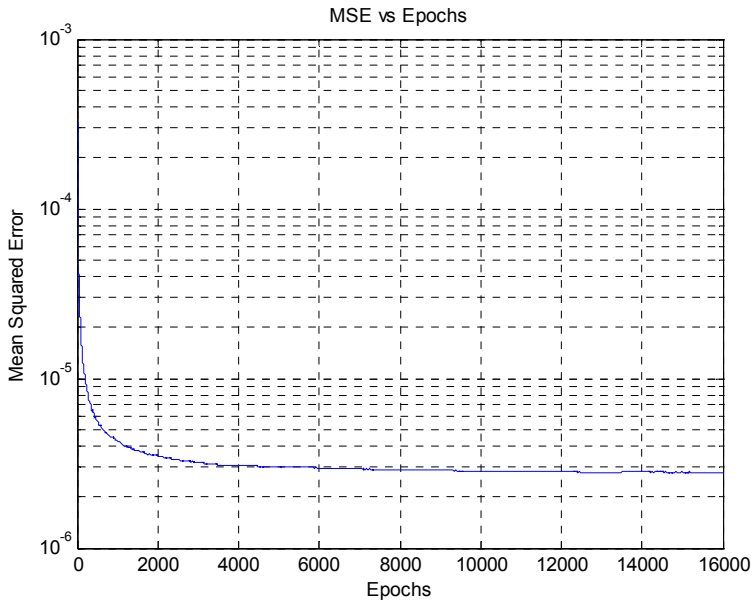

Figure 6.9 Training performance of ESN1 in terms of MSE

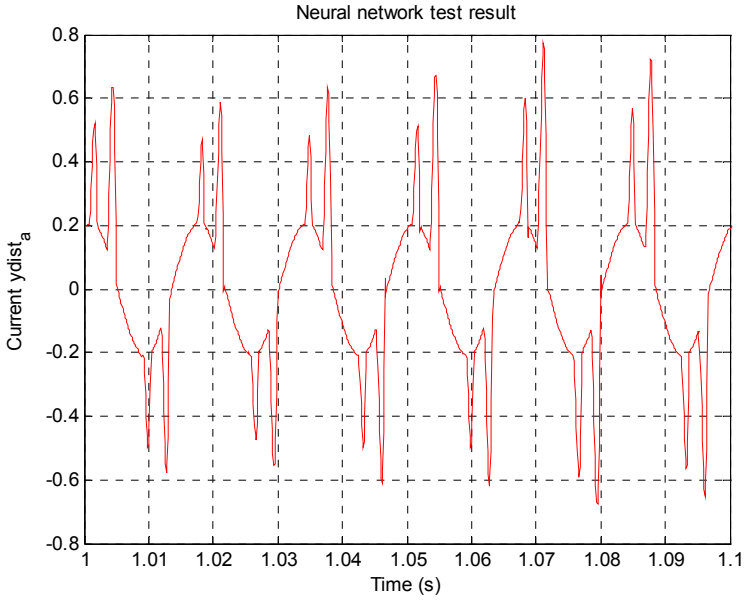

Figure 6.10 True phase A current waveform of the drive as predicted by ESN2

Once ESN1 has learned the admittance of the phase A of the VSD, the weights of ESN1 are transferred to ESN2. ESN2 is supplied with a clean sine wave voltage. The output of ESN2 is $\hat{i}_{a-dist}$ and Figure 6.10 shows what Figure 6.4 would have looked like if it were possible to isolate the VSD and supply it from a pure sine wave.

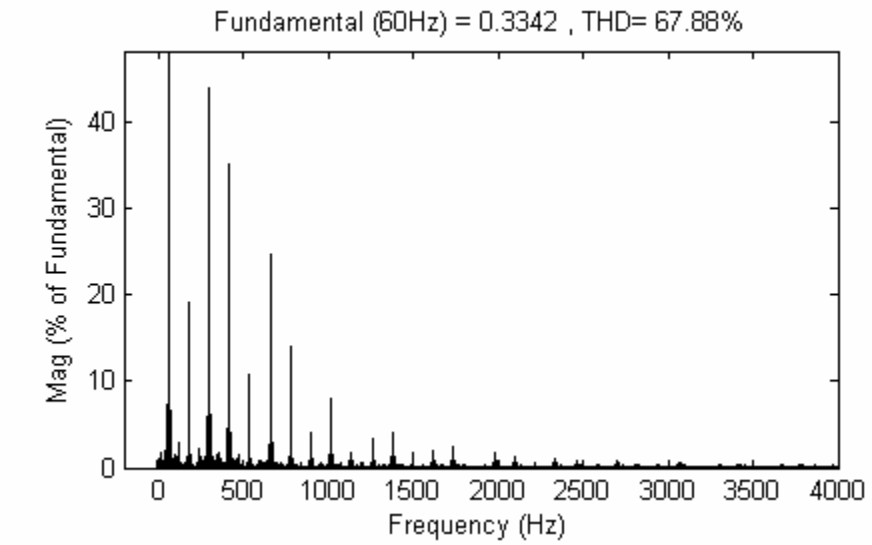

Figure 6.11 FFT spectrum of $\hat{i}_{a-dist}$ indicate a THD of 67.88%

Figure 6.11 shows the FFT spectrum of Figure 6.10. The true current distortion of $\hat{i}_{a-dist}$ is therefore 67.88% (instead of the 74.27% of Figure 6.6). This result agrees well with the measured value of 68.5% of Figure 6.7 where the VSD was supplied by a 0.2% distorted voltage.

Similar to phase A, the scheme is also applied to phase B and phase C of the VSD. Figure 6.12 shows the training result for Phase B. Figure 6.13 shows the training result for Phase C.

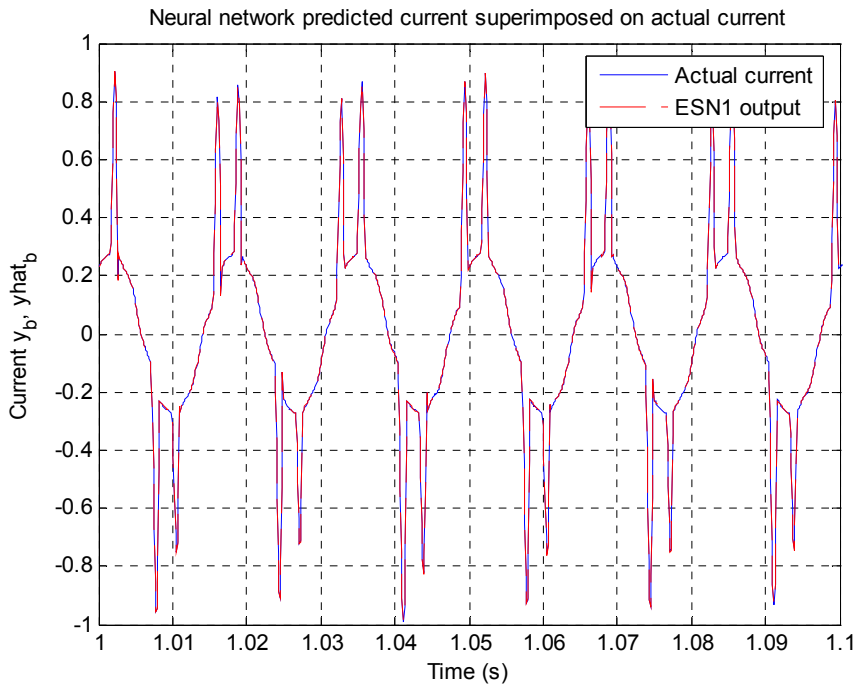

Figure 6.12 ESN1output superimposed on actual phase B drive current

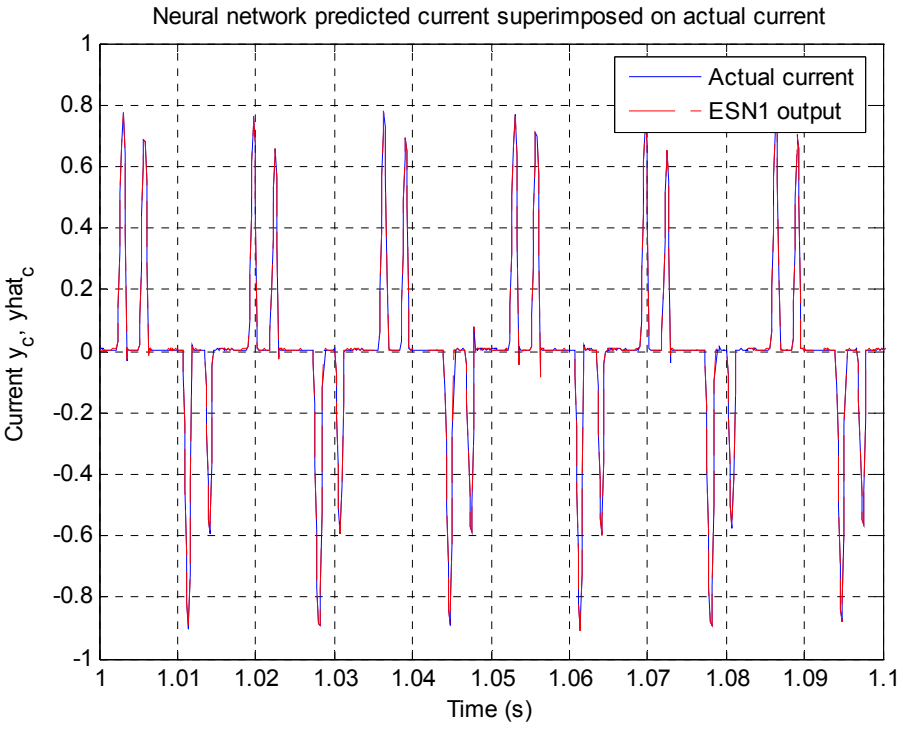

Figure 6.13 ESN1output superimposed on actual phase C drive current

The parameter e_m introduced in chapter 4 is computed for all three phases and the results are summarized in Table 6.1.

Table 6.1: Summary of ESN Experimental Results

Phase	THD_d (Utility Supply) (Current)	THD_s (ESN2 Output) (Current)	THD_{CI} (Clean Supply) (Current)	e_m
A	74.27%	67.88%	68.5%	-9.41%
B	59.67%	49.02%	47.72%	-21.73%
C	152%	132.27%	132.47%	-14.92%

THD_d is the i_{THD} from a distorted v_{pcc} ,and THD_s is the i_{THD} from a mathematical sine wave, i.e. the output of ESN2. e_m can be $\pm$ depending on the type of load and the condition of the network. THD_{CI} is the distortion in the current with the switch S in position 2. This value is used for validating of the results obtained using the proposed scheme. Closeness of the value of THD_s to THD_{CI} is an indicator of the training performance of the ESN.

In an actual implementation of the proposed scheme, the value of THD_{CI} will not be required since it is not used in the training algorithm and nor will such a value be available in any real power system application.

The dominant current harmonics in power electronics loads are the 5^{th}, 7^{th}, 11^{th} and the 13^{th}. For applications like Dominant Harmonic Active Filtering [140], it may be of interest to use individual harmonic current distortion in e_m instead of the overall

harmonic current distortion. Table 6.2 shows the value of e_m for each dominant harmonic, computed from the experimental result of the variable speed drive current i_{drvA}.

Table 6.2: True Magnitude of Dominant Current Harmonics as Predicted by ESN2

Phase A of VSD	THD_d (Utility Supply) (% of Fundamental)	THD_s (ESN2 Output) (% of Fundamental)	$e_m = \left(\frac{THD_s - THD_d}{THD_s} \right)$
5th Harmonic	41.98%	43.69%	3.91%
7th Harmonic	38.22%	35.00%	-9.20%
11th Harmonic	29.44%	24.35%	-20.90%
13th Harmonic	20.02%	13.86%	-44.44%

6.6 Discussion on ESN Convergence

The above experiments show an important aspect of ESN training. The trained ESN closely approximates the actual output after the initial transient dynamics have washed out, which are caused by the initial untrained and random network starting state. Hence the training performance of the ESN is judged after the initial transients have passed. Depending on the ESN size and the sampling rate of the input data, typical range for the initial transients is about 10 cycles of the input data.

Sometimes with switching power electronic loads, the initial transients may be a problem. However with the present experiment, this problem does not arise.

The gradient descent algorithms are difficult to use with ESNs. The performance of this algorithm depends critically on the eigenvalue spread of the cross-correlation matrix R.

$$R = E[d(n)d(n)^T] \tag{6.11}$$

where $d(n)$ is the network's internal state.

The eigenvalue spread s of the cross-correlation matrix R is defined as;

$$s = \frac{\lambda_{\max}(R)}{\lambda_{\min}(R)} \tag{6.12}$$

When the eigenvalue spread is large, the LMS algorithm converges slowly and becomes inefficient. The adaptation of the spread of the cross-correlation matrix R to permit the use of gradient descent algorithms, without compromising the training performance, is still an important area of research [132].

Adapting ESN for online training is an issue which needs investigation; however preliminary results do indicate that ESNs could be used in the proposed methods. ESNs have fast convergence times compared to other neural network topologies [130].

6.7 Summary

This chapter investigates the application of a new kind of recurrent neural network called Echo State Networks (ESNs) for the problem of measuring the actual amount of harmonic current injected into a power network by a nonlinear load. The learning ability of an ESN is demonstrated by training it to identify the nonlinear characteristics of a VSD. The principles of ESN are based on the use of a Recurrent

Neural Network (RNN) as a dynamic reservoir. In order to compute the desired output dynamics, only the weights of connections from the reservoir to the output units are calculated. This is simply a linear regression problem. The size of the dynamic reservoir is kept similar to that of the hidden layer of the neural network topologies used in chapters 4 and 5. Issues of online training of ESNs still need some investigation. However the advantage of using ESNs lies in the fact that they provide a simpler method to train a RNN and the feasibility of using the dynamic reservoir with much higher number of neurons as compared to MLPNs or RNNs.

CHAPTER 7

ACTIVE FILTER APPLICATION

7.1 Introduction

The increased use of modern power electronics technologies by industries has resulted in an increase of harmonic distortion in the industrial power system in recent years. The improved efficiency and productivity provided by adjustable-speed drives (ASD), uninterruptible power supplies (UPS), etc is offset by the fact that the utility grid is being disturbed by these equipments because of their rectifier front ends. The switching nature of these rectifiers results in a pulsed input current with high harmonic content. Classic utility-side symptoms of harmonics problems are distorted voltage waveforms, blown shunt capacitor fuses, and transformer overheating. Capacitor losses are sensitive to harmonic voltages. Transformer losses are sensitive to harmonic currents.

With the increasing use of power factor correction capacitors installed in the grid for reactive power compensation and the inductance of the lines and transformers, severe *L-C* resonances may be triggered by the harmonic current generated by nonlinear loads. The harmonic current also causes higher losses in the lines and transformers of the utility grid. Harmonic standards, such as the IEEE 519, are strongly recommended by the utilities to alleviate such problems.

Passive *L-C* filters have been the traditionally preferred harmonic filtering solution mainly for their high efficiency, low-cost and simplicity. However, *L-C* filters are susceptible to source-sink resonances [133]. *L-C* filters also attract harmonic current

from ambient harmonic-producing loads and background distortion of grid voltages [134]. Filter loading due to background distortion is a key design issue [135]. The filter characteristics are affected by component tolerances, and the varying utility system impedances in case of system configuration changes and contingencies. Further, a stiff utility grid poses great difficulties for *L*-*C* filter design because sharp and precise tuning is required to sink a significant percentage of the load harmonic current. With all these problems, *L*-*C* filters may not meet the IEEE 519 standard.

Divan, Bhattacharya et al. [136] have been instrumental in proposing active filter systems have been proposed to mitigate harmonic current of industrial loads. Pure series and shunt active filters are suitable for small-rating nonlinear loads. Hybrid series and hybrid shunt active filters, which are characterized by a combination of passive *L*-*C* filters and active filters, are cost effective and practical for large-rated nonlinear loads. Active filtering implemented with pulse width modulated inverters provides good harmonic mitigation. However, a key issue for active filters is to find a control method, which quickly obtains the compensation reference current without errors. The control has two main blocks: the first one generates the control reference signals and the second one carries out the control method. It is, therefore, crucial to be able to recognize the harmonic components in a waveform and to reduce them to an acceptable level.

The research literature has identified two groups of spectrum estimation techniques from a data set. The simplest group of approaches uses Fourier based algorithms (FFT and DFT). These algorithms have certain limitations as listed in [137]. The second group of approaches employs more sophisticated techniques like wavelet transforms to track harmonics accurately, but involves complex computational processes [138]. A third trend

has emerged over the past couple of years regarding the use of neural network techniques for the control of active filters [139]. The authors of [140] have proposed a system that achieves harmonic isolation at the dominant harmonic frequencies, i.e., at the fifth and seventh harmonics (for six-pulse rectifier front ends), using square-wave inverters.

This chapter focuses on the generation of the control reference signal using a MLPN with backpropagation training algorithm. The synchronous reference frame based harmonic isolation method is integrated within the neural network to extract the dominant harmonics. The proposed method is demonstrated on a three phase thyristor controlled DC drive.

7.2 Synchronous Reference Frame

The application of synchronous reference frame (SRF) based harmonic extraction was introduced in [141]. A description of the method as used in this thesis is briefly introduced. The three phase currents i_a, i_b and i_c are transformed from three phase abc reference frame to two phase $d^s - q^s$ stationary reference frame currents i_d^s and i_q^s using;

$$\begin{bmatrix} i_d^s \\ i_q^s \end{bmatrix} = \sqrt{\frac{2}{3}} \begin{bmatrix} 1 & -\frac{1}{2} & \frac{1}{2} \\ 0 & \frac{\sqrt{3}}{2} & -\frac{\sqrt{3}}{2} \end{bmatrix} \begin{bmatrix} i_a \\ i_b \\ i_c \end{bmatrix} \tag{7.1}$$

The currents i_d^s and i_q^s are now transformed to a synchronously rotating $d^e - q^e$ reference frame by the unit vectors $\cos\omega_e$ and $\sin\omega_e$ as shown below;

$$\begin{bmatrix} i_q^e \\ i_d^e \end{bmatrix} = \begin{bmatrix} \cos\omega_e & -\sin\omega_e \\ \sin\omega_e & \cos\omega_e \end{bmatrix} \begin{bmatrix} i_q^s \\ i_d^s \end{bmatrix} \tag{7.2}$$

The frequency ω_e is derived from the harmonic order that needs to be isolated. It is important to note that the direction of the unit vector rotation has to comply with the sequence of the harmonic extracted. Figure 7.1 shows the transformation from abc to $d^e - q^e$ reference frame.

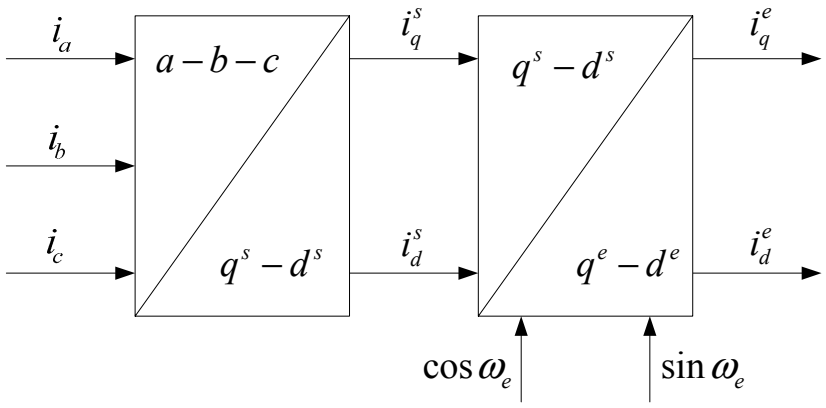

Figure 7.1 Block diagram showing abc to $d^e - q^e$ transformation

In the $d^e - q^e$ reference frame, components of ω_e appear as DC quantities and all other harmonics are transformed to non DC quantities. Using a low pass filter, the DC quantity can be accurately extracted. The DC component of the current is now retransformed back to the stationary reference frame using;

$$\begin{bmatrix} i_q^s \\ i_d^s \end{bmatrix} = \begin{bmatrix} \cos\omega_e & \sin\omega_e \\ -\sin\omega_e & \cos\omega_e \end{bmatrix} \begin{bmatrix} i_q^e \\ i_d^e \end{bmatrix} \tag{7.3}$$

Finally the components from the stationary reference frame are transformed back to three phase reference frame;

$$\begin{bmatrix} i_a \\ i_b \\ i_c \end{bmatrix} = \sqrt{\frac{2}{3}} \begin{bmatrix} 1 & 0 \\ -\frac{1}{2} & \frac{\sqrt{3}}{2} \\ -\frac{1}{2} & -\frac{\sqrt{3}}{2} \end{bmatrix} \begin{bmatrix} i_q^s \\ i_d^s \end{bmatrix} \tag{7.4}$$

Since a DC quantity in the $d^e - q^e$ reference frame exactly corresponds to the harmonic frequency of interest, extraction of the DC quantity by using the low pass filter ensures exact synthesis of the harmonic current in the *abc* reference frame. Figure 7.2 shows the filtering scheme.

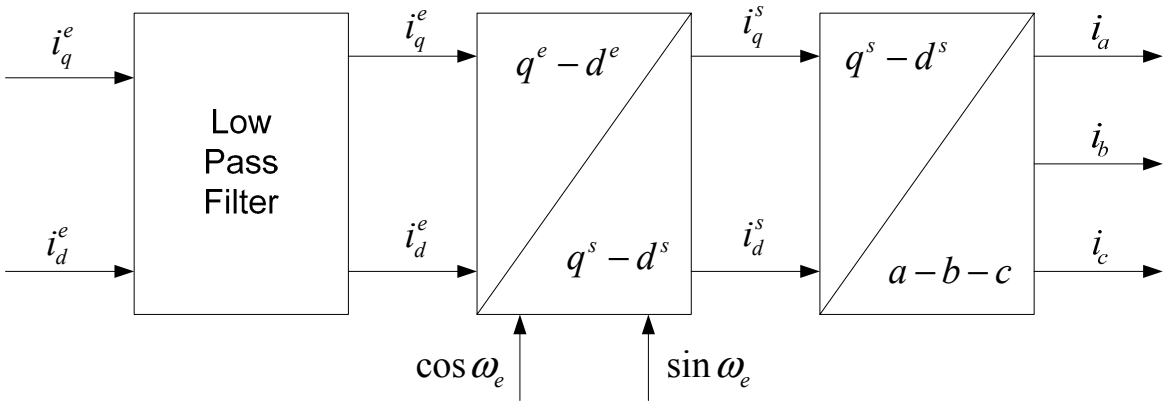

Figure 7.2 Block diagram showing $d^e - q^e$ to *abc* transformation

7.3 Proposed Scheme for Harmonic Isolation

A neural network based identifier is used to isolate the dominant harmonics from the rest of the current spectrum of a load. These isolated harmonics are then used with any standard active filter control scheme to mitigate the harmonics. A one-line diagram of a three-phase supply network having a sinusoidal voltage source v_s, network impedance L_s, R_s and several loads (one of which is nonlinear) connected to a PCC is shown in Figure 7.3.

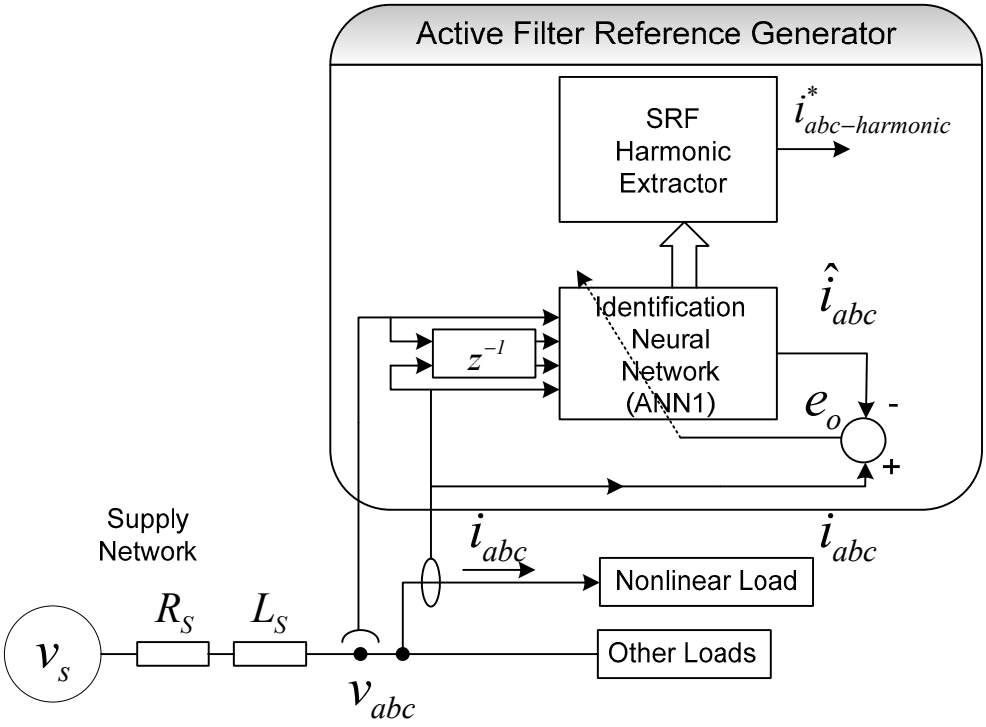

Figure 7.3 Proposed method for harmonic extraction

The nonlinear load injects distorted line current i_{abc} into the network. A MLPN is trained to identify the nonlinear characteristics of the load. This neural network is called the Identification neural network (ANN1) and is the same as the ANN1 described in chapter 4.

7.3.1 Training ANN1

The proposed method measures the instantaneous values of the three voltages v_{abc} at the PCC, as well as the three line currents i_{abc} at the k^{th} moment in time. The voltages v_{abc} can be line-to-line or line-to-neutral measurements. The neural network is designed to predict the one step ahead line current $\hat{i}_{abc}$ as a function of the present and delayed voltage vector values $v_{abc}(k)$, $v_{abc}(k-1)$ and $v_{abc}(k-2)$ as well as present and

delayed current vector values $i_{abc}(k)$, $i_{abc}(k-1)$ and $i_{abc}(k-2)$. When the $(k+1)^{th}$ moment arrives (at the next sampling instant), the actual instantaneous values of i_{abc} are compared with the previously predicted values of $\hat{i}_{abc}$, and the difference (or error e_o) is used to train the ANN1 weights (see appendix E for details). Initially the weights have random values, but after several sampling steps, the training soon converges and the value of the error e_o diminishes to an acceptably small value.

7.3.2 SRF Extractor

The method described in section 7.2 is used to extract the dominant harmonic components from the rest of the predicted current $\hat{i}_{abc}$. The extracted dominant harmonic current $i^*_{abc-harmonic}$ can now be used as the reference for any active filter algorithm. Many advanced current controller techniques exist for generating the compensating currents, however if the precise harmonic amplitude and phase is not extracted, harmonic compensation may not be successful.

7.4 Simulation Results

The proposed scheme of Figure 7.3 is applied to a simulated DC motor represented by a simplified RL-E model is fed from an inductive three-phase source through a six-pulse thyristor bridge. A pulse generator synchronized to the source voltages provides the trigger pulses for the six thyristors. The converter output current is controlled by a PI current regulator. The scheme is shown Figure 7.4.

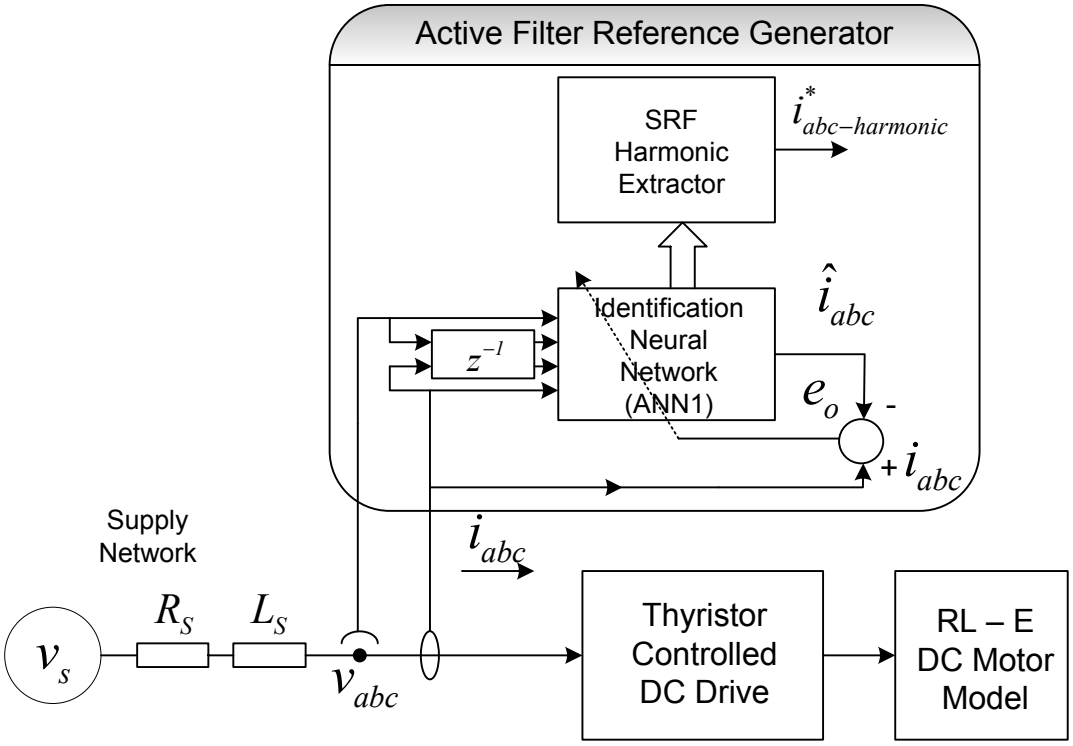

Figure 7.4 Harmonic extraction scheme applied to a DC drive

ANN1 is trained under various operating conditions of the dc drive. Once trained, ANN1 is tested with twenty cycles of voltage and current, with the 30 % step change applied to the drive reference current during the 10th cycle. This is done to test the dynamic response of the drive's current regulator and the ability of the neural network to identify such changes in current. Data acquisition rate is set at 512 samples per cycle. The output of ANN1 correctly tracks the actual current i_{abc} as shown in Figure 7.5. ANN1 quickly adapts to the step change, within 1 cycle, and keeps tracking the new current. This is one of the advantages of continual online training.

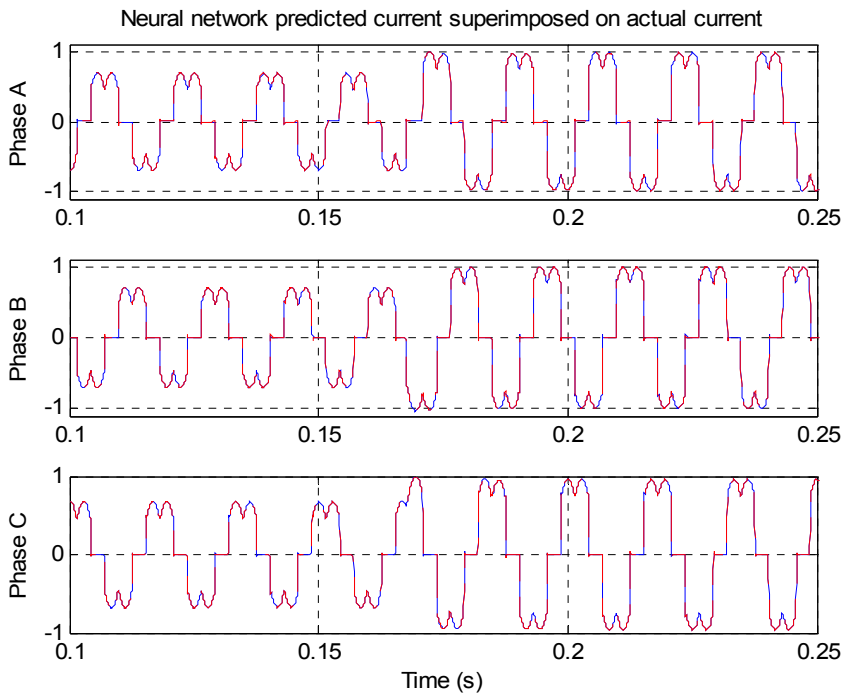

Figure 7.5 ANN1output superimposed on actual current to indicate convergence

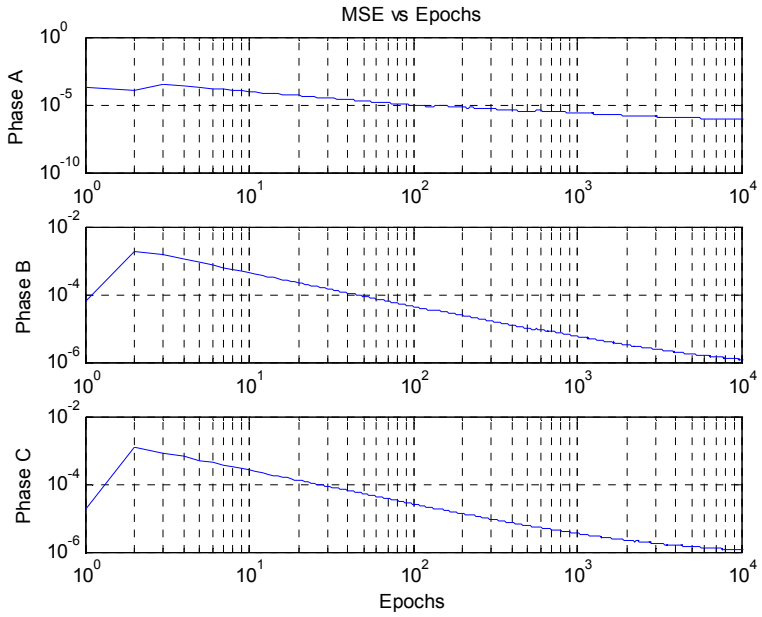

Figure 7.6 Training performance of ANN1 in terms of MSE

The training of the network continues until an acceptably small value of the MSE is reached as illustrated in Figure 7.6 for all three phase currents. For each phase, the final MSE value is less than 10^{-5} which is sufficiently small to indicate that the identification neural network is trained and has learned the load characteristics.

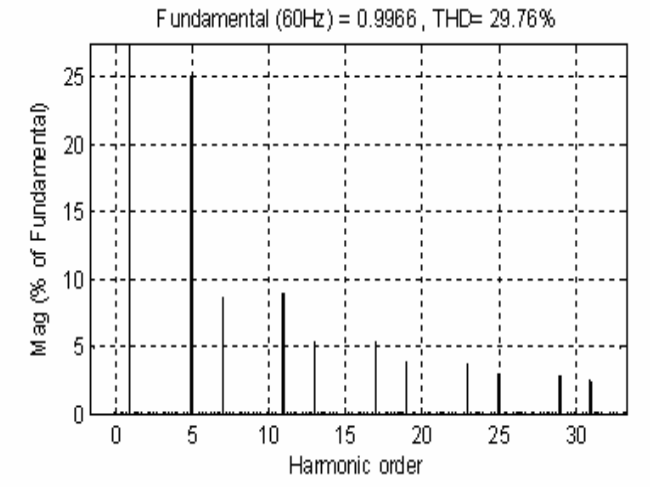

Figure 7.7 FFT spectrum of phase A current indicates a THD of 67.88%

Figure 7.7 shows the FFT spectrum of the phase A load current obtained using the powergui block of SIMULINK. At this point, the of the ANN1 is passed to the SRF Harmonic Extractor block in Figure 7.4. The performance of the SRF based control method is demonstrated by extracting the 5th and the 7th harmonics and comparing it with the values obtained from Figure 7.7. The i_{d5}^{e} and i_{q5}^{e} waveform is shown in Figure 7.8. Figure 7.9 shows the 5th harmonic current retransformed back in the *abc* reference frame.

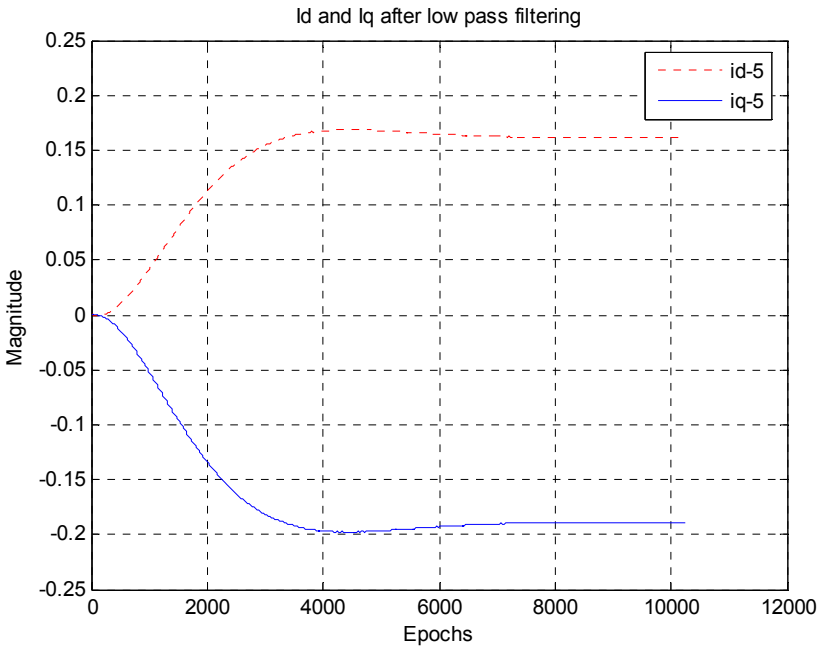

Figure 7.8 Fifth harmonic i_{d5}^{e} and i_{q5}^{e} after low pass filtering

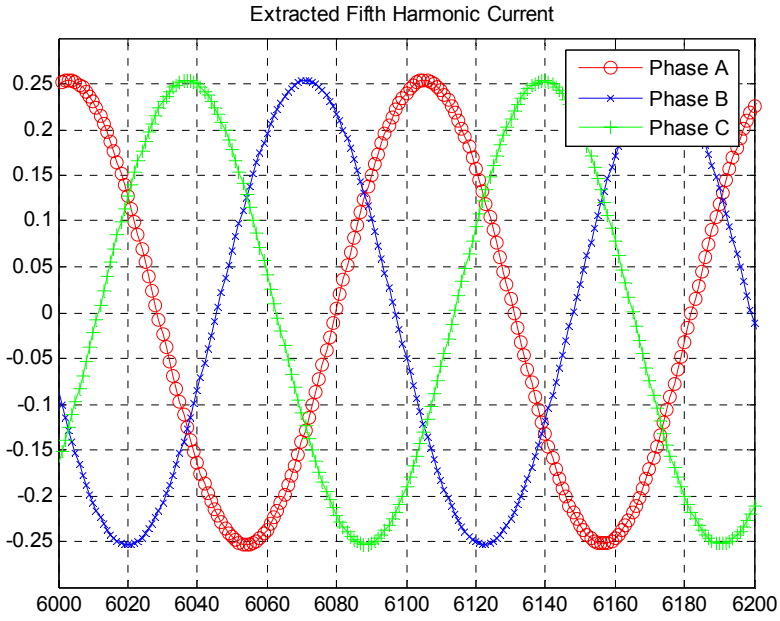

Figure 7.9 Fifth harmonic current in the *abc* reference frame

Extending the method, all the dominant harmonics can be extracted. Figure 7.10 and Figure 7.11 shows the result for the 7th harmonic current.

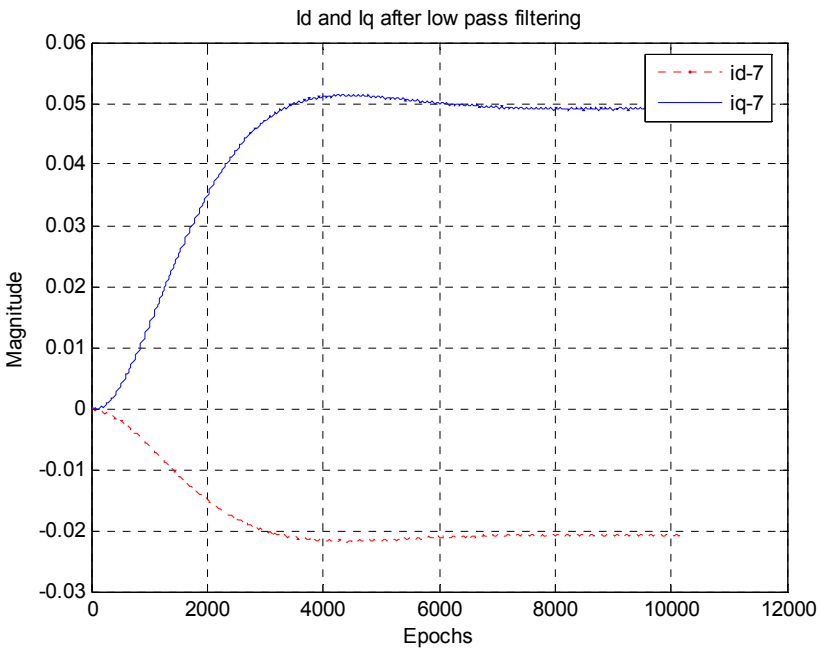

Figure 7.10 Seventh harmonic i_{d7}^{e} and i_{q7}^{e} after low pass filtering

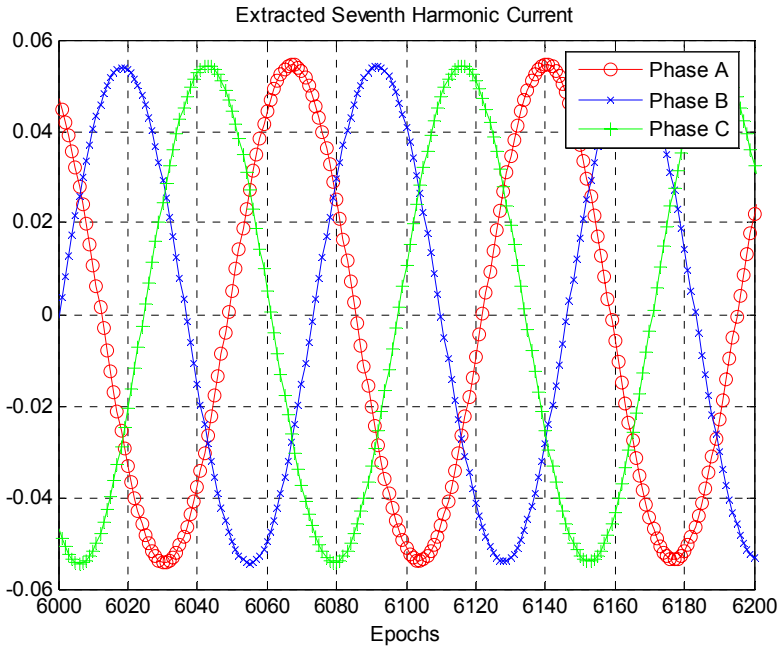

Figure 7.11 Seventh harmonic current in the *abc* reference frame

The harmonic current amplitude and phase values can now be used to generate the reference for the active filter. Table 7.1 provides the magnitude and phase values for the dominant harmonics, namely, 5^{th}, 7^{th}, 11^{th} and 13^{th}. The magnitude values are normalized. Comparison of these results with those from Figure 7.7 reveals that the neural network is able to extract the dominant harmonics accurately.

Table 7.1: Dominant Harmonics Amplitude and Phase Extraction

Harmonic	Phase A	Phase B	Phase C
5^{th} - Mag	0.2596 A	0.2642 A	0.2230 A
5^{th} - Phase	-132.2°	-12.3°	107.8°
7^{th} - Mag	0.0557 A	0.0568 A	0.0477 A
7^{th} - Phase	-110.5°	-9.55°	-129.0°
11^{th} - Mag	0.0843 A	0.0857 A	0.0725 A
11^{th} - Phase	36.26°	156.1°	-83.8°
13^{th} - Mag	0.0404 A	0.0412 A	0.0345 A
13^{th} - Phase	-86.09°	153.5°	33.86°

7.5 Summary

The increased use in recent years of nonlinear devices in industry has resulted in the increase of harmonic distortion in the industrial power system. The significant harmonics are almost always 5^{th}, 7^{th}, 11^{th} and the 13^{th} with the 5^{th} harmonic being the

largest in most instances. Active filter systems have been proposed by others to mitigate harmonic currents injected by the industrial loads. The most important requirement for any active filter is the precise detection of the individual harmonic component's amplitude and phase. Fourier transform based techniques provide an excellent method for individual harmonic isolation, but it requires a minimum of two cycles of data for the analysis, does not perform well in the presence of subharmonics which are not integral multiples of the fundamental frequency and most importantly introduces phase shifts in the harmonic components of the current.

To overcome these difficulties, this chapter proposed has proposed the use of a MLPN with back-propagation training to identify the harmonic characteristics of a nonlinear load. The operating principle of the synchronous-reference-frame-based harmonic isolation has been discussed. This proposed method has been applied to a thyristor controlled dc drive to obtain the simulated amplitude and phase of the dominant harmonics.

CHAPTER 8

CONCLUSIONS AND FUTURE WORK

8.1 Conclusions

Standards like IEEE 519 provide guidelines for controlling harmonic distortion levels that divide the responsibility between the utility and the customer. The utility has to maintain voltage distortion at the PCC below the specified limits and the customer has to limit the amount of harmonic current injection onto the utility system. However, disputes may arise between utilities and customers regarding who is responsible for the harmonic distortions due to the lack of a reliable single index which can precisely point out the source of the harmonic pollution. This thesis specifically addresses two important issues in this regard.

The fundamentals of harmonic studies and the related issues are reviewed in chapters 1 and 2. A detailed literature survey is presented to summarize the state of the art techniques that are pertinent to the methods proposed in this research.

Chapter 3 considers different neural network architectures, fundamentals of the algorithms used for the neural network training and their suitable adaptation to the problem in hand.

Chapter 4 explains the theoretical aspects of load modeling by neural networks. The proposed load modeling scheme is verified on a number of different power electronic circuits. It is shown that there is a difference in the current distortion of a load depending on whether the load is served by a clean voltage supply or a distorted voltage supply.

Validation of the results is established by supplying the test circuits from a California Instruments clean power source with no distortion.

Chapter 4 also introduces the dual of the load modeling scheme which is referred to as source modeling. The proposed source modeling scheme is verified in principle on a simulation circuit with two nonlinear loads. It is shown that the harmonic currents injected by a thyristor drive cause the voltage at the PCC to exceed the prescribed IEEE 519 limits. The proposed source modeling tool predicts the voltage distortion at the PCC if the thyristor drive was replaced by a clean sine wave current source. Validation of the source modeling scheme is established by comparing the voltage distortion at the PCC predicted by the neural network with a clean sine wave current input and the voltage measured at the PCC by replacing the thyristor drive by a clean current source in the simulation circuit.

Chapter 5 focuses on the feasibility of applying the proposed load modeling concept using actual field measurements without disrupting the operation of the customer. Measurements are taken at a site of a particular customer, and the results show the true impact on load current distortion due to changes in the distribution network. For this particular customer the predicted current distortion by the neural network, when the customer is assumed to be supplied with a clean sine wave voltage, is lower than the actual measured current distortion by a margin of approximately 20 % (phase A reduces by 23 %, phase B reduces by 21 % and phase C reduces by 17 %).

The reduction in the 7^{th} harmonic component is the principal factor responsible for the overall current THD reduction. Changes, as high as 63 %, in the B phase 7^{th} harmonic current is observed. The excess current distortion observed in the actual

measured current can be attributed to the source in this particular case. The load modeling scheme aids the detection of the true harmonic current distortion that can be attributed to a customer.

This thesis also introduces the theory for Echo State Networks in Chapter 6. ESNs are recently proposed for modeling complex dynamic systems and they are considered here because they provide a simple, yet power approach to calculate the output weights of a the network as against traditional the traditional approach of training the input and output weights of the network. The principles of ESN are based on the use of a RNN as a dynamic reservoir. A large (order of 100s of neurons) RNN is used as a "reservoir" of dynamics which can be excited by suitably presented input and/or feedback output. The connection weights of the reservoir network are not changed by training. In order to compute the desired output dynamics, only the weights of connections from the reservoir to the output units are calculated. This is simply a linear regression problem.

Online training of ESNs is an issue which needs to be resolved; however preliminary experimental results do indicate that ESNs could be used in the proposed scheme. ESNs demonstrate faster convergence times compared to other neural network topologies in identifying the nonlinear load admittance.

Chapter 7 proposes a possible application of the load modeling and source modeling schemes in the area of harmonic filtering. The precise detection of the individual current harmonic component's amplitude and phase is a necessity for any active filter control technique. To achieve the same, the characteristics of a nonlinear load are modeled using a MLPN. The output of the MLPN, which is the current injected by the nonlinear load into the power distribution network, is passed through a

synchronous-reference-frame block to isolate the dominant harmonics present in the nonlinear load current. The isolated harmonic currents can now be used as the compensation current reference. This proposed method is applied to a thyristor controlled dc drive to obtain the accurate amplitude and phase values of the 5^{th}, 7^{th}, 11^{th} and the 13^{th} harmonic currents.

The load modeling and source modeling methods proposed in this research avoids disconnecting or disrupting the operation of any loads from the system. The information provided by the load modeling scheme regarding the true harmonic current of a load could be used to penalize the offending customer. Experimental results confirm that an error in the measurement is made if the calculation of current THD is done by simply measuring the actual current of a nonlinear load. The information provided by the source modeling scheme regarding the impact on the voltage distortion level at the PCC, if the nonlinear load were to clean up its harmonic current, could be used to determine quantitatively the detrimental effect of a nonlinear load current on the voltage at the PCC.

On a practical system the neural network computations could be carried out on a DSP. A suitable A/D interface is required for acquiring the measured values of voltages and currents. Such a system could be installed permanently or be portable from one customer to another in order to simply monitor pollution levels at a particular PCC in the network.

8.2 Contributions

The new novel contributions of this research to the field of power engineering are summarized as follows:

- An elaborate step-by-step procedure is presented (Chapter 4) for implementing a neural network based identifier for identifying the characteristics of a nonlinear load using MLPN and RNN. It is further shown that the trained network could predict the true harmonic current distortion of a nonlinear load which is different from the actual measured current distortion of the nonlinear load.

- The presented experimental results have shown that there is a difference in the current distortion of a load depending on whether the load is served by a clean supply or a distorted supply. To quantify this difference, the index e_m is introduced. The values of e_m illustrate that this error could be positive for some loads and negative for others. Single-phase power electronic loads generate a great amount of triplen harmonics, and triplen harmonics are zero sequence. Three phase power-electronic loads on the other hand, do not generate triplen harmonics. Nontriplen harmonics generated by various single and three-phase loads are likely to have diversity effects due to phase cancellations and attenuation effects that cause the distortion variation in the PCC voltage. This explains why the index e_m is either positive or negative. One important finding from the above results shows that it is erroneous to reason intuitively that the current THD, when supplied from a distorted v_{pcc} should always be higher than if the v_{pcc} had no distortion.

- An elaborate step-by-step procedure is presented (Chapter 4) for implementing a neural network based identifier for predicting the change in

voltage distortion at the PCC if a nonlinear load was replaced by a current source with only fundamental and no harmonics, referred to as source modeling.

- The proposed methods of load modeling and source modeling are applied to actual field data (Chapter 5). The feasibility of training neural networks with snapshot data was established. Data from different commercially available meters are used for training the neural networks. Establishing a pure sinusoidal voltage at the PCC is not always feasible. Hence, for validating the site result, utility switching is performed to change the system impedance characteristics.

- The theory of Echo State Networks was introduced (Chapter 6). This is a new area of research and preliminary work has suggested that ESN could be used for the proposed work in this thesis.

- A neural network based scheme has been proposed to model the nonlinear characteristics of a load and further isolate the dominant harmonics of the load. This information could be used for generation of current reference in any standard active filter control algorithm (Chapter 7).

- This research has resulted in two patents, one issued and one pending [142], [143].

- Most of the work in this thesis has already been published or accepted for publication as one journal paper, three journal paper submissions and fourteen accepted conference papers of the various IEEE Societies [151]-[168].

8.3 Recommendations and Future Work

8.3.1 Generation of Impedance Plots

Generation of correct impedance versus frequency plots for a feeder circuit shows up any resonances present in the supply network. This still remains an important priority for utilities, but at present this has to be calculated from cable, transformer and network data which requires many man-hours to gather from utility field records. A power system itself is not a significant source of harmonics, but it becomes a contributor of problems when a resonance magnifies one or more harmonics.

Assuming all nonlinear loads can be represented as harmonic current injections, the harmonic voltage at each bus in a power system can be obtained by solving the following impedance matrix or nodal admittance equations for all orders of harmonics under consideration:

$$V_h = Z_h \cdot I_h \tag{8.1}$$

or

$$I_h = Y_h \cdot V_h \tag{8.2}$$

where V_h is the vector consisting of the h^{th} harmonic voltage at each bus that is to be determined. Z_h is the system harmonic impedance matrix, Y_h is the system harmonic admittance matrix, and I_h is the vector of measured or estimated harmonic currents representing the harmonic-generating loads at connected busses.

In (8.1) , Z_h can be obtained by using a *Z*-bus building algorithm for each harmonic of interest or from the inverse of Y_h in (8.2), but the harmonic effects on different power system components and loads need to be properly modeled [144]. Approaches for harmonic analysis based on (8.1) or (8.2) are commonly called current injection methods.

Current injection approaches are usually used in conjunction with fundamental frequency load flow computations. Through providing the network harmonic impedance or admittance and harmonic currents injected by nonlinear loads for all harmonics under consideration, the individual and total harmonic voltage distortions at each bus can be determined.

Observing (8.1), it is evident that harmonic impedance plays an important role in the system response to harmonics, especially when resonance occurs in the system. Resonance is defined as an amplification of a power system's response to a periodic excitation when the excitation frequency is equal to a natural frequency of the system. For a simple series LC circuit excited by a harmonic current, the inductive and capacitive reactance seen from the harmonic current source are equal at the resonant frequency f_r

$$f_r = \frac{1}{2\pi\sqrt{LC}} \tag{8.3}$$

In a power system, most significant resonance problems are caused by a large capacitor installed for displacement power factor correction or voltage regulation purposes. The resonant frequency of the system inductive reactance and the capacitor reactance often occurs near the fifth or seventh harmonic. However, resonant problems

occurring at eleventh or thirteenth harmonic are not unusual. There are two types of resonances likely to occur in the system:

- Series resonance and Parallel resonance.

Series resonance offers low impedance to the flow of harmonic current, and parallel resonance offers high impedance to the flow of harmonic current.

Series Resonance

As shown in Figure 8.1, if the capacitor bank is in series with the system reactance and creates a low impedance path to the harmonic current, a series resonance condition may result. Series resonance may cause high voltage distortion levels between the inductance and the capacitor in the circuit due low impedance path to the harmonic currents. Series resonance often causes capacitor fuse failures because of overload. The series resonant condition is given by

$$h_r = \sqrt{\frac{X_C}{X_L}} \tag{8.4}$$

where h_r is the harmonic order of the resonant frequency.

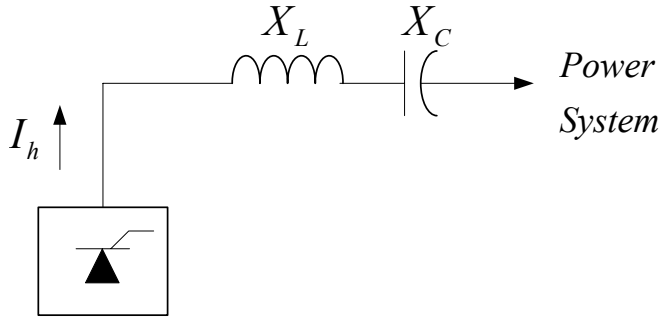

Figure 8.1 Series resonance circuit

Parallel Resonance

Figure 8.2 shows the circuit topology in which parallel resonance is likely to occur. Parallel resonance occurs when the parallel inductive reactance and the parallel capacitive reactance of the system are equal at a certain frequency, and the parallel combination appears to be a large impedance to the harmonic source. The frequency where the large impedance occurs is the resonant frequency. When parallel resonance exists on the power system, significant harmonic volt-drops cause distorted bus voltages. The distorted bus voltage may cause distorted currents flowing in adjacent circuits.

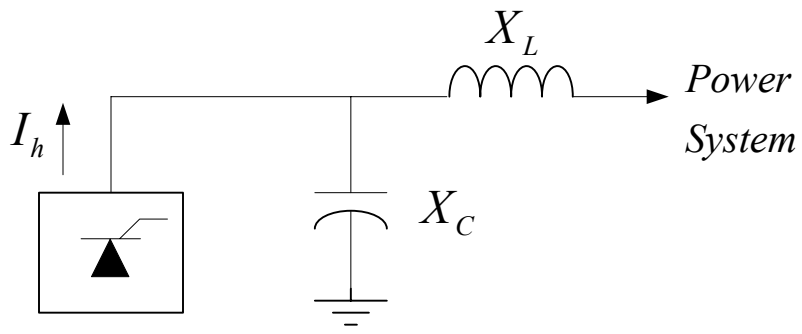

Figure 8.2 Parallel resonance circuit

When parallel resonance occurs in the circuit of Figure 8.2, the resonant frequency can be determined by

$$h_r = \sqrt{\frac{X_C}{X_L}} = \sqrt{\frac{MVA_{SC}}{MVAR_{CAP}}} \tag{8.5}$$

where MVA_{SC} is the short-circuit MVA at the harmonic-generating load connection point to the system and $MVAR_{CAP}$ is the MVAR rating of the capacitor. It

should be understood that this approximation is only accurate for systems with high X/R ratios.

Distributed Resonance

Another resonant scheme is shown in the distribution network of Figure 8.3. If some of the feeder inductance appears between groups of smaller capacitor banks, the system may present a combination of many series and parallel resonant circuits, although the resonant effects are somewhat less than that caused by one large resonant element. For this type of resonance problem, more sophisticated harmonic analysis programs [145] must be employed to predict the harmonic characteristics of the system.

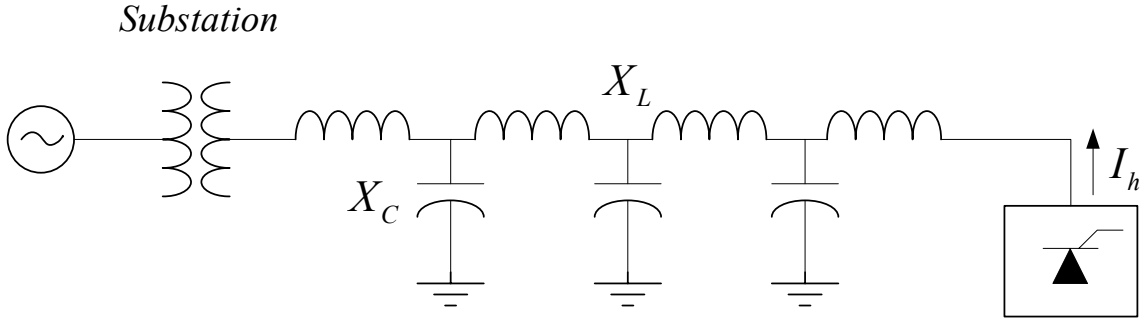

Figure 8.3 Distributed resonance circuit

A neural network can be used to learn the impedance of the feeder circuit. The trained neural network can now be supplied with a sinusoidal current with a frequency varying from 0 Hz to some predefined upper range, say 2.1 kHz. Dividing the output voltage of the neural network with its input current is the impedance of the feeder circuit. Creating a Bode plot will now provide the impedance versus frequency property of the feeder circuit. This would also throw some light on the frequency response characteristics of a neural network, which has not yet been investigated in great detail.

Some other recommendations can be made for continuing studies in this research field. These can be classified into two groups, namely theoretical/simulation and experimental recommendations.

8.3.2 Other Recommendations for Theoretical Work

The theoretical grounds for designing a harmonic monitoring meter for predicting the true harmonic current of a nonlinear load has been established through this research. The approach discussed in Chapter 6 needs a more detailed study and simulation. Especially the online training capability of ESNs needs to be established. From a theoretical perspective, three specific studies are suggested:

- Using algorithms like Particle Swarm Optimization (PSO) to find the optimum parameters of ESN.
- Using the concept of Echo States to design the hidden layer of MLPN and use online training to update only the output weights.
- Instead of computing the output weights of an ESN, use online training to train the output weights.

8.3.3 Recommendations for Experimental Work

The implementation of the load modeling and source modeling scheme in a commercially available power quality meter and evaluating its performance on a real-time basis would show the practicality of the proposed scheme for power engineers. The load modeling and source modeling schemes should also be implemented as a standalone dedicated hardware for a particular customer or site. This would enable the customer or the utility to have an accurate harmonic profile for a site.

APPENDIX A

IEEE 519 HARMONIC STANDARD

The requirements of current distortion and voltage distortion of IEEE 519 harmonic standard [146] - [150] are given below for reference.

Table A.1 Recommended practice for individual customers for voltages < 69 kV

Utility Voltage Limits < 69 kV						
Individual harmonic				Voltage THD		
3%				5%		
Customer Current Limits						
I_{SC} / I_L	$h < 11$	$11 \le h < 17$	$17 \le h < 23$	$23 \le h < 35$	$h \ge 35$	*TDD*
<20	4%	2%	1.5%	0.6%	0.3%	5%
20 - 50	7%	3.5%	2.5%	1%	0.5%	8%
50 - 100	10%	4.5%	4%	1.5%	0.7%	12%
100 - 1000	12%	5.5%	5%	2%	1%	15%
> 1000	15%	7%	6%	2.5%	1.4%	20%

Table A.2 Recommended practice for individual customers for voltage 69 - 161 kV

Utility Voltage Limits 69 - 161 kV	
Individual harmonic	Voltage THD
1.5%	2.5%
Customer Current Limits	

Table A.2 Continued

I_{SC} / I_L	$h < 11$	$11 \le h < 17$	$17 \le h < 23$	$23 \le h < 35$	$h \ge 35$	*TDD*
<20	2%	1%	0.75%	0.3%	0.15%	2.5%
20 - 50	3.5%	1.75%	1.25%	0.5%	0.25%	4%
50 - 100	5%	2.25%	2%	0.75%	0.35%	6%
100 - 1000	6%	2.75%	2.5%	1%	0.5%	7.5%
> 1000	7.5%	3.5%	3%	1.25%	0.7%	10%

Table A.3 Recommended practice for individual customers for voltage > 161 kV

Utility Voltage Limits > 161 kV						
Individual harmonic			Voltage THD			
3%			5%			
Customer Current Limits						
I_{SC} / I_L	$h < 11$	$11 \le h < 17$	$17 \le h < 23$	$23 \le h < 35$	$h \ge 35$	*TDD*
<50	2%	1%	0.75%	0.3%	0.15%	2.5%
≥ 50	3%	1.5%	1.15%	0.45%	0.22%	3.75%

APPENDIX B

PA-9 POWER PLUS ANALYZER SPECIFICATIONS

- APPLICABLE MEASUREMENT STANDARDS

  EN50160, IEEE 1159, IEEE 519, IEC 61000 SERIES

- VOLTAGE

  Voltage (4 Differential Input Channels)

  Voltage Range: Auto ranging between 20-300; 300-600 Vac/Vdc scales, true RMS through 63rd harmonic

  Voltage Accuracy: ±0.25% of reading ±0.05% of range through 63rd harmonic

- CURRENT

  Current (5 Channels)

  Current Resolution: 0.1% of Full Scale

  Current Accuracy: ±0.25% of reading ±0.05% of range through 63rd harmonic, plus the current probe accuracy

  Current Channels receive 0 to 1 Volt RMS from probes

- CREST FACTOR

  Voltage: 3.5 limited to 1500V peak (does not include impulse)

  Current: 1.4 of Full Scale at peak input

- VOLTAGE/CURRENT CONNECTORS

  V = 4 color coded pairs of safety banana jacks; I=5 Amp miniature circular connector; power provided for flexible CTs

- FREQUENCY

  Fundamental Frequency: 50 Hz or 60 Hz

  Frequency Response: dc to the 63rd harmonic with low pass anti-aliasing

  Filter Frequency Resolution: 0.01 Hz

  Frequency Accuracy: 0.01 Hz at 60 Hz

- SAMPLING RATE

  50/60 Hz: 256 sample/cycle

  Voltage and current for each phase are sampled simultaneously

- CHANNEL TO CHANNEL ISOLATION

  6000 Volts peak on voltage channels

- PHASE ANGLE ERROR

  ±1° referenced to first voltage channel at 60 Hz

- CONTROL

  Silicon rubber keypad, 4 cursor controls with select switch and 6 buttons (home, back, default, record, cursor select, & power on)

- TIME

Real Time Clock: internally maintained and updateable via computer

Time Accuracy: Better than ±0.005%

- POWER SUPPLY

  Primary Input 90-600 Vac, 50/60 Hz, 100-600 Vdc. Powered from channel 1 or auxiliary IEC computer-style power input

- BATTERY

  12 V backup battery included

  Battery Recharge Time: 16 hours

  Run Through Time: 15 minutes, below 90 V ac/110 V dc cutoffs. If recording, resume recording on power restoration

  Data Retention: 10 years with nonvolatile, solid-state flash memory

- ENVIRONMENTAL

  Operating Temperature: -4º to 122º F (-20º to +50º C) ambient temperature

  Humidity: Meets NEMA 4X, rain resistant; 90% noncondensing, not watertight

  Case: NEMA 4X, (IP54), nonconductive, corrosion resistant, rain resistant, not submersible

- COMMUNICATIONS

  RS-232: 3 wire up to 115200 baud rate, DB9 standard

  Modem (optional): Cellular compatible

External RS232 (Optional): For serial port access to instrument data while front lid remains closed

- DISPLAY

  Display Type: Backlit, 5 in. x 1.5 in., 240 x 64 pixels graphic LCD

  Display Operating Temperature: 32º to 122º F (0º to +50º C)

- OPTIONAL CUSTOMER DEFINED STARTUP SCREEN TEXT

  The factory presets two lines of the startup/about screen to customer specific data (i.e. owner contact information, lost/found message, etc.). Each line may contain up to 40 characters of text.

- MEMORY OPTIONS

  Standard: 12 megabytes internal flash

  Optional: Adapter for inserting external and removable compact flash memory cards (includes either a 64 MB or 128 MB card as specified with order)

- PHYSICAL

  Size: Portable — 13 x 10 x 6 in. (330 x 254 x 152 mm)

  Weight: 15 lbs (5.6 kg)

APPENDIX C

ELMAN RNN EXECUTION CYCLE COMPUTATIONS

A complete breakdown of the computations required for one Elman RNN execution cycle with a truncation depth of zero is shown below in Table C.1. The equations are in the same sequence as in Table 3.1. This makes the comparison between MLPN and RNN simpler to visualize. All the equations are in vector form. Most of the computations involve either addition or multiplication. Evaluation of the sigmoidal function is the only computationally demanding task.

Table C.1 Elman RNN Execution Cycle Computation

Equation	Multiplication	Addition	Sigmoidal
(3.1)	m(m+n)	m(m+n)	0
(3.2)	0	0	m
(3.3)	m	m	0
Forward Propagation	m(m+n+1)	m(m+n+1)	m
(3.4)	0	1	0
(3.5)	m	m	0
(3.6)	2m	0	0
(3.7): ΔV	2m+1	m	0
(3.7): ΔW	m(2m+2n+1)	m(2m+2n+1)	0
(3.8)	0	m(m+n)+m	0
Error Backpropagation	~m(2m+2n+5)	~2m(m+n+1)	0

APPENDIX D

CALIFORNIA INSTRUMENTS 5001 IX SPECIFICATIONS

The CI 5001ix AC power source referred to as HG in chapter 4 has been used as the pure sinusoidal voltage source for validating the load modeling results. The specifications of the power source are given below.

Output Specifications

Modes	AC, DC, AC+DC
Frequency	DC, 16 Hz - 500 Hz DC, 16 Hz - 819 Hz with -160 and/or -ABD option Supplemental specs.
Load regulation	± 0.5% DC to 100 Hz ± 0.6% 100 Hz to 500 Hz in high voltage range ± 2.2% 100 Hz to 500 Hz in low voltage range
Line Regulation	<± 0.1% for 10% line change
Output Noise (20 kHz to 1 MHz)	<250 mVrms typ. <500 mVrms max.
Harmonic Distortion (linear load)	Less than 1% from 16-66 Hz Less than 2% at 400 Hz
DC Offset	<20 mV
External Modulation depth	0 - 10%

Isolation Voltage	300 Vrms output to chassis
Output Relay	Push button controlled or bus controlled output relay
Output impedance	Programmable Z on 3001ix, 5001ix, 9003ix and 15003ix

Current Capability of 5001ix

Voltage Range	RMS	AC Peak	DC Current
135V	37.0	110.0	26
150V	33.3		23.2
270V	18.5	96.0	13
300V	16.7		11.6

Standard Measurements

Parameter	**Range**	**Accuracy* (±)**		**Resolution***
AC Measurements				
Frequency	16.00 - 500.0 Hz	0.01% + 0.01 Hz		0.01 Hz
		<100 Hz	100 - 500 Hz	
RMS Voltage	0 - 330 V	0.05 V + 0.02%	0.1 V + 0.02%	10 mV

RMS Current	0 - 40 A	0.05 A + 0.02%	0.1 A + 0.02%	1 mA
Peak Current	0 - 120 A	0.05 A + 0.02%	0.1 A + 0.02%	1 mA
Crest Factor	0.00 - 6.00	0.05	0.05	0.01
Real Power	0 - 6 kW	10 W + 0.1%	20 W + 0.1%	1 W
Apparent Power	0 - 6 kVA	10 VA + 0.1%	20 VA + 0.1%	1 VA
Power Factor	0.00 - 1.00	0.01	0.02	0.01

Harmonic Measurements

Parameter	**Range**	**Accuracy* (±)**	**Resolution**
Frequency			
Fundamental	16.00 - 500.0 Hz	0.01% + 0.01 Hz	0.01 Hz
Harmonics	32.00 Hz - 19.5 kHz		0.01 Hz
Phase	0.0 - 360.0°	2° typical	0.5°
Voltage	Fundamental	250 mV	10 mV
	Harmonics 2 - 50	0.1% + 250 mV +0.1% /1kHz	10 mV
Current	Fundamental	50 mA	10 mA
	Harmonics 2 - 50	0.1% + 50 mA +0.1% /1kHz	10 mV

*Accuracy specifications are valid above 100 counts. Accuracy specifications are times three for three phase mode. Harmonics frequency range in three phase mode is 32 Hz - 6.67 kHz.

System Features

Non Volatile Memory storage	6 complete instrument setups 200 user defined waveforms
Waveforms	
Waveform types	Sine Square Clipped Sine, 0 - 20% THD User defined
User defined waveform storage	Four groups of 50 user defined arbitrary waveforms of 1024 points for a total of 200. One group can be active at a time
Transient Programming	
Transient Types	
Voltage:	drop, step, sag, surge, sweep
Frequency:	step, sag, surge, sweep
Voltage and Frequency:	step, sweep
Transient List Parameters:	Voltage, Frequency, Time or cycles, Slew rate, Waveform shape, Phase angle, Repeat
Transient lists storage	up to 32 transient steps per list
Time resolution	1 msec
Time range	1 msec - 9999 sec
Maximum slew rate	50 usec for 10% to 90% of full scale change into resistive load
Waveform Acquisition	
Channels	Voltage and Current for each phase

Memory Depth	4096 samples/channel
Maximum Sample Rate	39.0625 Ks/s
Triggering	Auto, Phase, Transient
Trigger Delay	
Pre-trigger	0 - 104 msec 1 phase 0 - 312 msec 3 phase
Post-trigger	0 - 1000 msec

APPENDIX E

BACKPROPAGATION ALGORITHM FOR THREE PHASE SYSTEMS

A modified scheme, illustrated in Figure 5.7, is required to process the three phase voltage and current waveforms. Essentially, the modified neural network structure now has three phase voltages or currents along with two time delayed values of the vector, as well as a bias as inputs. So the actual number of inputs to the neural network is ten.

For a general neural network with n inputs including the bias and m neurons in the hidden layer, r outputs, the dimension of the input weight matrix W is $m \times n$ and dimension of the output weight matrix V is $r \times m$.

The output error vector $\begin{bmatrix} e_{0a} & e_{0b} & e_{0c} \end{bmatrix}^T$ is a 3 element column vector and is calculated as;

$$\begin{bmatrix} e_{0a} & e_{0b} & e_{0c} \end{bmatrix}^T = y_{abc}(k+1) - \hat{y}_{abc}(k+1) \tag{E.1}$$

The output error vector is backpropagated through the MLPN to determine the errors $\underline{e}_d$ and $\underline{e}_a$ in the decision vector $\underline{d}$ and activation vector $\underline{a}$. The decision error vector $\underline{e}_d$ is obtained by back-propagating the output error vector $\begin{bmatrix} e_{0a} & e_{0b} & e_{0c} \end{bmatrix}^T$ through the output weight vector V;

$$\underline{e}_d = V \cdot \begin{bmatrix} e_{0a} & e_{0b} & e_{0c} \end{bmatrix}^T \tag{E.2}$$

where the decision error vector $\underline{e}_d \in R^m$.

The activation errors e_{ai} are given as a product of the decision errors e_{di} and the derivative of the decisions d_i with respect to the activations a_i;

$$e_{ai} = \left(\frac{d}{da_i} d_i \right) e_{di}$$

$$= \left(\frac{d}{da_i} \left(\frac{1}{1+e^{(-a_i)}} \right) \right) e_{di}$$

$$= d_i \left(1 - d_i\right) e_{di}, \; i \in \{1, 2, ..., m\} \tag{E.3}$$

The derivative of a sigmoidal function can be expressed in terms of its inputs and outputs and computationally it results in multiplication and addition. The subscript i in equation (E.3) indicates element-wise multiplication of the vectors $\underline{d}$, $\underline{1-d}$ and $\underline{e}_d$.

The change in input weights ΔW and output weights ΔV at step k of the training process are calculated as;

$$\Delta W(k) = \gamma_m \Delta W(k-1) + \gamma_g \underline{e}_a \underline{x}^T$$

$$\Delta V(k) = \gamma_m \Delta V + \gamma_g \cdot \begin{bmatrix} e_{0a} & e_{0b} & e_{0c} \end{bmatrix}^T \cdot \underline{d}^T \tag{E.4}$$

where $\gamma_{m,} \gamma_g \in [0,1]$ are the momentum and learning gain constants respectively. The last step in the training process is the actual updating of the weights at step k;

$$W(k) = W(k-1) + \Delta W(k)$$

$$V(k) = V(k-1) + \Delta V(k) \tag{E.5}$$

BIBLIOGRAPHY

[1] R. C. Dugan, M.F. Mcgranaghan, and H.W. Beaty, "Electrical Power Systems Quality," McGraw-Hill, New York, 1995, ISBN 0070180318.

[2] G. J. Wakileh, "Power System Harmonics: Fundamentals, Analysis and Filter Design," Springer, Berlin Heidelberg New York, 2nd edition, 2001, ISBN 3540422382.

[3] A. McEachern, "Designing electronic devices to survive power-quality events," *IEEE Industry Applications Magazine*, vol. 6, no. 6, pp. 66 – 69, November-December 2000.

[4] M. F. McGranaghan, "Economic evaluation of power quality," *IEEE Power Engineering Review*, vol. 22, no. 2, pp. 8–12, February 2002.

[5] J. Arrillaga, M.H.J. Bollen, and N.R. Watson, "Power quality following deregulation," *Proceedings of the IEEE*, vol. 88, no. 2, pp. 246–261, February 2000.

[6] S. George and V. Agarwal, "A novel technique for optimizing harmonics and reactive power with load balancing under nonsinusoidal supply and unbalanced load conditions," in *Proceedings of the IEEE Power Electronics Specialist Conference (PESC03)*, Acapulco, Mexico, Vol. 4, pp. 1537 – 1541, June 2003.

[7] L. Cristaldi and A. Ferrero, "Harmonic power flow analysis for the measurement of the electric power quality," *IEEE Transactions on IEEE Transactions on Instrumentation and Measurement*, Vol. 44, Issue 3, pp. 683 - 685, June 1995.

[8] H. Sasaki and T. Machida, "A new method to eliminate ac harmonic currents by magnetic flux compensation-consideration on basic design," *IEEE Transactions on Power Apparatus and Systems*, pp. 380-385, 1971.

[9] L. Gyugyi and E. C. Strycula, "Active power filters," in *Proceedings of the IEEE Industry Applications Society Annual Meeting (IAS76)*, Chicago, Illinois, pp. 529 – 535, October 11-14, 1976.

[10] N. Mohan, H.A. Peterson, W.F. Long, D.R. Dreifuerst, and J.J. Vithayathil, "Active filter for ac harmonic suppression," *IEEE PES Winter Power Meeting,* paper WM95, New York, January 1977.

[11] M. Bollen, "Understanding Power Quality Problems, Voltage Sags and Interruptions," IEEE Press, New York, 2000, ISBN 0780347137.

[12] C. Sankaran, "Power Quality," CRC Press, 1st edition, 2001, ISBN: 0849310407.

[13] IEEE Standard 1159-1995, IEEE recommended practice for monitoring electric power quality, 1995.

[14] IEEE Standard 519-1992, IEEE Recommended Practices and Requirements for Harmonic Control in Electric Power Systems.

[15] S. Peeran, T. Barclay, K. Sanborn, R. Schnorr von Carolsfeld, and M. Shields, "Fault analysis through power quality metering," *IEEE Industry Applications Magazine*, vol. 5, no. 2, pp. 28–31, March-April 1999.

[16] I. Hunter, "Power quality issues-a distribution company perspective," *IEE Power Engineering Journal*, vol. 15, no. 2, pp. 75–80, April 2001.

[17] A.K. Khan, "Monitoring power for the future," *IEE Power Engineering Journal*, vol. 15, no. 2, pp. 81–85, April 2001.

[18] R. Tsukui, P. Beaumont, T. Tanaka, and K. Sekiguchi, "Power system protection and control utilizing intranet technology," *IEE Power Engineering Journal*, vol. 15, no. 5, pp. 249–255, October 2001.

[19] R. C. Dugan, S. S., M. F. McGranaghan, H. W. Beaty, "Electrical Power Systems Quality," McGraw-Hill Professional, 2nd edition, 2002, ISBN: 0-0713-8622-X.

[20] E. Acha, M. Madrigal, "Power System Harmonics, Computer Modeling and Analysis," John Wiley & Sons, England, 2001, ISBN 047152175-2.

[21] M. Mcgranaghan, " Controlling harmonics from nonlinear loads in commercial facilities," in *Proceedings of the IEEE International Conference on Harmonics And Quality of Power (ICHQP98)*, Athens, Greece, Vol. 2, pp. 872 – 877, October 14-16, 1998.

[22] E. L. Owen, "A history of harmonics in power systems," *IEEE Industry Applications Magazine*, vol. 4, no. 1, pp. 6 – 12, January – February 1998.

[23] IEEE Power System Harmonic Working Group, "Bibliography of Power System Harmonics, Part I and II," *IEEE PES Winter Power Meeting,* Paper 84 WM 214-3, January/February 1984.

[24] J. Arrillaga, B.C. Smith, N.R. Wood, and A.R. Wood, "Power System Harmonic Analysis," John Wiley & Sons, England, 1997, ISBN 0471975486.

[25] J. Arrillaga, N.R. Watson, and S. Chen, "Power System Quality Assessment," John Wiley & Sons, England, 2001, ISBN 0471988650.

[26] F. Peng, "A new approach to harmonic compensation in power systems - The combined system of shunt passive and series active filters," PhD thesis, Nagaoka University of Technology, Nagaoka, Japan, 1989.

[27] M. Fauri and P. Ribeiro, "A novel approach to nonlinear load modeling," in *Proceedings of the 6th International Conference on Harmonics in Power Systems (ICHPS'94),* Bologna, Italy, September 1994.

[28] G. Heydt and A. Risal, "Apparatus and method to identify harmonic producing loads," U.S. Patent number 5,508,623, April 16 1996.

[29] D. Rice, "A detailed analysis of six-pulse converter harmonic currents," *IEEE Transactions on Industry Applications*, vol. 30, pp. 294.304, March/April 1994.

[30] A. Mansoor, W.M.Grady, R.S. Thallam, M.T. Doyle, S.D. Krein and M.J. Samotyj, "Effect of supply voltage harmonics on the input current of single-phase diode bridge rectifier loads," *IEEE Transactions on Power Delivery*, Vol. 10, Issue 3, pp. 1416 - 1422, July 1995.

[31] T.S. Key and Jih-Sheng Lai, "Costs and benefits of harmonic current reduction for switch-mode power supplies in a commercial office building," *IEEE Transactions on Industry Applications*, Vol. 32, Issue. 5, pp. 1017-1025, September/October 1996.

[32] S. Bhattacharya and D.M. Divan, "Utility Interface Issues of Power Electronic Converters - Case Studies of Active Filter Applications," tutorial notes of Industrial Power Converter Committee (IPCC), IAS 1995, Orlando, FL, October 9-13, 1995.

[33] Roger C Dugan, Surya Santoso, Mark F. McGranaghan, H. Wayne Beaty, "Electrical Power Systems Quality," McGraw-Hill Professional, 2nd edition, 2002, ISBN: 0-0713-8622-X.

[34] J.C. Li and Y.P. Wu, "FFT algorithm for the harmonic analysis of three-phase transformer banks with magnetic saturation," *IEEE Transactions on Power Delivery*, Vol. 6, Issue 1, pp. 158 - 161, Jan 1991.

[35] Ned Mohan, Tore M. Undeland and William P. Robbins, "Power Electronics: Converters, Applications and Design," Wiley, 3rd edition, 2002, ISBN 0-4712-2693-9.

[36] Muhammad H. Rashid, "Power Electronics: Circuits, Devices and Applications," Prentice Hall, 3rd edition, 2003, ISBN 0-1310-1140-5.

[37] V. Sharma and A.C. Thomson, "Power system harmonic guidelines and how to evaluate the impact of customer generated harmonics," in *Proceedings of the IEEE Communications, Computers and Power in the Modern Environment (WESCANEX 93)*, Saskatoon, Canada, pp. 797 - 800, May 1993.

[38] Electromagnetic Compatibility (EMC)-Part 3: Limits-Section 6:Assessment of Emission Limits for Distorting Loads in MV and HV Power Systems, IEC 1000-3-6,1996.

[39] A. McEachern, W.M. Grady, W.A. Moncrief, G.T. Heydt, and M. McGranaghan, "Revenue and Harmonics: An evaluation of some proposed rate structures," *IEEE Transactions on Power Delivery*, Vol. 101, Issue 1, pp. 474 - 482, January 1995.

[40] A. Ferrero, L. Peretto, and R. Sasdelli, "Revenue metering in the presence of distortion and unbalance: myths and reality," in *Proceedings of the International Conference on Harmonics and Quality of Power (ICHQP98),* Athens, Greece, Vol. 1, pp. 42-47, October 14-16, 1998.

[41] K. Srinivasan, "On Separating Customer and Supply Side Harmonics," *IEEE Transactions on Power Delivery*, Vol. 11, Issue 2, pp. 1003 - 1012, April 1996.

[42] C. Li and W. Xu, "On Defining Harmonic Contributions at the Point of Common Coupling," *IEEE Power Engineering Review*, Vol. 22, No.7, pp. 44-45, July 2002.

[43] W. Xu, and Y. Liu, "A Method for Determining Customer and Utility Harmonic Contributions at the PCC," *IEEE Transactions on Power Delivery*, Vol. 15, Issue 2, pp.804-811, April 2000.

[44] W. Xu, "Status and Future Directions of Power System Harmonic Analysis," in *Proceedings of the IEEE PES General Meeting,* Denver, Colorado, Vol. 1, pp.756-761, June 6-10, 2004.

[45] W. Xu and Y. Liu, " A method to determine customer harmonic contributions for incentive based harmonic control applications," in *Proceedings of the IEEE Power Engineering Society Summer Meeting*, Vol. 1 , pp. 361 - 366, July 1999.

[46] W. Xu and X. Liu, "An Investigation on the Validity of Power Direction Method for Harmonic Source Determination," *IEEE Transactions on Power Delivery*, Vol. 18, No. 1, pp. 214-219, Feb. 2003.

[47] C. Li, W. Xu and T. Tayjasanant, "A Critical Impedance Based Method for Identifying Harmonic Sources," *IEEE Transactions on Power Delivery*, Vol. 19, No. 2, pp. 671-678, April 2004.

[48] A. A. Moustafa, A. M. Moussa, and M. A. El-Gammal, "Separation of customer and supply harmonics in electrical power distribution systems," in *Proceedings of IEEE International Conference on Harmonics and Quality of Power(ICHQP00),* Orlando, FL, Vol. 1, pp. 208 – 213, October 1-4, 2000.

[49] G. Moreau, H.H. Le, G. Croteau, G. Beaulieu, and E. Portales, "Measurement system for harmonic impedance of the network and validation steps," in *Proceedings of the IEEE International Symposium on Quality and Security of Electric Power Delivery Systems, CIGRE/PES 2003,* pp. 69 – 73, October 8-10, 2003.

[50] W. Xu, E. Ahmed, X. Zhang and X. Liu, "Measurement of Harmonic Impedances: Practical Implementation Issues and Solutions," *IEEE Transactions on Power Delivery*, Vol 17, No. 1, pp. 210–216, Jan. 2002.

[51] A. de Oliveira, J.C. de Oliveira, J.W. Resende, and M.S. Miskulin, "Practical approaches for AC system harmonic impedance measurements," *IEEE Transactions on Power Delivery*, Vol.6, No.4, pp. 1721-1726, October 1991.

[52] A.D. Lorenzi, P. Bettini and L. Zanotto, "Harmonic Impedance Measurements and Calculations in the EHV Transmission Network," in *Proceedings of the IEEE International Conference on Harmonics and Quality of Power (ICHQP02)*, Rio de Janeiro, Brazil, Vol. 1, pp. 162 – 168, October 6-9, 2002.

[53] J. P. Rhode, A.W. Kelley, and M.E. Baran, "Line Impedance Measurement: A Nondisruptive Wideband Technique," in *Proceedings of the IEEE Industry Applications Society Annual Meeting (IAS 1995),* Orlando, FL, Vol.3, pp. 2233 - 2240, October 9-13, 1995.

[54] M. C. Di Piazza, P. Zanchetta, M. Sumner and D.W.P. Thomas, "Estimation of load impedance in a power system," in *Proceedings of the IEEE International Conference on Harmonics And Quality of Power (ICHQP00)*, Orlando, FL, Vol. 2, pp. 520-525, October 1-4, 2000.

[55] B. Palethorpe, M. Sumner and D.W.P. Thomas, "Power system impedance measurement using a power electronic converter," in *Proceedings of the IEEE International Conference on Harmonics And Quality of Power (ICHQP00)*, Orlando, FL, Vol. 2, pp. 280 – 213, October 1-4, 2000.

[56] Y. Baghzouz, and O. T. Tan, "Probabilistic Modeling of Power System Harmonics," *IEEE Transactions on Industry Applications*, Vol. IA-23, No. 1, pp. 173-180, January/February 1987.

[57] Y.G. Hegazy and M.M.A. Salama, "Probabilistic representation of harmonic currents produced by AC/DC static power converters," in *Proceedings of the IEEE Industry Applications Society Annual Meeting (IAS 1995),* Orlando, FL, Vol.2, pp. 1689 - 1695, October 9-13, 1995.

[58] Y. Baghzouz, "An overview on probabilistic aspects of harmonics in power systems," in *Proceedings of the IEEE Power Engineering Society General Meeting(PES05)*, San Francisco, CA, pp. 2813 - 2815, June 18-22, 2005.

[59] A. Testa, D. Castaldo and R. Langella, "Probabilistic aspects of harmonic impedances," in *Proceedings of the IEEE Power Engineering Society Winter Meeting, 2002*, Vol. 2 , pp. 27 - 31, Jan 2002.

[60] P.F. Ribeiro, "An overview of probabilistic aspects of harmonics: state of the art and new developments," in *Proceedings of the IEEE Power Engineering Society General Meeting(PES05)*, pp. 2342 - 2345, June 18-22, 2005..

[61] Jung-Wook Park, R.G. Harley, and G.K. Venayagamoorthy, "Adaptive-critic-based optimal neurocontrol for synchronous generators in a power system using MLP/RBF neural networks," *IEEE Transactions on Industry Applications*, Vol. 39, Issue 5, pp. 1529 – 1540, September/October 2003.

[62] G. K. Venayagamoorthy and R.G. Harley, "Two separate continually online-trained neurocontrollers for excitation and turbine control of a turbogenerator," *IEEE Transactions on Industry Applications*, Vol. 38, Issue 3, pp. 887 – 893, May/June 2002.

[63] B. K. Bose, "Artificial neural network applications in power electronics," in *Proceedings of the IEEE Industrial Electronics Society Annual Conference(IECON01),* Denver, Colorado, Vol. 3, pp. 1631 – 1638, November 29 – December 2, 2001.

[64] M. A. El-Sharkawi, "What role can neural networks play in power system engineering," *IEEE Power Engineering Review*, Vol. 14, Issue 2, pp. 14, February 1994.

[65] R. M. Tallam, T. G. Habetler and R. G. Harley, "Continual on-line training of neural networks with applications to electric machine fault diagnostics," in *Proceedings of the IEEE Power Electronics Specialist Conference(PESC01)*, Vancouver, Canada, Vol. 4, pp. 2224 – 2228, June 17-21, 2001.

[66] N. Pecharanin, H. Matsui and M. Sone, "Harmonic detection using neural networks," in *Proceedings of the IEEE International Conference on Neural Networks (ICNN95),* Perth, Australia, Vol. 2, pp. 923-926, November 27-December 1, 1995.

[67] J. R. Vazquez, P. Salmeron, J. Prieto and A. Perez, "Practical implementation of a three-phase active power line conditioner with ANNs technology," in *Proceedings of the IEEE Industrial Electronics Society Annual Conference(IECON02)*, Seville, Spain, Vol. 1, pp. 739 – 744, Nov 5-8, 2002.

[68] M. Bostanci, J. Koplowitz and C.W. Taylor, "Identification of power system load dynamics using artificial neural networks," *IEEE Transactions on Power Systems*, Vol. 12, Issue 4, pp. 1468 - 1473, Nov 1997.

[69] S. Osowski, "Neural network for estimation of harmonic components in a power system," *IEE Proceedings on Generation, Transmission and Distribution*, Vol. 139, Issue 2, pp. 129 – 135, March 1992.

[70] W. L Keerthipala, L. T. Chong, "Artificial neural network model for analysis of power system harmonics," in *Proceedings of the IEEE International Conference on Neural Networks (ICNN95),* Perth, Australia, Vol. 2, pp. 905-910, November 27- December 1, 1995.

[71] R. K. Hartana and G. G. Richards, "Harmonic Source Monitoring and Identification using neural Networks," *IEEE Transactions on Power Systems*, Vol. 5, Issue 4, pp. 1098 - 1104, November 1990.

[72] L. L. Lai and W. L. Chan, "Real-time frequency and harmonic evaluation using artificial neural networks," *IEEE Transactions on Power Delivery*, Vol. 14, Issue 1, pp. 52 - 59, January 1999.

[73] I. El-Amin and I. Arafah, "Artificial neural networks for power systems harmonic estimation," in *Proceedings of the IEEE International Conference on Harmonics And Quality of Power(ICHQP98)*, Athens, Greece, Vol. 2, pp. 999 – 1009, October 14-16,1998.

[74] M. Rukonuzzaman, A.A.M Zin, H. Shaibon, and K. L. Lo, "An application of neural network in power system harmonic detection," in *Proceedings of the IEEE World Congress on Computational Intelligence, IEEE International Joint Conference on Neural Networks (IJCNN98)*, Anchorage, Alaska, Vol. 1, pp. 74 – 78, May 4-8, 1998.

[75] C. R. van Niekerk, A. P. J Rens and A.J. Hoffman, "Identification of types of distortion sources in power systems by applying neural networks," *IEEE AFRICON*, Mbabane, Swaziland, Vol. 2, pp. 829 – 834, October 2002.

[76] H. Mori, and S. Suga, "Power system harmonics prediction with an artificial neural network," in *Proceedings of the IEEE International Symposium on Circuits and Systems (ISCAS91)*, Singapore, Vol. 2, pp. 1129 –1132, June 11-14, 1991.

[77] Simon Haykin, "Neural Networks – A comprehensive foundation," Prentice Hall, 2nd edition, 1998, ISBN 0-1327-3350-1.

[78] D. Rumelhart, G. Hinton and R. Williams, "Learning internal representations by error propagation," in Parallel Distributed Processing, volume 1, chapter 8, pp. 318– 362. MIT Press, 1986, ISBN: 10:0-26263112-1

[79] M. J. L. Orr, "Introduction to radial basis function networks," Technical report, Centre for Cognitive Science, University of Edinburgh, 1996.

[80] G. Cybenko, "Approximation by superpositions of a sigmoidal function," *Mathematics of Control, Signals and Systems*, Vol. 2, pp. 303–314, 1989.

[81] H. White, "Connectionist nonparametric regression: Multilayer feedforward networks can learn arbitrary mappings," *Neural Networks*, Vol.3, Issue5, pp. 535 –549, Elsevier Science Limited, ISSN: 0893-6080, 1990.

[82] Paul J. Werbos, "The Roots of Backpropagation: From Ordered Derivatives to Neural Networks and Political Forecasting," Wiley, 1st edition, 1994, ISBN 0-471-59897-6.

[83] T. Kohonen, "The self organizing map", *IEEE Transactions on Neural Networks*, Vol.1, Issue. 1, pp. 1464-1480, March 1990.

[84] W.T. Miller, R.S. Sutton, and P.J. Werbos, "Neural Networks for Control," MIT Press, Cambridge, Massachusetts, 1990, ISBN 0-262-13261-3.

[85] B. Burton and R.G. Harley, "Reducing the computational demands of continually online-trained artificial neural networks for system identification and control of fast processes," *IEEE Transactions on Industry Applications*, Vol. 34, Issue 3, pp. 589 – 596, May/June 1998.

[86] Jung-Wook Park, R.G. Harley, and G.K. Venayagamoorthy, "Comparison of MLP and RBF Neural Networks Using Deviation Signals for On-Line Identification of a Synchronous Generator," in *Proceedings of the IEEE PES Winter Meeting, 2002,* Vol.1, pp.274-279, January 2002.

[87] M. Mozer, "Neural net architectures for temporal sequence processing," in *Time Series Prediction: Forecasting the Future and Understanding the Past*, editors A. Weigend and N. Gershenfeld, pp. 243–264. Addison-Wesley, 1993.

[88] A. Lapedes and R. Faber, "Nonlinear signal processing using neural networks: Prediction and signal modeling" Technical Report LA-UR-87-2662, Los Alamos National Laboratory, Los Alamos, New Mexico, 1987.

[89] J. Elman, "Finding structure in time," in *Proceedings of Cognitive Science*, Issue 14, pp. 179–211, 1990.

[90] P. J. Werbos, "Backpropagation Through Time: What It Does and How to Do It," *Proceedings* IEEE, Vol.78, No.10, pp. 1550-1560, October 1990.

[91] Y. Bengio, S. Simard, and P. Frasconi, "Learning long-term dependencies with gradient descent is difficult," *IEEE Transactions Neural Networks*, Vol. 5, Issue 2, pp. 157–166, April 1994.

[92] R.J. Williams and D. Zisper, "A learning algorithm for continually running fully recurrent neural networks," in *Proceedings of Neural Computation 1,* pp. 270 – 280, 1989.

[93] S. Geman, E. Bienenstock and R. Doursat, "Neural Networks and the Bias/Variance Dilemma," in *Proceedings of Neural Computation*, Issue 4, pp. 1–58, 1992.

[94] S. Lawrence, C. L. Giles, and A. C. Tsoi, "What size neural network gives optimal generalization?: Convergence properties of backpropagation," Technical Report UMIACS-TR-96-22 and CS-TR-3617, Institute for Advanced Computer Studies, University of Maryland, College Park, 1996.

[95] A. Blum, "Neural Networks in C++: An Object-Oriented Framework for Building Connectionist Systems," John Wiley & Sons , New York, pp. 80, ISBN: 047155202X, 1992.

[96] M. J. A. Berry and G. Linoff, "Data Mining Techniques," Wiley Computer Publishing, pp. 323, ISBN: 0471470643, 1997.

[97] D. R. Hush and B. G. Home, "Progress in Supervised Neural Networks," *IEEE Signal Processing Magazine*, pp. 8-39. January 1993.

[98] E. B. Baum and D. Haussler, "What Size Net Gives Valid Generalization?," *Neural Computation*, no. 1, pp 151-160, 1989.

[99] V. N. Vapnik and A.Ya. Chervonenkis, "On the Uniform Convergence of Relative Frequencies of Events to Their Probabilities," *Theory of Probability and Its Application*, vol. 16, no. 2, pp 264-280, 1971.

[100] G.T. Heydt, S.P. Hoffman, A. Rishal, R.I. Sasaki, and M.J. Kemper, "The impact of energy saving technologies on electric distibution system power quality," in *Proceedings of the IEEE International Sysmposium of Industrial Electronics (ISIE 1994)*, Santiago, Chile, pp. 176-181, May 25-27, 1994.

[101] Y.H. Yan, C.S. Chen, C.S. Moo and C.T. Hsu, "Harmonic analysis for industrial customers," *IEEE Transactions on Industry Applications*, Vol. 30, Issue. 2, pp. 462- 468, March/April 1994.

[102] V.E. Wagner, "Effects of harmonics on equipment," *IEEE Transactions on Power Delivery*, Vol. 8, Issue 2, pp. 672 - 680, April 1993.

[103] D.P. Manjure and E.B. Makram, "Impact of Unbalance on Power System Harmonics," in *Proceedings of the IEEE International Conference on Harmonics And Quality of Power (ICHQP02)*, Rio de Janeiro, Vol. 1, pp. 328 – 333, October 6-9, 2002.

[104] F.P.Marafao, S.M.Deckmann and J.A.G. Marafao, "Power factor analysis under nonsinusoidal and unbalanced systems," in *Proceedings of the IEEE International Conference on Harmonics And Quality of Power (ICHQP02)*, Rio de Janeiro, Vol. 1, pp. 266 – 271, October 6-9, 2002.

[105] P.E. Sutherland, "Harmonic measurements in industrial power systems," *IEEE Transactions on Industry Applications*, Vol. 31, Issue. 1, pp. 175- 183, January/February 1995.

[106] Z. Staroszczyk and A. Chwaleba, "High accuracy harmonics identification and power measurements in power systems," in *Proceedings of the IEEE Instrumentation and Measurement Technology Conference (IMTC94)*, Hamamatsu, Japan, Vol. 3, pp. 1305 – 1308, May 10-12, 1994.

[107] R. Arseneau, "What is measured by digital revenue meters?," in *Proceedings of the IEEE Power Engineering Society General Meeting(PES05)*, pp. 1384 - 1386, June 18-22, 2005.

[108] E.J. Davis, A.E. Emanuel and D.J. Pileggi, "Harmonic Pollution Metering: Theoretical Considerations," *IEEE Transactions on Power Delivery*, Vol. 15, Issue 1, pp. 19 - 23, Jan 2000.

[109] M. Munday and D.G. Hart, "Methods for electric power measurements," in *Proceedings of the IEEE Power Engineering Society Summer Meeting, 2002*, Vol. 3 , pp. 1682 - 1685, July 2002.

[110] C. Gherasim, J. Van den Keybus, J. Driesen and R. Belmans, "DSP implementation of power measurements according to the IEEE trial-use standard 1459," *IEEE Transactions on Instrumentation and Measurement*, Vol. 53, Issue 4, pp. 1086 - 1092, Aug 2004.

[111] I. Yamamoto, K. Matsui, K. Tsuboi, and F.Ueda, "A harmonic meter using a phase locked loop," in *Proceedings of the IEEE International Symposium on Industrial Electronics (ISIE 2001),* Pusan, Korea, Vol.1, pp. 543 – 548, June 12-16, 2001.

[112] J.M. Moreno-Eguilaz and J. Peracaula, "A PC-based tool for evaluation of harmonics and power in three-phase power electronic converters," in *Proceedings of the IEEE Workshop on Computers in Power Electronics (COMPEL 2000)*, Blacksburg, Virginia, pp. 55 – 58, July 16-18, 2000.

[113] S.C. Smith and M.J. Devaney, "Fourier based three phase power metering system," in *Proceedings of the IEEE Instrumentation and Measurement Technology Conference(IMTC 2000)*, Baltimore, MD, Vol. 1, pp. 30 – 35, May 1-4, 2000.

[114] T. Yamaguchi, K. Matsui, K. Tsuboi, and F.Ueda, "A simple and low cost measuring method for harmonics in the power system," in *Proceedings of the IEEE Industry Applications Society Annual Meeting (IAS 98),* St. Louis, MO, Vol.3, pp. 2360 - 2363, October 8-12, 1998.

[115] A. Carullo, M. Parvis and A. Vallan, "Low-cost power meter for the characterisation of inverter-fed electrical machines," in *Proceedings of the IEEE Instrumentation and Measurement Technology Conference (IMTC 1997)*, Ottawa, Canada, Vol. 1, pp. 270 – 275, May 19-21, 1997.

[116] V.A.Katic, "Computer Based Harmonic Measurement Systems: Discussion and A Realization," in *Proceedings of the International Conference on Harmonics in Power Systems (ICHPS92),* Atlanta, GA, pp. 16 - 22, September 22-25, 1992.

[117] L. Saint, J.J. Mesas, and S. Herraiz, " Study of harmonic cancellation between AC/DC converter currents," in *Proceedings of the International Conference on*

Harmonics and Quality of Power (ICHQP04), Lake Placid, NY, pp. 148-153, September 12-15, 2004.

[118] S. Hansen, P. Nielsen, and F. Blaabjerg, "Harmonic cancellation by mixing nonlinear single phase and three phase loads," *IEEE Transactions on Industry Applications*, Vol. 36, Issue. 1, pp. 152-159, January/February 2000.

[119] W.M. Grady, A. Mansoor, E.F. Fuchs, P. Verde and M. Doyle, "Estimating the net harmonic currents produced by selected distributed single-phase loads: computers, televisions, and incandescent light dimmers," *IEEE Power Engineering Society Winter Meeting, 2002*, Vol. 2 , pp. 1090 – 1094, January 2002.

[120] A. Capasso, R. Lamedica and A. Prudenzi, "Estimation of net harmonic currents due to dispersed nonlinear loads within residential areas," in *Proceedings of the IEEE International Conference on Harmonics And Quality of Power (ICHQP98)*, Vol. 2, pp. 700 – 705, October 14-16,1998.

[121] Y. Wang and W. Xu, "An Investigation on the Reactive Power Support Service Needs of Power Producers," *IEEE Transactions on Power Systems*, Vol. 19, No.1, pp. 586 – 593, February 2004.

[122] S. Chen, "A quantitative analysis of the data acquisition requirements for measuring power quality phenomena," *IEEE Transactions on Power Delivery*, Vol. 18, Issue 4, pp. 1575 - 1577, Oct 2003.

[123] D.D. Sabin, " Analysis of harmonic measurement data," in *Proceedings of the IEEE Power Engineering Society Summer Meeting, 2002*, Vol. 2 , pp. 941 - 945, July 2002.

[124] H. Jaeger, "Reservoir Riddles: Suggestions for Echo State Network Research," in *Proceedings of the IEEE International Conference on Neural Networks (IJCNN05)*, Montreal, Canada, Vol.2, pp. 905 – 910, July 31- August 4 2005.

[125] D. Prokhorov, "Echo State Networks: Appeal and Challenges," in *Proceedings of the IEEE International Conference on Neural Networks (IJCNN05)*, Montreal, Canada, Vol.2, pp. 905 – 910, July 31- August 4 2005.

[126] M. Cernansky and M. Makula, "Feed-forward Echo State Networks," in *Proceedings of the IEEE International Conference on Neural Networks, (IJCNN05)*, Montreal, Canada, Vol.2, pp. 905 – 910, July 31- August 4 2005.

[127] K. Bush and C. Anderson, "Modeling reward functions for incomplete state representations via echo state networks," in *Proceedings of the IEEE International Conference on Neural Networks (IJCNN05)*, Montreal, Canada, Vol.2, pp. 905 – 910, July 31- August 4 2005.

[128] M. Salmen and P.G. Plogger, " Echo State Networks used for motor control," in *Proceedings of the IEEE International Conference on Robotics and Automation, ICRA05*, Barcelona, Spain, pp. 1953-1958, April 18-22, 2005.

[129] K. Ishu, T. van der Zant, V. Becanovic and P. Ploger, "Identification of motion with echo state network," in *Proceedings of the IEEE OCEANS 04*, Vol. 3, pp. 1205 – 1210, Kobe, Japan, November 9-12, 2004

[130] H. Jaeger, "The echo state approach to analysing and training recurrent neural networks," GMD Report 148, German National Research Center for Information Technology, 2001.

[131] H. Jaeger, "Short term memory in echo state networks**,"** GMD Report 152, German National Research Center for Information Technology, 2001.

[132] B. Liebald, "Exploration of effects of different network topologies on the ESN signal crosscorrelation matrix spectrum," Bachelor of Science (B.Sc.) thesis, International University Bremen, Spring 2004.

[133] H. Fujita and H. Akagi, "A practical approach to harmonic compensation in power systems – Series connection of passive and active filters," *IEEE Transactions on Industry Applications*, Vol. 27, pp.1020-1025, November/December 1991.

[134] M. Rastogi, N. Mohan, and A. Edris, "Hybrid active filtering of harmonic currents in power system," *IEEE Transactions on Power Delivery*, Vol. 10, pp.1994-2000, October 1995.

[135] M. McGranagham, and D. Mueller, "Designing Harmonic Filters for Adjustable Speed Drives to Comply with IEEE- 519 Harmonic Limits," *IEEE Transactions on Industry Applications*, Vol. 5, Issue 2, pp.312-318, March/April 1999.

[136] S. Bhattacharya and D. Divan, "Active filter solutions for utility interface of industrial loads," in *Proceedings of the International Conference on Power Electronics, Drives and Energy Systems*, New Delhi, India, pp. 1078-1084, January 8-11, 1996.

[137] T. A. George, and D. Bones, "Harmonic power flow determination using the fast Fourier transform", *IEEE Transactions on Power Delivery*, Volume: 6 Issue: 2, April 1991, pp. 530 –535.

[138] J.F. Chicharo and T.S. Ng, "Gradient-based adaptive IIR notch filtering for frequency estimation," *IEEE Transactions on Acoustics Speech and Signal processing*, Vol. 35, Issue 3, pp.769-777, 1990.

[139] P. Salmeron and J.R. Vazquez, "Practical design of a three phase active power line conditioner controlled by artificial neural networks," *IEEE Transactions on Power Delivery*, Vol. 20, Issue 2, pp.1037-1044, April 2005.

[140] P. Cheng, S. Bhattacharya and D. Divan, "Experimental verification of dominant harmonic active filter for high power applications," *IEEE Transactions on Industry Applications*, Vol. 36, pp.567-577, March/April 2000.

[141] S. Bhattacharya, D. Divan and B. Banerjee, "*Synchronous frame harmonic isolator using active series filter*," in *Proceedings of the EPE-Firenze*, Italy, Vol. 3, pp. 30-35, September 1991.

[142] R. Harley, F. Lambert, T. Habetler and J. Mazumdar, "System and Method for Determining Harmonic Contributions from Nonlinear Loads," United States Patent 7013227 issued March 2006.

[143] R. Harley, D. Divan, F. Lambert and J. Mazumdar, "Determining the impact of nonlinear load harmonics on the PCC voltage distortion," United States Patent application 11/337630 filed January 2006.

[144] Task Force on Harmonics Modeling and Simulation, "Modeling and Simulation of the Propagation of Harmonics in Electric Power Networks Part I : Concepts, Models and Simulation Techniques," *IEEE Trans. on Power Delivery,* Vol.11, No.1, January 1996, pp. 452-465.

[145] Superharm Software by Electrotek Inc.

[146] T. Hoevenaars, K. LeDoux and M. Colosino, "Interpreting IEEE STD 519 and meeting its harmonic limits in VFD applications," in *Proceedings of the IEEE Industry Applications Society 50th Annual Petroleum and Chemical Industry Conference, 2003*, Houston, TX, pp. 145 – 150, September 15-17, 2003.

[147] S.M. Halpin, "Overview of revisions to IEEE standard 519-1992," in *Proceedings of the* IEEE International Symposium on Quality and Security of Electric Power Delivery Systems, CIGRE/PES 2003, pp. 65 – 68, October 8-10, 2003.

[148] S.M.R. Rafiei, R. Ghazi and H.A. Toliyat, "IEEE-519-based real-time and optimal control of active filters under nonsinusoidal line voltages using neural networks," *IEEE Transactions on Power Delivery*, Vol. 17, Issue 3, pp. 815 - 821, July 2002.

[149] A. Ludbrook, "IEEE 519-harmonic current goals and diversity-a proposal," in *Proceedings of the IEEE Power Engineering Society Summer Meeting, 2001*, Vol. 2 , pp. 797 - 800, July 2001.

[150] M. McGranaghan, "Overview of the guide for applying harmonic limits on power systems-IEEE P519A," in *Proceedings of the International Conference on Harmonics and Quality of Power (ICHQP98),* Athens, Greece, pp. 462-469, October 14-16, 1998.

[151] J. Mazumdar, R. Harley, F. Lambert and G.K. Venayagamoorthy, "Using a neural network to distinguish between the contributions to harmonic pollution of non-

linear loads and the rest of the power system," *IEEE Transactions on Power Electronics*, accepted for publication.

[152] J. Mazumdar, G.K. Venayagamoorthy, R.G. Harley, and Frank Lambert, "System and Method for Determining Harmonic Contributions from Non-Linear Loads", *IEEE Transactions on Industry Applications*, under review, submitted January 23, 2006.

[153] J. Mazumdar, R. Harley and G.K. Venayagamoorthy, "Recurrent Neural Networks Trained with Backpropagation Through Time Algorithm to Estimate Harmonic Currents Injected from Single and Three Phase Nonlinear Loads," *IEEE Transactions on Industrial Electronics*, under review, submitted April 05, 2006.

[154] J. Mazumdar, R. Harley, F. Lambert, G.K. Venayagamoorthy and M.L. Page, "Application of Echo State Networks for Determining Nonlinear Load Harmonics," *IEEE Transactions on Neural Networks*, under review, submitted August 23, 2006.

[155] J. Mazumdar, R. Harley, T. Habetler and F. Lambert, "Using a neural network to discriminate between the contributions of the power electronic load and the power system to harmonic pollution," *in Proceedings of the IEE International Power Electronics Conference (IPEC 2005)*, Niigata, Japan, pp. 874-878, April 4-8, 2005.

[156] J. Mazumdar, R. Harley, F. Lambert and G.K. Venayagamoorthy, "Detection of non-linear load harmonics using a neural networks," *in Proceedings of the International Conference on Power Systems Operation and Planning (ICPSOP 2005)*, Praia, Cape Verde, pp. 115-119, May 22-26, 2005.

[157] J. Mazumdar, R. Harley, F. Lambert and G.K. Venayagamoorthy, "Using a neural network to distinguish between the contributions to harmonic pollution of non-linear loads and the rest of the power system," *in Proceedings of the IEEE Power Electronics Specialist Conference (PESC 2005)*, Recife, Brazil, pp. 366-371, June 12-16, 2005.

[158] J. Mazumdar, R. Harley, F. Lambert and G.K. Venayagamoorthy, "A novel method based on neural networks to distinguish between load harmonics and source harmonics in a power system," *in Proceedings of the Inaugural IEEE PES 2005 Conference and Exposition in Africa (PES Durban 2005)*, Durban, South Africa, July 11-15, 2005.

[159] J. Mazumdar, R. Harley and F. Lambert, "System and method for determining harmonic contributions from non-linear loads using recurrent neural networks," *in Proceedings of the IEEE International Joint Conference on Neural Networks (IJCNN 2005)*, Montreal, Canada, pp. 366- 371, July 31 – Aug. 4, 2005.

[160] J. Mazumdar, R. Harley and F. Lambert, "System and method for determining harmonic contributions from non-linear loads," *in Proceedings of the IEEE Industry Applications Society Annual Meeting (IAS 2005)*, Kowloon, Hongkong, pp. 2456-2463, Oct 2-6, 2005.

[161] J. Mazumdar, R. Harley and F. Lambert, "Identifying harmonic contributions from non-linear loads using neural networks," *in Proceedings of the IEEE International Conference on Intelligent Systems Application to Power Systems (ISAP 2005)*, Washington D.C., pp. 117-122, Nov. 6-10, 2005.

[162] J. Mazumdar, R. Harley, F. Lambert and G.K. Venayagamoorthy, "A novel method for predicting harmonic current injection from non-linear loads using neural networks," *in Proceedings of the IEEE Industrial Electronics Society Annual Conference (IECON 2005)*, Raleigh, North Carolina, pp. 952-957, Nov. 6-10, 2005.

[163] J. Mazumdar, R. Harley, F. Lambert and G.K. Venayagamoorthy, "Predicting Load Harmonics in Three Phase Systems Using Neural Networks," *in Proceedings of the IEEE Applied Power Electronics Conference (APEC 2006)*, Dallas, Texas, pp. 1738-1744, Mar. 19-23, 2006.

[164] J. Mazumdar, R. Harley, F. Lambert and G.K. Venayagamoorthy, "Monitoring the True Harmonic Current of a Variable Speed Drive Under Nonsinusoidal Supply Conditions," *in Proceedings of the IEEE Power Electronics Specialists Conference (PESC 2006)*, Jeju, Korea, pp. 1-7, June 18-22, 2006.

[165] J. Mazumdar, G.K. Venayagamoorthy, R. Harley and F. Lambert, "Echo State Networks for Determining Harmonic Contributions from Nonlinear Loads," *in Proceedings of the IEEE International Joint Conference on Neural Networks (IJCNN 2006)*, Vancouver, Canada, pp. 1695-1701, July 16-21, 2006.

[166] J. Mazumdar, R. Harley, F. Lambert, G.K. Venayagamoorthy and M.L. Page, "Intelligent Tool for Determining the True Harmonic Current Contribution of a Customer in a Power Distribution Network," *in Proceedings of the IEEE Industry Applications Society Annual Meeting (IAS 2006)*, Tampa, Florida, Oct 8-12, 2006.

[167] J. Mazumdar, R.G. Harley and G.K. Venayagamoorthy, "Synchronous Reference Frame Based Active Filter Current Reference Generation Using Neural Networks," *in Proceedings of the IEEE Industrial Electronics Society Annual Conference (IECON 2006)*, Paris, France, pp. 4404 – 4409, Nov. 7-10, 2006.

[168] J. Mazumdar, G.K. Venayagamoorthy and R.G. Harley, "Application of Neural Networks for Data Modeling of Power Systems with Time Varying Nonlinear Loads," submitted for review to *IEEE Symposium on Computational Intelligence and Data Mining (CIDM 2007)*, Honolulu, Hawaii, Apr 1-5, 2006.

VITA

Joy Mazumdar was born in Bombay, India in 1973. He received his bachelor's degree in electrical engineering from Shivaji University, India in 1994 and master's degree in electrical engineering from the University of Central Florida in 2002. In 1995, he joined Siemens Automation and Drives Division in India as a power electronics engineer and was with Siemens till 2000. He joined Georgia Institute of Technology in the Fall of 2002 for his PhD study.

Joy's present research focuses on applying neural network techniques to distinguish between load harmonics and source harmonics in a power system. His other research interests include neural network topologies, power quality issues and utility applications of power electronics.

Joy Mazumdar is an IEEE student member since 2000. He is also a member of the IEEE Industry Applications, Power Engineering, Power Electronics, Industrial Electronics and Computational Intelligence societies. He won the IEEE engineering award at the Future Energy Challenge 2001 competition and several other IEEE student grants. He has authored over 15 conferences publications and 4 transaction publications. His research resulted in two patents, one issued and one pending.